

This dissertation has been
microfilmed exactly as received 66-14,200

COTA, Harold Maurice, 1936-
SEMICONDUCTIVITY AND CATALYTIC
ACTIVITY: THE DECOMPOSITION OF
HYDROGEN PEROXIDE VAPOR ON
NICKEL OXIDE SINGLE CRYSTALS.

The University of Oklahoma, Ph.D., 1966
Engineering, chemical

University Microfilms, Inc., Ann Arbor, Michigan

THE UNIVERSITY OF OKLAHOMA

GRADUATE COLLEGE

SEMICONDUCTIVITY AND CATALYTIC ACTIVITY:
THE DECOMPOSITION OF HYDROGEN PEROXIDE
VAPOR ON NICKEL OXIDE SINGLE CRYSTALS

A DISSERTATION

SUBMITTED TO THE GRADUATE FACULTY

in partial fulfillment of the requirements for the

degree of

DOCTOR OF PHILOSOPHY

BY

HAROLD MAURICE COTA

Norman, Oklahoma

1966

SEMICONDUCTIVITY AND CATALYTIC ACTIVITY:
THE DECOMPOSITION OF HYDROGEN PEROXIDE
VAPOR ON NICKEL OXIDE SINGLE CRYSTALS

APPROVED BY

7. Mark Johnson
Shen D. Quinlan
Frank Caulfield
Richard Prosser
William J. ...

DISSERTATION COMMITTEE

ACKNOWLEDGMENT

The author takes pleasure in acknowledging the encouragement and help of Dr. F. Mark Townsend throughout this research. Dr. James W. Fulton's and Dr. R. H. Perry's comments during the initial stages of the research were also an encouragement. The stimulating and frank discussions with and comments from Dr. E. E. Kohnke, Dr. A. Cosgarea, Dr. R. A. Ross, Dr. G. Parravano, Dr. J. B. Wagner, Jr., Mr. J. B. Price, Dr. A. B. Hart, and Dr. M. Sumita were valued highly by this author. These people all took time out from their own research efforts to show interest and assist the work presented here in various ways.

The special glassblowing talents of Father Norman Alexandre and his interest in the research during the experimental program are gratefully acknowledged. The excellent work of Mr. Leonard Milacek, who X-rayed and analyzed the diffraction patterns, was a definite contribution. The staff of the University's Osage Computer Laboratory was of definite assistance during the computational phase of this project. Mr. Lee Ho is acknowledged for the photograph of the nickel oxide surface.

Financial support for this work came from the Department of Chemical Engineering and Materials Science, through the approval of

Professors R. D. Daniels, O. K. Crosser, and C. M. Sliepcevich.

In addition to the department for research and teaching assistantships, the Dow Chemical Company is acknowledged for a fellowship and the Monsanto Chemical Company for a scholarship.

Acknowledgment to my wife, Judith, for her continued encouragement and support is gratefully given.

ABSTRACT

A study of the vapor phase decomposition catalyzed by nickel oxide single crystals has been carried out in an isothermal flow reactor. Catalyst pretreatment consisted of annealing the crystals at various temperatures and in several atmospheres. This produced crystals with non-stoichiometric concentration. A compensation effect was observed between the specific rate constant and the apparent activation energy. The catalytic activity was therefore characterized by the amount of decomposition per unit area.

The single crystals were characterized by measuring the electrical conductivity in the same temperature range covered by the kinetic study. It was found that the temperature coefficient of the resistivity was related to the temperature at which pretreatment was conducted. Equations are developed which allow one to predict the amount of non-stoichiometry or the lattice defect concentration from the low temperature conductivity data.

The kinetic parameters were compared with the electrical characteristics of the single crystal and it was found that the maximum activity occurred with the catalytic pretreatment of 1000°C . As the calculated

nickel vacancy concentration increases the catalytic activity first increases then begins to decrease.

The results of this study indicate that meaningful kinetic data can be obtained with this highly ideal system even on the low surface area provided. The application of these techniques to simultaneous measurement of the kinetic and solid state properties is discussed.

TABLE OF CONTENTS

	Page
LIST OF ILLUSTRATIONS	xi
LIST OF TABLES.	xiii
Chapter	
I. INTRODUCTION	1
A. General Concepts	
B. Present Approach	
II. PREVIOUS INVESTIGATIONS.	12
A. Hydrogen Peroxide Vapor Decomposition	
1. Related Studies in the Liquid Phase	
B. Electronic Characterization of NiO	
1. Conduction Model	
2. Defect State	
3. Electrical Conductivity	
a. Equilibrium region	
b. Intermediate region	
c. Low temperature region	
d. Low temperature conductivity with lithium impurities	
e. Surface or boundary conductivity	
4. Conductivity and Chemisorption	
5. Electrical Conductivity and Catalysis	
a. Nitrous oxide decomposition	
b. Oxidation of carbon monoxide	
c. Formic acid decomposition	

	Page
6. Seebeck Coefficient	
III. EXPERIMENTAL APPARATUS AND PROCEDURES . . .	40
A. Preparation of the NiO Crystals	
1. Cleaving	
2. Orientation of Crystal	
3. Pretreatment of the Crystals	
B. Kinetic Apparatus	
1. Raw Materials	
2. Flow Control	
3. Cleaning the Glassware	
4. Vapor Generation	
5. Reactor	
a. Tube reactor	
b. Fluid jacketed reactor	
6. Geometric Surface Area	
C. Electrical Measurements on NiO Single Crystals	
1. Resistivity-Seebeck Cell	
2. Two Point Probe Measurements	
3. Low Temperature Measurements	
a. Seebeck coefficient	
b. Resistivity	
4. Attempted Measurement of Electrical Properties During Reaction	
IV. EXPERIMENTAL RESULTS AND DISCUSSION	71
A. Kinetic Results	
1. Effect of Temperature	
2. Compensation Effect	
3. Order of Reaction	
4. Effect of Surface Area	
5. Effects of Flow Rate	
6. Reproducibility	

B. Electronic Characterization of Catalyst

1. Electrical Conductivity
2. Comparison with Two Point Probe
3. Estimation of Concentration of Nickel Vacancies
4. Room Temperature Measurements of Resistance
5. Seebeck Measurements
 - a. Low temperature
 - b. High temperature

C. Correlation between Electrical and Kinetic Properties

V.	CONCLUSIONS	109
	LITERATURE CITED	111
	NOMENCLATURE	124
APPENDICES		
A.	DERIVATION OF RELATION BETWEEN CONDUCTIVITY PARAMETERS AND NICKEL VACANCY CONCENTRATION	127
B.	IMPURITY CONCENTRATION OF NiO SINGLE CRYSTALS GROWN BY VERNEUIL METHOD	128
C.	DEIONIZED DISTILLED WATER	129
D.	CALIBRATION OF THERMOCOUPLES	134
E.	LOCATION OF CRYSTALS IN THE TUBE REACTOR.	136
F.	GEOMETRIC SURFACE AREAS	137
G.	CALCULATED KINETIC PARAMETERS, RUNS 2/1-2/6	142
H.	ELECTRICAL CONTACTS.	143
I.	CALCULATION OF RESISTIVITY	146

	Page
J. KEL-F COATINGS	148
K. DECOMPOSITION OF HYDROGEN PEROXIDE VAPOR ON BOROSILICATE GLASS	149
L. EXPERIMENTAL EXIT CONCENTRATION PARAM- ETERS.	162
M. BEST FIT COEFFICIENTS TO CONCENTRATION PARAMETER-TEMPERATURE RELATION	164
N. CALCULATED PSEUDO RATE CONSTANTS AND DECOMPOSITION.	167
O. APPROACH TO SATURATION.	169
P. APPARENT ACTIVATION ENERGY OF SURFACE REACTIONS IN EXTERNAL FLOW SYSTEMS	171
Q. EXPERIMENTAL RESULTS FROM TUBE REACTOR NUMBER 1	173
R. EXPERIMENTAL EXIT CONCENTRATION PARAM- ETER-RUN 2/12	175
S. LOW TEMPERATURE RESISTIVITY	176
T. CALCULATION OF THE SEEBECK COEFFICIENT.	178

LIST OF ILLUSTRATIONS

Figure		Page
1.1	Two Dimensional Energy Level Representation of a P-Type Surface	7
2.1	Temperature Dependence of Conductivity for NiO from Literature	23
3.1	Etch Pits on Cleavage Surface of NiO from Run 2/13, x 150	40
3.2	Flow Diagram of Kinetic Apparatus	48
3.3	Glass Reactors	53
3.4	Resistivity-Seebeck Coefficient Apparatus	59
3.5	Two Point Probe Apparatus	63
3.6	Low Temperature Seebeck Cell	66
3.7	Low Temperature Resistance Measuring Apparatus	68
4.1	Dependence of Exit Concentration Parameter on Reactor Temperature	76
4.2	Representative Arrhenius Plot of Kinetic Data, Run 2/12B	77
4.3	Compensation Effect on NiO	80
4.4	Effect of Geometric Surface Area on Decomposition of H ₂ O ₂ , Runs 2/7-2/9	84
4.5	Effect of Flow on Over-All Rate Factor	87

Figure		Page
4.6	Temperature Dependence of Resistance for NiO	94
4.7	Annealing Temperature versus Electronic Activation Energy of NiO	95
4.8	Catalytic Activity versus Electronic Activation Energy of NiO	104
4.9	Effect of Pretreatment Temperature on Nickel Vacancy Concentration in NiO	106
4.10	Effect of Oxygen Mole Fraction of Atmosphere during Pretreatment on Vacancy Concentration in NiO . .	106
4.11	Effect of Nickel Vacancy Concentration on Catalytic Activity	108

LIST OF TABLES

Table		Page
1.1	Origin of Concepts used in Heterogeneous Catalysis . . .	4
2.1	Simultaneous Adsorption-Conductivity Studies on Polycrystalline NiO	35
3.1	Description of the NiO Boules	40
3.2	Pretreatment Conditions of the NiO Crystals	45
4.1	Experimental Kinetic Parameters Obtained with NiO Single Crystals having only Cleaved Surfaces . . .	78
4.2	Decomposition at Two Different Hydrogen Peroxide Concentrations at 165 ^o C	82
4.3	Effect of Crystal Surface Area on Decomposition of H ₂ O ₂ at 165 ^o C	85
4.4	Effect of Flow Rate on Observed Kinetics in Run 2/12 .	86
4.5	Resistivity Temperature Coefficients of NiO Crystals	96
4.6	Estimation of the Relative Ni Vacancies	98
4.7	Seebeck Coefficients	102

CHAPTER I

INTRODUCTION

The phenomena of catalysis is of significant economic importance to society. Motivation to solve the associated complex physico-chemical problems has stimulated a tremendous amount of fundamental catalytic research in the last ten years throughout the world. The problem has reduced to an attempt to understand the nature of the catalytic process in order to predict and control the selectivity and rate of reaction as desired.

It is now generally accepted that all catalytic reactions involve chemisorption. Chemisorption is accompanied by the formation of primary bonds. Various types of interaction are possible with the surface of a solid catalyst. Catalytic reactions are also visualized to progress via one or more intermediates that can be considered unstable compounds. The methods of study and the theoretical interpretation of the nature of the phenomena draw from the fields of physics, chemistry and chemical engineering. The interconnection of all the views and results is expected, but not yet realized.

Semiconductor catalysis is the subject of this study. Semiconducting oxide surfaces have a particularly important place in heterogeneous catalytic research (136). Nickel oxide has been used extensively in fundamental studies. Of the transition metal oxides its electronic properties are best understood. The oxide used here is in the form of single crystals with crystallographic cleavage planes exposed to the reactant.

Hydrogen peroxide vapor decomposition is measured on this catalyst. This reaction is relatively simple, and very sensitive to surface conditions (129).

An isothermal flow reactor is used and kinetic data obtained on the catalysts with total geometric surface areas of 2 cm^2 . The electronic state is characterized by direct current resistivity measurements. Seebeck coefficients were also determined on several crystals.

The experimental techniques developed for this study are of value in obtaining an insight into the relation between catalytic activity and the electronic state of the catalyst. The rate of hydrogen peroxide decomposition and the catalyst resistivity change with temperature. A compensation effect is observed with this system which is in agreement with earlier work. The electrical properties of the catalyst have been found to be dependent on the pretreatment temperature. A comparison is made between a catalytic activity, characterized by the amount of decomposition per unit area, and parameters calculated from the

electrical measurement on the catalysts after reaction.

A. General Concepts

A unified theory of catalysis does not exist. Much remains obscure about the interaction between reactants on even the simplest surface. Questions regarding the nature of the reaction intermediate, its bonds with the surface, and the connection between chemisorption and catalysis are basic. On the other hand, the theory of solids requires more quantitative information about surfaces and how surface and bulk properties are related.

A catalyst is a dynamic participant in chemical reaction phenomena in that a definite interaction between the surface and reacting species exists. The condition of the surface influences both the catalytic properties and other physicochemical properties of a semiconductor. With such a material one has an especially sensitive reflection of surface conditions in the electrical properties of the solid.

The correlation between the electronic structure of solids and their catalytic activity was generally accepted in 1943 (31, 131). Prior to that time much of the ground work was done in developing concepts to explain the observed phenomena. In the last two decades efforts have been directed toward formulation of a more quantitative description as well as applying both new techniques and materials (128).

Since several excellent reviews of the development of this field of heterogeneous catalysis are available (5, 31, 59, 153), no comprehensive

review is given here. In rapidly reviewing some of the early concepts, however, one becomes aware how our thinking today has been influenced by past contributions. With the purpose of calling to mind some relevant concepts as well as historically placing the contributors Table 1.1 is presented.

TABLE 1.1
ORIGIN OF CONCEPTS USED IN HETEROGENEOUS
CATALYSIS

Concept of Study	Approximate Date	Investigator
Specific interaction between catalyst surface and adsorbed reacting molecules.	1825	Faraday (85)
Composition and group structure related to activity.	1884	Ostwald (85)
Unstable intermediate compound.	1902	Sabatier, Ipatieff (48,122)
Bohrs theory characterizes catalyst and activity.	1916	Pisarzhevskii (153)
Nature of forces between solid and adsorbed gases.	1918	Langmuir (87)
Active site.	1925	Taylor (141)
Estimation of intermediate interaction energy.	1928	Brönsted, Polanyi (18)
Electronic factors describe nature of bonds in chemisorption.	1928	Roginskii (116)
Adsorption depends on lattice spacing.	1929	Balandin (6)

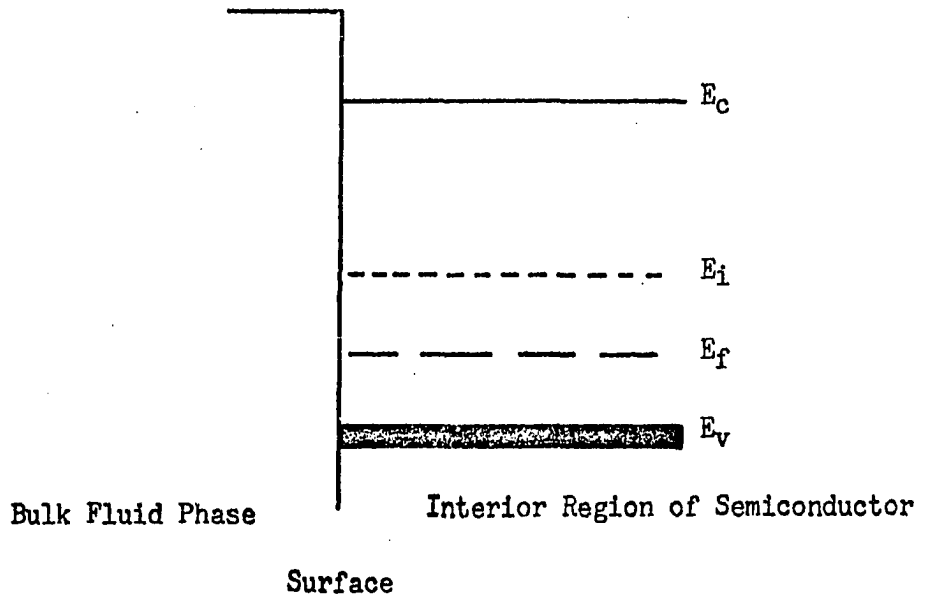
TABLE 1.1--Continued

Concept of Study	Approximate Date	Investigator
Potential energy changes of atom or molecule approaching surface.	1932	Lennard-Jones (91)
Ionization of adsorbed species during chemisorption effected by surface electrons.	1932	Nyrop (106)
Lattice defects, electrical conductivity, catalytic activity and electron transfer.	1938	Wagner, Hauffe (155)
Activated adsorption and electron surface states.	1939	Pollard (114)
Absolute rate theory applied to surface reactions.	1940	Laidler, Eyring, Glasstone (86)
Catalytic control rules experimentally verified.	1949	Gray, Garner, Stone (44)
Importance of Fermi level revealed.	1950	Dowden (31), Volkenstein (154)
Electron transfer and rectification theory.	1952	Hauffe (57), Aigrain (1), Weisz (156)
Quantitative treatment of earlier work presented.	1960, 1966	Garrett (38), Lee (90)

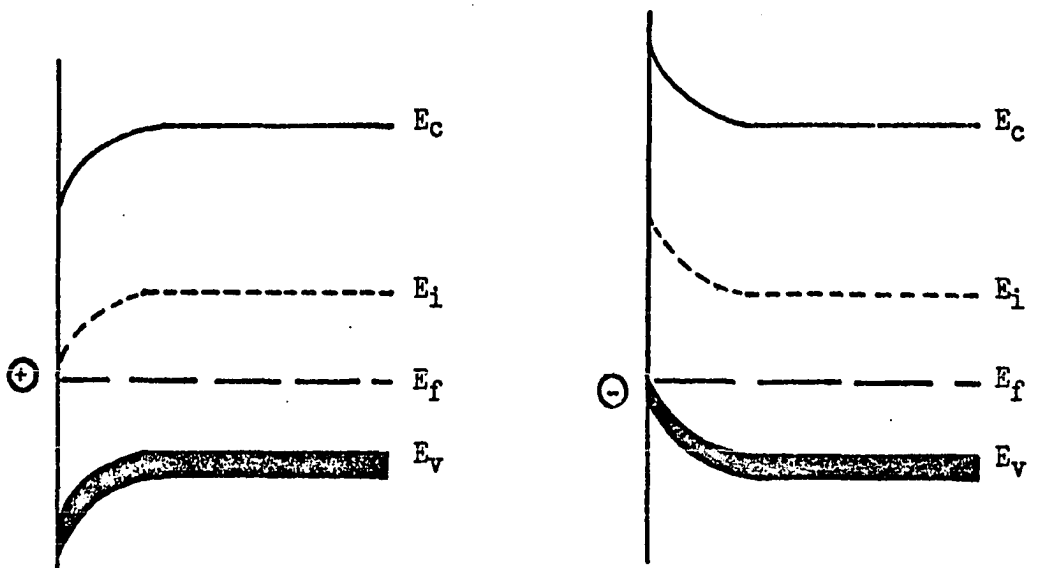
Ehrlich (34) at the 1965 International Congress of Catalysis pointed out that the failures of the theory are easier to document than are the successes and stressed the power of the experimental approach. The current theory is adequately reviewed in the papers cited in Table 1.1.

In this dissertation the general concepts involved in the simple boundary layer theory of adsorption will be mentioned. It does not adequately describe the observed phenomena; however, it stimulated much research in the last fifteen years. Further, these concepts are still drawn upon to describe, at least qualitatively, the phenomena.

In the boundary layer treatment chemisorption is visualized to occur on the surface of the semiconductor by the formation of ions resulting from electron exchange with the surface. The concentration of charge carriers, which is relatively small in a semiconductor, is thereby affected to considerable depths. The adion-solid system must maintain electrical neutrality, in other words, an opposite charge will exist in the surface layer. This so called space charge layer has been treated mathematically in the same manner as surface states arising in electrical contacts of solids. Conceptually the two dimensional energy level diagram, Figure 1.1, is useful. The ordinate axis in Figure 1.1 is assumed to be parallel to the plane surface. This is graduated in terms of energy units usually with respect to a specified level or band. The abscissa represents distance from the surface into the bulk of the crystal. A P-type semiconductor is characterized by parameters such as the work function Φ , density of acceptor levels N_D at E_i , located above the filled band E_v , with the Fermi level assumed halfway between (Figure 1.1a). These acceptor levels may arise from non-stoichiometry, localized charge defects, and/or adsorbed species (157). The concentration of



a.



b. Positive Charge on Surface
Depletion Limited

c. Negative Surface Charges
Accumulation

Figure 1.1. Two Dimensional Energy Level Representation of a P-Type Surface

charge carriers in a nondegenerate, one carrier P-type semiconductor at equilibrium (121, 99) is:

$$N_D = N_0 \exp \frac{E_f - E_i}{kT} \quad (1)$$

where k is the Boltzman constant and T the absolute temperature. If in the process of chemisorption electrons are transferred to the solid, the concentration of carriers (positive holes) decreases in the space charge region. Since the Fermi level at the surface remains unchanged, E_i must increase represented by a bending of the bands, from equation (1). As chemisorption proceeds the electrons will have to overcome a potential barrier. The Mott-Schottky theory of rectification has been applied to obtain the depth of the boundary layer and the rate of carrier flow across the potential barrier (58, 157). The modified form of this theory (38, 56, 89) can, in principle, be used to predict the reaction rate constant without kinetic data, given enough data on adsorption and solid state properties.

The main contribution of the theory has been its descriptive and sometimes qualitatively correct model. When successful it has given insights into the nature of catalysis and new perspective and direction to experiments.

B. Present Approach

A reliable answer as to which parameters of a solid body are decisive for its catalytic characteristics is only possible in special

cases (132). Such things as geometric, acid, chemical, and electronic factors are of interest. The domain of the electronic factor is that of metal and semiconductor catalysis. In all chemical reactions accelerated by solid catalysts, the interaction of the reacting molecules with the current carriers and lattice defects play a significant role. Based on the knowledge of the electronic properties of a crystal, it seems that the examination of semiconductors as catalysts should lend itself to the study of the mechanism of catalysis.

One of the main problems in any experimental work is the exact nature of the surface. Boudart (17) and others have suggested the use of evaporated metal films to obtain well defined surfaces. Single crystal films would be expected to be most ideal. Films of oxide crystals have in the past been prepared by vapor deposition of the metal followed by oxidation (33) and also by the Cech-Alessandrini halide decomposition technique (20). This latter method is reported to give very good single crystals (12). One would expect that single crystals with well defined crystallographic planes would be the best real surface on which to carry out a study.

Single crystals are desirable from another aspect, viz, interpretation of the electrical properties. In any study where one is trying to relate surface and bulk electrical properties to the catalytic activity several complications develop when sintered compacts and powders are used. Interpretation of the measurements due to the highly undefined

state of the solid is the main problem. In considering bulk and surface electrical properties, the effect of impurities, and deviations in stoichiometry and their relation to catalytic activity, it is believed that measurements on single crystals of controlled composition are superior (38, 88, 69, 32). Using concepts from solid state theory in the interpretation of catalysis should be most successful with a single crystal.

In the past it has been difficult to obtain large single crystals of the semiconducting oxides. At the present time many large oxide crystals are available commercially, some at reasonable cost. The choice of which transition metal oxide to use in this study was based on the fact that the solid state of nickel oxide is best understood and under continual study. This together with the fact that nickel oxide has been used in many prior fundamental studies (24, 72, 41, 74, 108, 158) made it the first choice. Nickel oxide boules were obtained from Marbeni-Iida and cleaved and treated in this laboratory.

Reactions which combine high reactivity and molecular simplicity are particularly applicable to basic gaseous-solid interaction studies (136). Monomolecular reactions such as the decomposition of ammonia, phosphine, other hydrides, nitrous oxide, and formic acid (85) have been useful. With this type of reaction there is a good chance to learn more about the relationship and application of solid state theory to catalysis. From previous work with the vapor decomposition of hydrogen peroxide, it is clear that there are certain features of this reaction which make it

particularly attractive for such a study. The vapor phase decomposition of hydrogen peroxide vapor has been shown to be completely heterogeneous at temperatures below 400°C (129). The decomposition is characterized by: (a) being highly irreversible, (b) having no side reactions, (c) having all the reaction occurring at the catalytic surface, (d) possessing kinetics sensitive to small changes in surface treatment, (e) exhibiting a rapid surface reaction (125). These properties are ideal for the study of catalysis on semiconductor surfaces. Industrial interests in the slow oxidation of hydrocarbons have stimulated studies of the decomposition of hydrogen peroxide on various surfaces including transition metal oxides (51, 94, 101, 144). Also electrochemical studies connected with fuel cell development have been interested in the nickel oxide-hydrogen peroxide system (80).

CHAPTER II

PREVIOUS INVESTIGATIONS

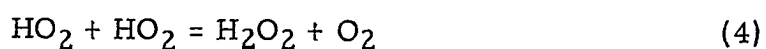
A. Hydrogen Peroxide Vapor Decomposition

Interest in the decomposition of hydrogen peroxide goes back to L. J. Thenard in 1818. Progress in understanding the mechanism has been slow and basic questions remain unanswered. The majority of the reported studies are with aqueous solutions, that is, in the liquid phase. Not until relatively recently has the vapor phase reaction been investigated. A review of these studies up to 1955 has been given by Schumb (129). The earliest studies measured the decomposition on glass and various metals at temperatures of less than 100°C . Results indicated a first order reaction. Later (53, 92, 95) the reaction on pyrex and quartz walls using temperatures up to 540°C was considered. The most recent work has been to a large extent under the influence of P. A. Giguere in Canada, C. N. Satterfield in the United States, and independently by A. B. Hart and A. D. Walsh in Scotland.

Giguere's group has been interested primarily in the thermal decomposition of hydrogen peroxide vapor, i. e., the homogeneous

mechanism above 400°C (4, 39, 40). Since these authors were primarily interested in the homogeneous reaction their study of the heterogeneous reaction has been to find suitable surfaces on which the homogeneous effects could be isolated. Soft glass, Pyrex, quartz and metallized surfaces were investigated. Apparent activation energies of between 13.4 and 19 kcal/mole in the range 0 to 140°C were reported on these surfaces although the rate varied by 15 from surface to surface. This difference was related to variation in adsorbed molecules. In the range between 140 to 200°C the reaction was found to be very rapid with a negligible temperature coefficient. The hydrogen peroxide molecule was visualized as oriented with the weak O - O bond strained so that any low thermal action could break the bond. No compensation effect was observed. It was concluded that all surfaces decompose hydrogen peroxide vapor at moderate temperatures. For the truly elementary homogeneous reaction the activation energy should be 52 kcal/mole, the energy associated with breaking the O - O bond. The homogeneous activation energy found was 48 kcal/mole.

Low temperature, static experiments (39) indicated the following non-chain mechanism for the homogeneous reaction.





This was based not only on pressure changes but also auxiliary information from spectroscopy, mass spectrometry, and electrical discharge work. These same conclusions are supported by Yeung (162).

C. N. Satterfield's group at Massachusetts Institute of Technology has added extensively to the understanding of heat and mass transfer effects associated with the vapor phase decomposition. Satterfield and Stein (126) determined the rate of decomposition as a function of temperature and composition on borosilicate, boric oxide and aluminum surfaces. Assuming the reactants are adsorbed in a monolayer on active sites where the reaction proceeds, the following equation gave the best fit of 15 equations tested.

$$r = \frac{K_{\text{H}_2\text{O}_2} P_{\text{H}_2\text{O}_2}^2}{(1 + K_{\text{H}_2\text{O}_2} P_{\text{H}_2\text{O}_2} + K_{\text{H}_2\text{O}} P_{\text{H}_2\text{O}})^n} \quad (7)$$

where r = rate of decomposition of hydrogen peroxide vapor

K = adsorption-equilibrium constants for subscripted component

P = partial pressure of subscripted component

n = constant having the value 1, 2 or 3

Hydrogen peroxide is visualized to be adsorbed on two adjacent sites and dissociating to form two adsorbed OH radicals. The remaining steps are visualized using equations (2) through (5). The active site may be assumed to be an electron donor site. Stein reports that this mechanism is also

consistent with the steps proposed for homogeneous and heterogeneous catalytic decomposition of the liquid.

Harris's (53) study of this reaction is related to the fact that hydrogen peroxide has been observed in the product gas of the slow combustion of hydrocarbons. Professor A. D. Walsh and colleagues (23, 65, 156) have similarly become involved with hydrogen peroxide vapor decomposition in their work with the slow oxidation of various fuels. Aside from obtaining a better understanding of various surfaces with respect to vapor decomposition, a non-chain Lindeman mechanism originally proposed for the homogeneous reaction (equations 2-6) explained certain discrepancies of other studies. The first step is written,



where M can be either H_2O_2 , H_2O , CO_2 , N_2 , O_2 , or He. The rate decreases in this same order. By keeping M large first order reaction behavior is observed. In the range between 241 - 420°C the reaction was found to be first order since the time for one half of the peroxide to react was independent of concentration.

The complete details of their interesting study are unpublished. They found it convenient to classify three types of surfaces. The first, category 1 surfaces, preserved hydrogen peroxide. Included were acidic surfaces such as new or HF-rinsed quartz and Pyrex, boric acid, phosphoric acid, and acidic oxides such as GeO_2 and TiO_2 . Category 2

surfaces included metallic oxides and salts. Reactions on Category 2 surfaces were not diffusion controlled. In the third category the surface adsorbed and destroyed hydrogen peroxide extremely rapidly, and the overall reaction was therefore diffusion limited. Silver and other noble metals are examples of this latter class.

These kinetic studies have shed light on the phenomena, but they leave much to be desired. The interaction of the catalyst and reactants is only observed indirectly and there is little hope of improving things relying only on a kinetic approach. The value of using concepts developed in the general electron theory of catalysis mentioned in section 1A in elucidating the mechanisms is evident.

The first to apply these ideas to hydrogen peroxide vapor decomposition was Hart and Ross (55, 54, 118). Their papers, published several years after the original work (119), are of value in drawing some conclusions about the chemical or electronic nature of the catalyst and its activity. The first published paper (54) reports that decomposition on sintered mixed oxides steadily increases with temperature from 38 to 100°C. A higher catalyst annealing temperature also increases the catalytic decomposition; however, annealing above about 600°C results in less activity. A decrease in the magnetic susceptibility after exposure to hydrogen peroxide vapor was related to a change in the oxidation state of the surface. In this study the equimolar mixtures were of Mn_2O_3 and PbO , ZnO , NiO , or CuO and Fe_2O_3 .

The decomposition on oxide surfaces in the form of vacuum deposited metal films, metal slips and compressed slips of bulk oxide was measured using a flow reactor (55). At a given temperature the oxide producing the largest amount of decomposition was considered to be most active. When this could not be used as a criteria the catalyst with the smallest activation energy was considered most active. In this manner the following activity series was obtained.

Mn_2O_3 is more active than $PbO > Ag_2O > CoO/Co_2O_3 > Cu_2O > NiO$
(green) $> CuO > Fe_2O_3 > CdO > ZnO = SnO_2 > glass$ (pyrex).

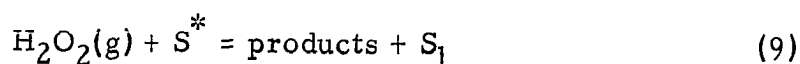
In other words, the P-type oxides were the most active followed by the N-type and then the insulators based on the bulk type of semiconductivity. These data were obtained using sintered compacts and oxidized metal films.

Hart, McFadyen and Ross then considered the implication of their work as it related to possible mechanisms. The "active site" was identified as a position where electron exchange is favorable, such as,

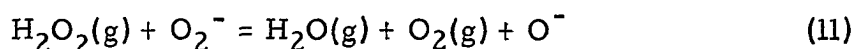
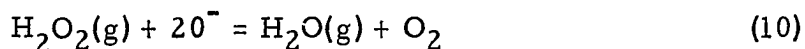
(a) an excess electron trapped at the surface, i. e., a vacant anion, or an impurity,

(b) a hole held at the surface by cation vacancy.

The proposed rate controlling process is formulated as,



where S^* may be O^- , O^{2-} , HO^- , a metal ion, or a species from H_2O_2 , e.g., HO_2^- . S^* is an active surface site and S_1 is able to return to S^* in a step which is not rate controlling. They attributed a fast disturbance of surface equilibrium when a sudden change in the concentration of H_2O_2 occurred as due to the disturbance of (S^*). At low temperatures the surface may take part in a simple cycle transfer of electrons between the oxide and the H_2O_2 where either of the following are controlling:



Based on equation (9), one can write a rate expression.

$$r = \bar{P}_{H_2O_2} \cdot (S^*)$$

where r = rate of decomposition

(S^*) = surface activity of species S^*

$\bar{P}_{H_2O_2}$ = partial pressure of hydrogen peroxide

These authors believed the key to the mechanism is connected with the change in (S^*) when a sudden change is made in the concentration of H_2O_2 , disturbing the surface equilibrium.

In their final paper (118), decomposition on compressed sintered samples of pure and doped NiO in three forms is reported. The P-type oxide (doped with Li_2O) was more active than the N-type form (doped with Ga_2O_3). This is the same trend shown by the bulk activity pattern.

Also at 100°C an activity pattern was reported to be, nonstoichiometric NiO > stoichiometric NiO > Ni/NiO (119).

In these three papers the purpose was to relate changes of catalytic activity due to changes in the partial pressures and the temperature (kinetic variables) to the known transport properties of the solid films (bulk semiconductivity).

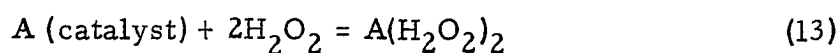
The rate equation used to describe all their data was,

$$r = k (\bar{P}_{\text{H}_2\text{O}_2}) (\bar{P}_{\text{O}_2})^{1/8} (\bar{P}_{\text{H}_2\text{O}})^{-1/2} \quad (12)$$

where the terms have the same meaning as before. The temperature range covered was 38°C to 135°C and the partial pressure of hydrogen peroxide varied from 0.32 to 9.96 mm of Hg. The temperature coefficient on a nickel-flashed film was determined to be 11.0 ± 0.5 kcal per g-mole in the temperature range of 60°C to 160°C. A compensation effect was noted (119).

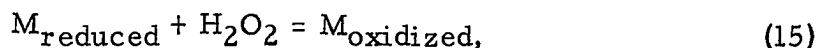
1. Related Studies in the Liquid Phase

Several authors (126, 85) have indicated a connection between catalysis in the vapor and liquid. Some related studies of liquid phase decomposition will now be mentioned. Baxendale (11) indicates the development of two theories. The intermediate product theory is expressed by

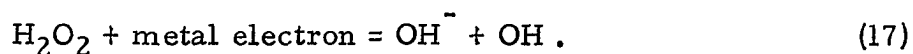


where an unstable peroxidic compound is assumed to decompose on catalyst A as indicated.

The other theory is based on the assumption that a catalyst, M, can exist in at least two oxidation states. Since hydrogen peroxide can act as both an oxidation and a reducing agent, it is possible to write,



Schumb (129) cites J. Weiss as the first to indicate an electron transfer between heterogeneous catalyst and substrate by proposing the rate controlling step in the decomposition to be,



Studies of the catalytic effect of nickel oxide on hydrogen peroxide in the liquid phase are limited. The studies prior to 1955 indicate that nickel exerts virtually no catalytic effect in acid solution. Acid treatment of nickel oxide deposited on nickel depressed the activity for surface decomposition (80). In basic solution nickel hydroxide has only mild activity. One active form appears to be the nickel oxide-silica gel mixture (129).

A recent study of the decomposition on lithium and chromium-doped nickel oxide (93) showed that the rate of decomposition was proportional to the pH of the solution, being a maximum at pH 12-13. The activation energy is lower for a higher electron hole concentration in nickel oxide. The change in work function determined by contact potential

with respect to platinum has been correlated with the activity (taken as the specific rate constant) in the decomposition of 0.25 molar hydrogen peroxide (164). The conclusions from this study were that the Fermi level near the surface controls the rate of reaction, a lowering of the Fermi level is reflected by a rise in the work function and a lowering of the activity. Donor type molecules are adsorbed on nickel oxide.

In recent years the liquid phase decomposition has been used to characterize activity on several different types of catalysts. The assumption made in these studies is that a first order process is occurring (28, 29, 71, 73, 76, 146, 147, 163, 164).

B. Electronic Characterization of Nickel Oxide

1. Conduction Model

The carrier transport properties of NiO are characterized by the electrical properties of the solid. Since catalysis and chemisorption are surface phenomena a connection with the electrical properties of the surface is expected. Many have been active in directing research to increase the understanding of transition metal oxide properties. The interest is reflected in the informal proceedings of the 1965 Buhl Conference (127) attended by two hundred scientists gathered from all over the world to discuss the transport and magnetic properties of transition metal compounds with particular emphasis on NiO.

The present ideas on the conduction mechanism start with the work of de Boer and Verwey (27), who developed a theory to explain the

fact that nickel oxide is an insulator when stoichiometric. Assuming d-electrons are localized at metal ions, conduction could take place if ions of the same element, but of different valency, existed on crystallographically equivalent lattice points, and if there is a temperature high enough to overcome the high energy barrier. Conduction could also take place if imperfections are present; created by: non-stoichiometry, selected impurities, grain boundaries, heat treatment and plastic deformation (145). The contributions of Mott (102), Morin (99), Yamashita (161), Heikes (61, 62), and Van Houten (150) are the foundations of current progress. The need for more experiments on well defined samples to clear up contradiction between experimental results and their interpretation is recognized as a necessity (151). The experimental results available in the literature are largely obtained with nickel oxide that is non-stoichiometric or doped with lithium. The non-stoichiometric results from the literature are compared in Figure 2.1.

The energy-level model of the transition metal oxides is unique in that the energy bands important for semiconductivity are related to inner electronic bands of the atoms in the structure. A filled and empty band originates from the 2p anion levels and the 4s cation levels, respectively, as in zinc oxide. The 3d levels of the cations are only partially filled. In nickel oxide the overlap of the wave functions of the 3d electrons is considered so small that a 3d band does not exist. The 3d electrons are localized on individual ions and can move from one ion to the

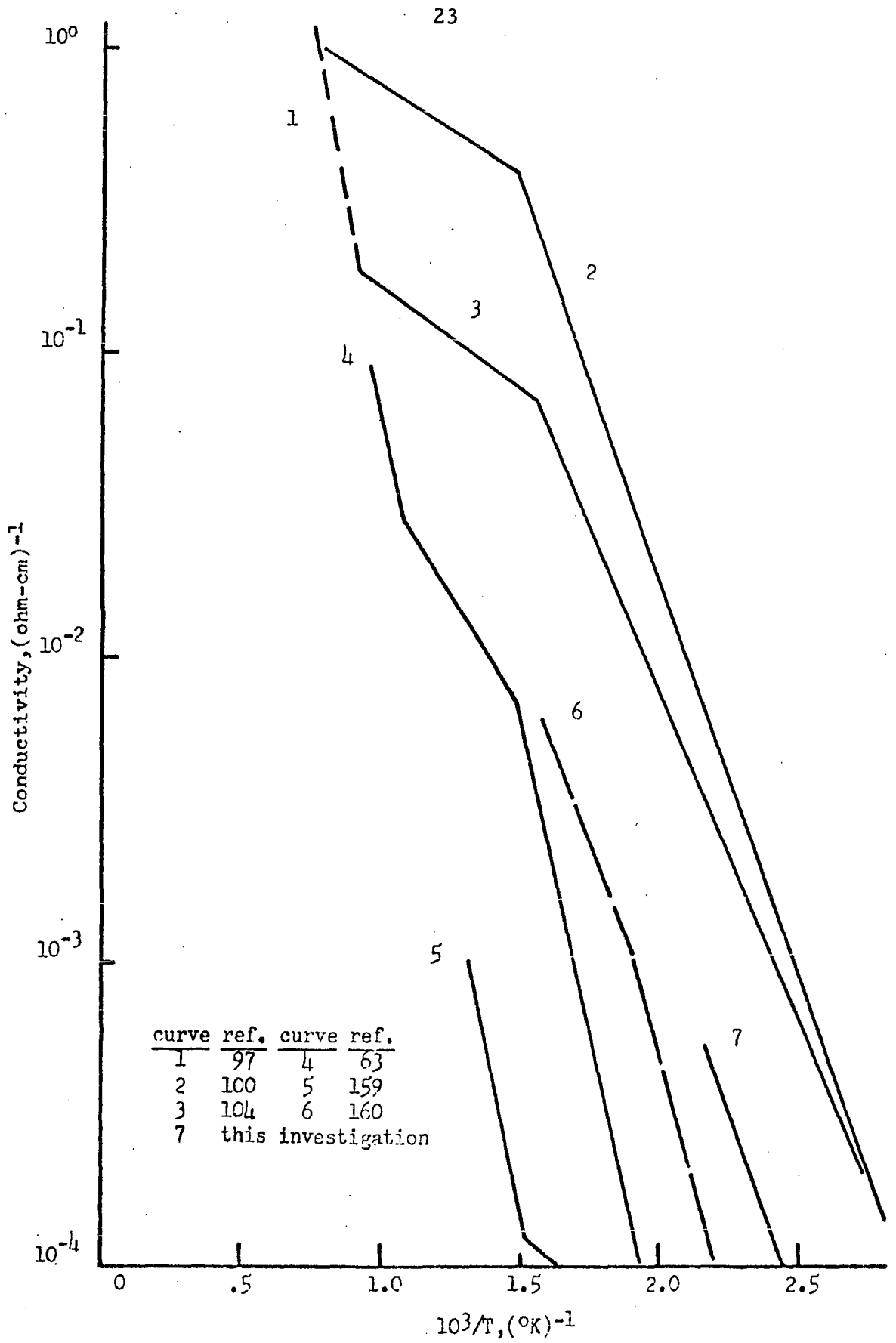


Figure 2.1. Temperature Dependence of Conductivity for NiO.

next by a sort of hopping or diffusion process.

In ordinary semiconductors the activation energy is considered to be the energy required to excite an electron into the conduction band. With an impurity concentration of 10^{-6} to 10^{-4} cm^{-3} , degeneracy results and the conductivity becomes metallic in nature. In lithium doped nickel oxide no such results have been obtained. Van Houten (150) visualized the extra positive charge carriers associated with lithium impurities or nickel vacancies as attracted to that site because it has an effective negative charge. The activation energy for charge transfer is thus a combination of an energy to loosen the carrier and to transfer it once freed. The transport energy is required due to self trapping caused by an induced lattice polarization field that is associated with a long residence time. To explain the mobility activation factor the Mott-Gurney hopping mechanism (103) is used.

Both Morin (99) and Van Houten (150) have given useful energy level diagrams. Yamashita (161) calculated the order of magnitude of the d-band width by an approximate quantum mechanical treatment. The results showed the 3d band width is 0.1 electron volts.

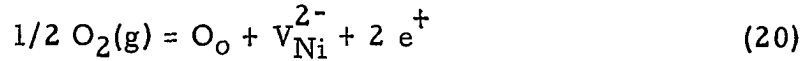
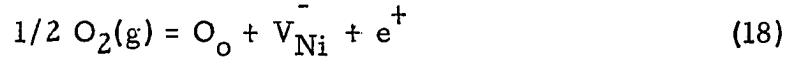
Boreshov (16) among others (43, 59, 153) has suggested that one of the primary reasons for the failure of the extended theory of catalysis on semiconductors is the fact that the oxide semiconductor, e.g., NiO, may not follow the simple band theory of solids. This is based on the fact the 3d levels of the first row transition elements are only

partially filled and one would expect, therefore, metallic conduction in the ionic oxide crystals. Such oxides as Cr_2O_3 , Mn_2O_3 , NiO , CoO , and CuO have insulating properties. To explain this it has been suggested that if the overlap of the wave functions of the 3d electrons is very small, the band formed is very narrow or nonexistent. The typical band conduction model breaks down. Several Soviet scientists argue that in nickel oxide carriers probably move in a narrow band (82, 165). Even if there is no band conduction, a recent study has confirmed that if nondegenerate, the single band statistics can be used with NiO . In the case of a depletion space charge, a Mott-Schottky approximation was applied. A space charge region due to exhaustion of holes near the surface was observed (121). For a degenerate semiconductor the Boltzman distribution does not apply and no density of states function is known for hole-hopping conductors. In this case the dependence of the space charge curvature with the applied potential cannot be derived.

Hubbard (68) is developing a theory to relate the various properties of solids following the band theory type conduction and those having hopping conduction. A pseudo particle density of states function with a variable atomic separation in crystalline array is used in the treatment. The main contribution of theory has been its descriptive and sometimes qualitatively correct model. When successful it has given insight into the nature of catalysis and given new direction to experiments.

2. Defect State

The lattice defect state characterizing non-stoichiometric NiO has been represented by a cation vacancy and hole in the valence band. Using the notation of Swalin (138) the interaction of oxygen with the nickel oxide is represented by the following set of equations.



where O_o = oxygen ion on an oxygen lattice site,

V_{Ni} = nickel vacancy having an effective charge of 1

V_{Ni}^{2-} = nickel vacancy having an effective charge of 2

e^+ = hole in the Ni²⁺ (ed⁸) levels

Since there is no widely accepted notation used in thermodynamics of defects the above equations have appeared in a variety of equivalent forms. With nickel oxide the hole or carrier is most often symbolized by Ni³⁺ while the nickel vacancy by Ni□. For further details on notation refer to Kroger and Vink (81).

Equations (18) and (20) have both been used in the literature to derive the dependency of conductivity, σ , upon the partial pressure of oxygen, \bar{P}_{O_2} , in the surrounding atmosphere at equilibrium. It can be shown that,

for singly ionized vacancy,

$$\sigma \propto \bar{P}_{O_2}^{1/4};$$

for doubly ionized vacancy,

$$\sigma \propto \bar{P}_{O_2}^{1/6}.$$

Hauffe (60) indicates that at temperatures above 1000°C reaction (19) becomes noticeable, yielding as the overall equation (20) with oxygen pressure dependence of $1/6$. This is based on Mitoff's results (97). Choi and Moore (22) suggest that Mitoff's data are in better accord with equation (18). Eror (36) found that in the temperature range of 800° to 1200°C equation (18) and the corresponding $1/4$ power dependence are observed.

In the first study relating conductivity to defect structure, Van Baumbach and Wagner (10) established a $1/4$ power dependence in the range between 800° and 1000°C . Hauffe (60) indicates that from 600° to 1000°C with oxygen partial pressures of between 10^{-4} to 1 atmosphere, the dependence is between $1/4$ and $1/4.5$.

The principles making it possible to correlate conduction with stoichiometry and impurity content are well accepted (67). Mitoff's work has been useful in the quantitative determination of defect concentration. The treatment is based on the hopping conduction model of Heikes and Johnson (62). They assumed charge carriers were not free to move through the lattice without additional energy. The carrier remains on a site for a time greater than the vibrational frequency of the

lattice. The work to overcome the potential barrier is the activation energy ΔG . For electron-transfer materials this corresponds to the free energy of activation, rather than energy gaps, as would be the case in standard semiconductors (67). The fraction of carriers above this energy for the nondegenerate semiconductor is $\exp(-\Delta G/kT)$ where k is the Boltzman constant and T the absolute temperature. By considering two parallel crystal planes the perpendicular flux of carriers is obtained by multiplying the above by the probability a jump will occur. The resulting equation resembles the diffusion equation and, by analogy, the Einstein equation relating diffusivity and mobility, μ , can be used to obtain an expression for carrier mobility. It is assumed that the conductivity, σ , which is the inverse of resistivity, ρ , can be written,

$$\sigma = \frac{1}{\rho} = e\mu(\text{Ni}^{3+}) \quad (21)$$

The temperature dependence of the conductivity is proportional to the product $T^{-1} \exp(-\Delta G/kT)$. The relative effect of the T^{-1} is small and is usually neglected (67, 150). Mitoff (97) has derived a useful equation for the electrical conductivity from the above concepts by replacing the free energy of activation with an enthalpy of activation and accounting for the entropy by either an experimentally determined constant or an assumed constant. The electrical conductivity is then given by,

$$\sigma = C'(\text{Ni}^{3+}) \exp\left(-\frac{\Delta H_{\oplus}^*}{RT}\right) \quad (22)$$

where C^I = constant including the jump frequency and entropy term,
 ΔH_{\oplus}^* = activation enthalpy for carrier jump.

At temperatures above which equilibrium is established, the concentration of nickel vacancies is related by (20) to the number of carriers, and is given by,

$$Ni = C^{III} \bar{P}_{O_2}^{1/6} \exp(-\Delta H_f^0/3RT) \quad (23)$$

where C^{III} = constant,

ΔH_f^0 = enthalpy of formation for the equilibrium reaction.

Substituting this expression into equation (22), noting that $(Ni^{3+}) = 2(Ni\Box)$ gives,

$$\sigma = C^I \bar{P}_{O_2} \exp\left(-\frac{\Delta H_f^0}{3RT} - \frac{\Delta H_{\oplus}^*}{RT}\right) \quad (24)$$

Relating the conductivity to the defect structure under equilibrium conditions, Mitoff found; $H_f^0 = 53,400$ cal/g-mole, $H_{\oplus}^* = 5500$ cal/g-mole, $C^{III} = 0.11$ g-mole, where \bar{P}_{O_2} is expressed in atmospheres and the vacancy concentration is expressed as vacancies per ion pair. On the basis of the interrelationship between the conduction regions it is possible to relate quantitatively the defect concentration to the parameters of the low temperature conductivity curve. See Appendix A.

3. Electrical Conductivity

In discussing the previous electrical conductivity studies with nickel oxide it is convenient to present the results graphically in Figure 2.1.

Because of the large number of studies only representative curves from the various studies are shown. Three definite regions can be recognized and each corresponds to a different mechanism of electrical conduction. Each of these conductivity regions will now be discussed separately.

a. Equilibrium region. Mitoff's paper (97) shows that above 1050°C single crystal nickel oxide maintains equilibrium with the surrounding atmosphere with heating and cooling rates as high as 125°C per hour. Below this temperature the crystal cannot maintain equilibrium if the cooling rate is too high. This can be seen by looking at Figure 2.1. The change in slope from that of the dotted line indicates that the cooling rate is too rapid to maintain equilibrium. Mitoff observed that below 900°C equilibrium is not maintained even at cooling rates as low as 2°C per hour. It is interesting to note that several polycrystalline samples fall on the extrapolated equilibrium line at much lower temperature than do single crystals. The slope of this line is 0.772 eV/g-mole .

b. Intermediate region. Below 1050°C a given defect concentration can be 'frozen in' by selecting various cooling rates such as 161°C per hour. This causes a bend in the conductivity versus reciprocal absolute temperature curve. The slope of this portion of the curve is 0.24 eV/g-mole and it seems to be independent of cooling rate. Theory suggests that it corresponds to the average activation energy for conduction. It is assumed in this region that the concentration of defects remains constant; that is, cooling is so rapid that chemical equilibrium is not

maintained and the surrounding gas has no effect on the defect concentration. Eror (36) has found that this activation energy is a function of the partial pressure of oxygen at the time the crystal was in the equilibrium region. Eror's slope of 0.29 eV agrees closely with the polycrystalline samples of Herbst (63) and the single crystal work of Yamaka (160), while Morin's (100) and Thorton's (145) single crystal data, as well as Nachman's (104) polycrystalline data, are in agreement with Mitoff.

c. Low temperature region. In lowering the temperature to near the crystallographic Néel point (37, 78) another bend occurs, although sometimes it is not observed with polycrystalline samples (160).

The exact temperature at which this transition occurs is independent of the defect concentration (104). Van Houten (150) observed a variation in the transition temperature with sintered pure nickel oxide from 198 to 308°C. Small variations in the heat treatment were suggested as the cause. Wright and Andrews (159) observed a low temperature transition between 315° and 376°C. Two other values, 341°C (104) and 393°C (63) have been reported with polycrystalline samples. Single crystal data is scarce in this region; however, the reported values of 485°C (145) and 394°C (100) are consistent with the polycrystalline results. Heikes (61) believes this phenomena is not related to the Néel point, as from the theory it is not expected to vary this much, but rather related to some impurity or property of nickel vacancies. A second

magnetic transition at temperatures somewhat below the Néel point have been discussed by Cimino et. al., (24) but the relation is not clear. It is evident that the slope in this region varies from sample to sample (from 0.22 to 0.69 eV/g-mole). Hogarth (66) showed that the activation energy for conduction between 111°C and 393°C increased as the logarithm of oxygen pressure. Nachman (104) has suggested that this activation energy corresponds to conduction by thermally activated hopping. Snowden and Saltsburg (134) have verified that room temperature conduction is indeed by the hopping processes. Heikes (61) found the temperature dependence faster than predicted by hopping alone and postulates a magnetic contribution.

d. Low temperature conductivity with lithium impurities. Because the low temperature conduction mechanism is similar to that of lithium doped nickel oxide (104) a brief description of some low temperature results are given. Aliyama reported (77) that the Néel temperature decreases as lithium is added to NiO. In attempting to shed more light on the conduction mechanism of nickel oxide, Koide (77) made extensive resistivity measurements on lithium doped NiO single crystals in the range of 25°C to 743°C. A low temperature transition similar to the above was observed to take place near the Néel point. The transition temperature decreased with the decrease of the impurity content. The activation energies he found, denoted by E_1 above the transition temperature and E_2 below, are given below.

<u>Lithium Content,</u> <u>mole%</u>	<u>E_1, eV</u>	<u>E_2, eV</u>	<u>$E_2 - E_1$, eV</u>
0.0	0.667	0.910	.243
0.93	0.234	0.344	.110
1.36	0.143	0.237	.094

$E_2 - E_1$ is governed by the change in difference of the energy of self-trapped state and the activated state. Both $E_2 - E_1$ and the Néel point decrease with the addition of lithium up to 0.025%. The transition temperature coincides with the Néel point. E_2 is related to antiferromagnetic ordering.

e. Surface or boundary conductivity. Nachman (104) found the values of carrier concentration calculated using conductivity and Seebeck results and those found by chemical analysis did not agree. To explain this, grain boundary conduction is suggested, that is, if nickel oxide is prepared at not too high a temperature, the current carriers, Ni^{3+} , are distributed in a thin layer at the surface of the grains. The mean electrical conductivity is then determined by equation (21) using the mobility in the surface layer, and the concentration averaged over the whole grain. Also, if the internal domain has only a few carriers, for example, if chemisorbed oxygen has not diffused too far into the bulk, the experimentally determined Seebeck coefficient represents the surface layer.

Thornton (145) has studied the relation between single crystal and polycrystalline electrical conductivity, concluding: polycrystalline

conductance is higher than in a single crystal, conductivity of the boundary is considerably higher than bulk, and the same mechanism controlling bulk conduction controls conduction in grain boundary regions.

4. Electrical Conductivity and Chemisorption

Bielanski (13) suggests electrical conductivity can be used to characterize a semiconductor catalyst two ways. The first uses the initial conductivity shown by a catalyst before coming into contact with the reactants while the second approach relates the activity and the changes in the conductivity during the reaction.

One of the first to explore these ideas in a systematic approach was T. J. Gray (42). The change in electrical conductivity during adsorption and desorption of oxygen on nickel oxide as well as the change during the oxidation of CO were measured. The assumption was that the measured electrical conductivity change was only due to a change in the surface conductivity which in turn could be related directly to the number of carriers transferred in the process of chemisorption. Unfortunately, this neat formalism did not prove as useful as anticipated.

Although many studies have been performed studying conductivity changes during adsorption and catalysis (Table 2.1), most of the work has been performed on powders which are not well defined, this limits the usefulness of the results, as pointed out previously.

It should be pointed out that classical adsorption studies have

also been reported with nickel oxide using monometric techniques (72, 21, 30, 46, 70, 79, 83).

TABLE 2.1
SIMULTANEOUS ADSORPTION - CONDUCTIVITY STUDIES
ON POLYCRYSTALLINE NICKEL OXIDE

Gas Adsorbed	Reference	Gas Adsorbed	Reference
O ₂	10, 42, 75, 84, 124*	acetone	13
cyclohexane	75	H ₂	10, 13, 42
n-hexene-1	75	N ₂ O	84
H ₂ O	13	CH ₆	75
isopropanol	13	CO	10, 13, 42, 75
CO ₂	13, 75		

*Single crystal NiO used.

5. Electrical Conductivity and Catalysis

Only a limited number of studies have been made in which an attempt was made to use electrical conductivity to help characterize the solid state during chemical reaction. Recent studies using sintered catalysts are mentioned below.

a. Nitrous oxide decomposition. Nitrous oxide decomposition has been studied more than any other reaction on nickel oxide. Kuchynka (83) concluded from adsorption measurements along with electrical

conductivity change: that the character of nitrous oxide bonding on nickel oxide changes with temperature, the selectivity is connected to the chemical character of the N_2O - oxide bond, chemisorption is not accompanied by charge transfer, and the rate limiting step is connected with the formation of gaseous oxygen.

b. Oxidation of carbon monoxide (25). This standard reaction of catalytic research has been studied on nickel oxide using electrical conductivity and kinetic techniques. Two extremes are revealed: the surface saturated with chemisorbed oxygen which promotes oxidation, and a surface saturated with carbon monoxide (13). The authors indicate that the results confirm the value of conductivity measurements for catalytic research, if applied with kinetic data, since changes in conductivity are a sensitive indication of surface changes.

c. Formic acid decomposition (9). The electrical and kinetic properties of the nickel oxide-chromic oxide-formic acid system were studied over a range of temperatures. Initial reaction rates were used to characterize the kinetics, and an Arrhenius type temperature coefficient was found to characterize the electrical properties. Sintered materials ignited below $700^{\circ}C$ were reduced partially to metallic nickel by the formic acid. With nickel oxide it was shown that the activation energy for the decomposition of formic acid decreases as the electron hole concentration increases.

Until the present time no work has been reported in which

catalysis has been carried out on well-defined nickel oxide single crystals in which the solid state character was defined in terms of parameters related to the electrical conductivity.

6. Seebeck Coefficient

The Seebeck coefficient, θ , is also useful in characterizing the electronic state of single crystals. This property of the solid state is measured by applying a temperature difference, ΔT , across a sample and measuring the EMF generated, ΔE . The coefficient is defined as,

$$\theta = \frac{\Delta E}{\Delta T} \quad (25)$$

The coefficient is related to the Fermi level through the equation,

$$\pi = \theta T = E_f + A \quad (26)$$

where A = scattering parameter, a constant,

T = absolute temperature,

E_f = Fermi level with respect to the filled $\text{Ni}^{2+} (3d^8)$,

π = Peltier coefficient.

Some authors (104) have assumed the constant A to be negligible in the particular temperature range of interest here.

In studies with polycrystalline nickel oxide samples it has been found that the value of the Seebeck coefficient on a given crystal does not vary much with temperature and thus investigators (99, 104, 109, 150) found that the product θT , which is proportional to the Fermi level, increased slightly with temperature. On the other hand the magnitude of

the coefficient varied greatly from study to study due apparently to differences in impurity concentration. For example, with polycrystalline non-stoichiometric NiO, Nachman (104) found that with an excess oxygen concentration of 0.2×10^{-4} atoms per NiO molecule the coefficient was about $700 \mu v/^{\circ}K$, while at 9.7×10^{-4} the value was about $100 \mu v/^{\circ}K$. Van Houten also found that as the excess oxygen increased the Seebeck coefficient decreased; here, however, lithium impurity was being added (150). At equilibrium it has been reported (159),

$$\theta = -\frac{k}{en} \log P_{O_2} \pm \text{constant} \quad (27)$$

where P_{O_2} = pressure of oxygen,

$n = 5$ to 6.3 ,

k = Boltzman constant,

e = electronic charge.

Parravano (110), in a study with polycrystalline NiO, found that in the presence of various gases the unsteady state change of the Seebeck coefficient was of value in interpreting adsorption studies. For example, with NiO at $115^{\circ}C$ and an oxygen pressure of 4.05×10^{-1} mm. Hg. the value of θ dropped from $595 \mu v/^{\circ}C$ to about $547 \mu v/^{\circ}C$ in about 100 minutes. A relation was derived between the observed change in the Seebeck coefficient and the positive hole concentration:

$$\frac{N_c}{N_o} = \exp \left[-\left[\frac{\theta_c - \theta_o}{k} \right] \right] \quad (28)$$

where N corresponds to the carrier concentration and the subscripts "o" and "c" represent the values of the indicated parameter before and after chemisorption, respectively.

Finally, several authors (32, 52, 166) have indicated the value of using a point contact at constant temperature on a crystal at room temperature to give a qualitative idea of crystalline heterogeneity. A series of recent papers has applied this principle to obtain quantitative values of the distribution of the Seebeck coefficient over the surface of the crystal with germanium and polycrystalline CuO (8,163).

CHAPTER III

EXPERIMENTAL APPARATUS AND PROCEDURES

A. Preparation of the NiO Crystals

Five nickel oxide single crystals were purchased from the Fuji Titanium Industry Co., Ltd., Osaka, Japan through their representatives, Marubeni-Iida Co., Ltd., in Chicago, Illinois. These crystals were reported to be prepared from raw materials of the following purity: NiO 99.92 + %, Co 0.003%, and Fe 0.006%. A detailed analysis of representative single crystals is given in Appendix B. A description of the crystals is given in Table 3.1.

TABLE 3.1

DESCRIPTION OF THE NiO BOULES

Lot No.	Weight, grams	Diameter, mm	Length, mm
1519	8.5	5-8.5	22
1526	9.5	5-8	33
1525	10.5	4.6-8	33.5
1520	15	5-9	37
1305	22	5-10	40

These crystals were grown in an oxidizing atmosphere by Verneuil's flame fusion method (152).

1. Cleaving

In order to obtain a well defined crystal surface it was necessary to cleave the crystals. The first method tried began with a dip in liquid nitrogen until thermal equilibrium was obtained as indicated by the termination of vigorous boiling taking place on the crystal surface. A No. 8 Exacto blade was used to cleave the crystal held in place by clay. A small hammer provided the force required to cleave the crystal. Crystals smaller than 10.5 grams cleaved with no complications. In going to the larger crystals only the small tips gave a uniform cleavage plane.

Later in the work another technique similar to that of Hall (49) was found to give much better results with less waste, even with larger crystals. This technique made it possible to remove the edges of the crystal resulting in a sample with only (100) planes exposed. Crystals were obtained having widths of only one millimeter.

The Exacto cutting edge was placed on the corner of the crystal instead of parallel to an edge. A force was applied with the ball end of a ball peenhammer. In most cases only a light tap was required to affect the cleavage. All the time the crystal rested on high density alumina with extra pieces of alumina to contain the pieces created by the process.

The surface of the cleaved crystals was essentially smooth and flat on a macroscopic scale. Microscopic examination of the crystal indicated that the surface was not always simple. One of the more interesting surfaces is shown in Figure 3.1. Prior to this picture the crystal had been etched 7 minutes in boiling nitric acid. This is one of the catalysts in run 2/13. Etch pits are evident on the surface. These pits are more clearly defined than previously published (139). On some of the samples random cracks appeared on the surface. Patterns of lines were observed with reflected light on the crystal surface.

No documentation of these structures was made but they are similar to those found by Saito (123).

2. Orientation of Crystal

Crystal growth was in the $[100]$ direction and upon cleavage a (100) crystallographic plane was exposed. To verify the orientation of the NiO cleaved surfaces a sample was selected at random. The sample was mounted in plastic to ensure that the polishing would be as close to parallel to the cleavage plane as possible. A No. 320 AB carbimet wet paper was used until scratches appeared in the direction of polishing. No. 600 grit paper was then used in a direction perpendicular to the above. The sample was polished with Linde Abrasive with a Bueler polishing cloth. X-ray diffraction was performed using a Jarrel-Ash High Intensity Microfocus Unit with a Laue Reflection Camera. The (100) orientation of the cleaved surface was confirmed. In a similar

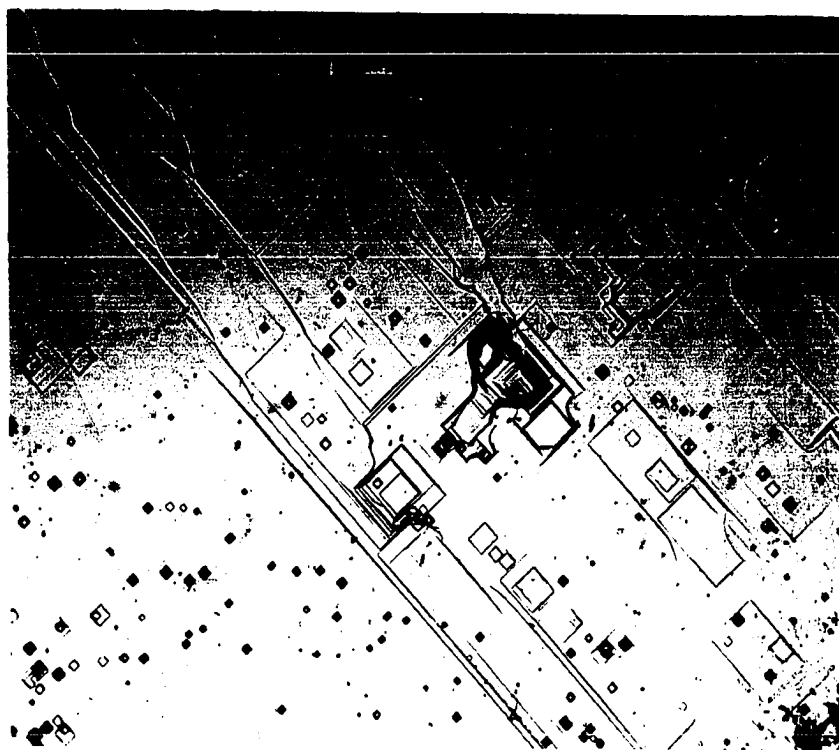


Figure 3.1. Etch pits on cleavage surface of NiO from
Run 2/13. x 150.

manner a large crystal was mounted and X-rayed as received. Results indicated that the plane perpendicular to the axis of growth was the (100) plane.

Other orientations could be obtained by using various cutting machines (140), but this was not attempted. The chemical methods required to remove strains and damaged surface layers would introduce other effects which were avoided in the present work.

3. Pretreatment of the Crystals

As in other catalytic work it is necessary to control and specify the pretreatment as completely as possible. In selecting pretreatment conditions the object is to vary reproducibly both the catalytic and electrical properties of the NiO single crystals. The variables are partial pressure of oxygen in the surrounding atmosphere, the temperature and time of the heat treatment, and the cooling rate. It is necessary to anneal crystals made by the Verneuil method (22). The annealing usually has been similar to that used by Roth and Slack (120, 133). This treatment consists of heating crystals at temperatures ranging from 1450 to 1600° for a few hours in an argon atmosphere containing a small amount of oxygen and cooling slowly to room temperature. This procedure usually results in simple domain structure (123). Annealing in dry nitrogen for 40 hours between 1000 and 1470° C has also been used (22).

In view of the results reported in Chapter 2, one would expect a reproducible surface if the nickel oxide crystal was allowed to reach

chemical equilibrium with the surround atmosphere and then quenched the crystal. Two other possibilities, pulsing, with hydrogen above 400°C (124) and cleaving in vacuum (149), both in place techniques, were considered impractical for the present study. The treatments used are given in Table 3.2.

TABLE 3.2
PRETREATMENT CONDITIONS OF NiO CRYSTALS

Run	Crystal*	Temperature °C	Time, hours	Atmosphere mole% O ₂	Cooling Rate °C/hr.	Cooling Time minutes
1	9.5	1000	21	71.8	1286 500 221	9 24 38
2	9.5, 22	1000	20	50.2	same as 1	
3	8.5	1500	4	75.7	38	
5	same as 2					
6	same as 2					
7** 8** 9**	random combination of all crystals	920	29	air	2460	
10**	8.5	1400	10	34.5	1029	23
11**	same as 1					
12**	8.5	920	17	air	100	
13**	9.5	1400	15	100	same as 10	

* Identified by weight, see Table 3.1.

** Only 100 planes exposed.

In the pretreatment anneal above 920°C , an 1800 watt, Heraeus glowbar furnace was used. Temperature was controlled with a Foxboro potentiometric controller, model number 4043-40E, using a Pt-Pt 10% Rh thermocouple as the control element.

The samples were placed on high purity alumina boats furnished by the Research Instrument Co. of Norman, Oklahoma. These supported and protected the crystals from contamination during high temperature firing. A brilliant turquoise color was left by the crystal on the alumina at each point of contact, even at 920°C . This has been observed before (45).

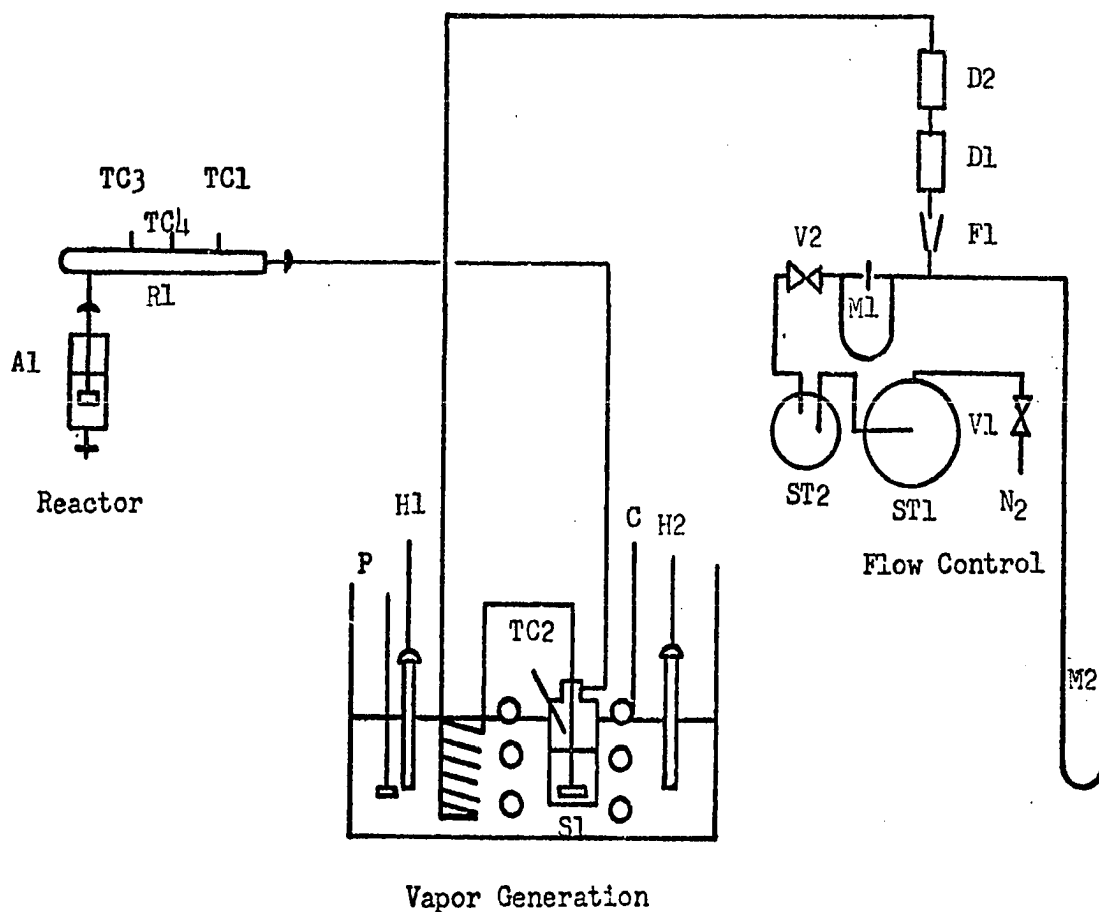
A Morganite Triangle H-5, 1-1/8" O. D., 7/8" I. D., mullite tube was used as the furnace tube allowing the desired atmosphere to be maintained. Although the manufacturer specified the maximum safe cooling rate to be 200°C per hour, for the conditions described the cooling rates reported in Table 3.2 were used without breakage. The atmosphere was controlled by passing helium and 99.72% oxygen through two separate Brooks rotometers from the cylinders, regulating each stream by means of the regulator needle valves. The helium was Grade A quality obtained from the U. S. Bureau of Mines. The oxygen was obtained from Big 3 Welding Supply Company. The gases were mixed prior to introduction into the furnace in a 500 cubic inch tank. The mixture passed into the furnace by a Vycor tube held in place with Carborundum Fiberfrax ceramic bulk fiber. The most rapid heating rates were

obtained by setting the powerstat at 25, 30 and 35 amps successively in 30 minute intervals. Cooling was obtained by shutting off the power completely, and either letting the entire system reach room temperature or pulling the mullite tube out of the furnace at 200°C.

The 920°C anneal took place in the 584 watt section of a 1750 watt Hevi-Duty multiple unit combustion furnace. In the 950° and 1000° pretreatments a Vycor combustion tube was used, limiting the maximum temperature but permitting rapid cooling rates. These rates were obtained by cutting the power and opening the upper half of the furnace after 30 seconds, exposing the tube to the surrounding atmosphere. Oxygen content in the furnace atmosphere was determined with a Beckman GC-2A chromatograph. A six foot column was packed with Linde 5A molecular sieve and operated at 40°C with a filament current of 65 milliamperes. Nitrogen gas was used as a carrier, hence both a helium peak and an oxygen peak were observed. The mole percent oxygen was calculated by peak height techniques. The values determined appear in Table 3.2.

B. Kinetic Apparatus

Isothermal study of the decomposition of hydrogen peroxide vapor was carried out in an apparatus similar to that of Hart and Ross (55, 119) and Satterfield and Yeung (125). Figure 3.2 is the system flow diagram.



- | | |
|-------------------------------|--------------------------|
| A1. absorber | P. stirrer |
| C. refrigeration coils | R1. glass reactor |
| D1, D2. carrier gas purifiers | S1. saturator |
| F1. Brooks rotometer tube | ST1, ST2. surge tanks |
| H1, H2. heaters | TC1-TC4. thermocouples |
| M1. capillary manometer | V1. regulator valve |
| M2. system manometer | V2. Nupro metering valve |

Figure 3.2. Flow Diagram of Kinetic Apparatus.

1. Raw Materials

The hydrogen peroxide used in this study was a 98% solution furnished by F. M. C. Corporation and a 50% solution provided by the Solvay Process Division of Allied Chemical Corporation. Both were used without further purification. Dry nitrogen from Big 3 Welding Supply Co. had an estimated purity of 99.7% and was the carrier.

Before the nitrogen gas contacted the hydrogen peroxide solution, it passed through two gas purification bulbs in series, D1 and D2 of Figure 3.2. D1 was filled with CaCl_2 and magnesium perchlorate, while D2 was filled with silica gel and soda lime. Each bulb had its ends plugged with Pyrex glass wool.

2. Flow Control

The flow rate of nitrogen into the system was controlled by V2, a Nypro fine metering valve, B4MA2. The back pressure of the system was fixed during all the runs, being set by the needle valve V1 on the pressure regulator. Originally the flow rate was monitored with a Brooks rotometer, F1, having either a 1A-15-1 tube with glass float or a 3-15-4 tube with stainless steel float. To reduce oscillation of the rotometer float at low flow, ST1 a 500 cubic inch tank, and ST2, a one liter flask with a capillary inlet, were used as surge tanks. More consistent results, however, could be obtained using a capillary manometer type flowmeter, M1. Calibration with a soap bubble flowmeter resulted

in a precision of ± 3 cc/minute at 200 cc/minute.

3. Cleaning the Glassware

Extreme care must be exercised to achieve the most inert borosilicate reactor. The glass to be used in constructing the reactor were thoroughly rinsed with deionized distilled water (See Appendix C) and then rinsed with reagent grade ethanol. After draining most of the ethanol, reagent grade nitric acid was carefully added. Care must be taken in this operation since an extremely violent reaction sometimes occurs. After the fumes had subsided, water was added and the pieces dried. The precleaned glassware was then ready to use in the construction of the reactor. After glass blowing and subsequent annealing, the same sequence was repeated with the exception of the initial water rinse. The final step consisted of only two water rinses.

The rest of the glassware in the system was rinsed with ethanol, water, and contacted with vapors of nitric acid carried in nitrogen followed by thorough rinsing with water. Since the temperature of these surfaces is always 24°C , negligible reaction takes place.

The interconnecting lines were made of borosilicate glass tubing. Tygon flexible plastic tubing having the formulation R-3604 A joined long lengths of glass tubing to various pieces of the apparatus. This tubing was furnished by U. S. Stoneware Co. Only borosilicate surfaces were in contact with the $\text{N}_2\text{-H}_2\text{O}_2$ stream once it left saturator

Sl. Absorber A-1 was lubricated with Fluorolube GR-544 furnished by the Hooker Chemical Company. The Fluorolube was tested and found to cause negligible decomposition at room temperature under the conditions used. This lubricant was also used in the ball and socket joint connecting the saturator and the reactor.

4. Vapor Generation

To reduce temperature variations within the reactor due to the highly exothermic reaction and to simplify the kinetic treatment, a low initial concentration of hydrogen peroxide vapor is desired. This was obtained by passing nitrogen bubbles through 40ml of hydrogen peroxide solution. These bubbles were generated by passing the gas through a fritted cylinder in a standard gas washing bottle. Previous studies have shown that near a saturation concentration can be obtained by using only one such bottle (119) using similar conditions. The concentration of the hydrogen peroxide in the vapor depends on both the concentration of the solution in Sl and its temperature. The concentration of the solution is not expected to change very much due to either distillation or decomposition (119), if the apparatus is clean. The temperature of the hydrogen peroxide solution was controlled by means of a water thermostat. The solution in Sl can be maintained either above or below room temperature.

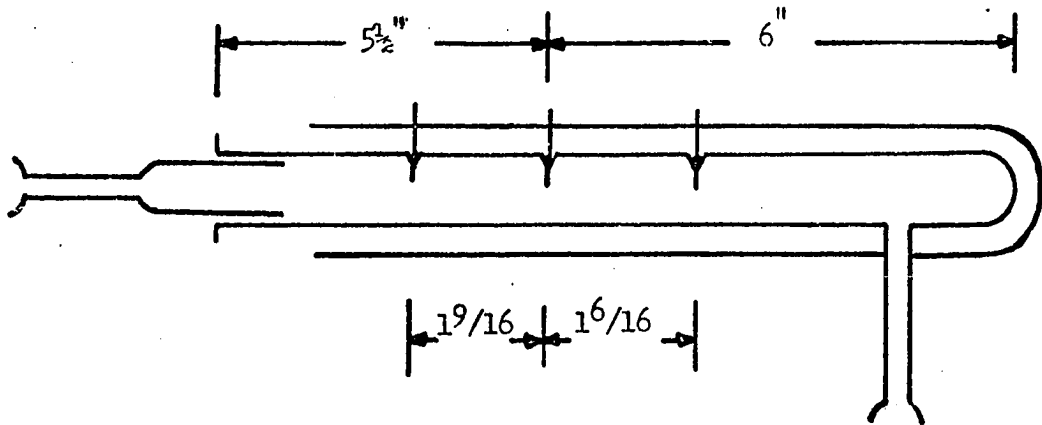
Two bath temperatures were used in the work reported here,

13.5°C and 24°C. Steady state operation of a Tecumseh-refrigeration unit, C, maintained the solution at a temperature of 13.5°C as measured by thermocouple TC2 and a mercury-in-glass thermometer in the water bath. The higher temperature was obtained by letting the water bath reach room temperature, which was maintained at a constant temperature of $24 \pm 1^\circ\text{C}$. In either case, the temperature variation was not detected with TC2, and from this it is assumed that the solution temperature was known $\pm .5^\circ\text{C}$.

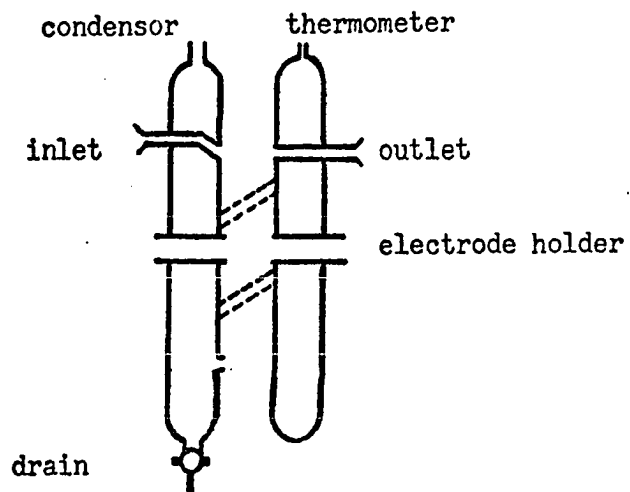
Intermediate temperatures could be obtained by using the refrigeration unit and knife heaters controlled with a precision thermostat.

5. Reactor

a. Tube reactor. The simple tube reactor shown in Figure 3.3a gave the most satisfactory kinetic results. Not until the utmost care was taken in the glass-blowing and handling of the glass were satisfactory results achieved. For further comments see the borosilicate treatment described in Appendix K. This reactor consisted of a $\text{T } 14/20$ outer fitting joined to a 12mm section of tubing closed at one end with a 3" long 5mm diameter sidearm at right angles to the larger tube's axis. A connector was designed so that the reactor could be removed easily from the rest of the system, and also for the addition or removal of catalyst. It consisted of a $\text{T } 12/5$ socket joint and $\text{T } 14/20$ inner glass



a. Tube Reactor



b. Fluid Jacket Reactor

Figure 3.3. Glass Reactors.

grinding. Three indentations were made for thermocouples. After wrapping one layer of asbestos paper over the glass, the tube was wrapped uniformly with nichrome wire. Several more layers of asbestos sheet were used to cover this wire. Iron constantan thermocouples were placed semi-permanently into the wells with the aid of Thermo-coat HT high temperature adhesive (Omega Engineering Company). The thermocouples were calibrated at one point against a reference thermocouple as outlined in Appendix D. A slight temperature gradient existed over this reactor tube during operation as shown below.

<u>Powerstat setting volts</u>	<u>TC1, °C</u>	<u>TC4, °C</u>	<u>TC3, °C</u>
10 v	63	66	64
16	121	127	124
18	134	141	138
20	166	175	170
22	201	210	208

Independent sectional heaters were added to improve this condition, but were inadequate. By carefully applying insulation it was possible to keep the temperature difference between TC₄ and TC₃ within 2°C. In reporting the temperatures the geometric average between the thermocouples bounding the catalyst was used.

Initially the reactor flow rate was set and after four hours operation at 200°C, a blank run was made. This consisted of attaching

adsorber A1 containing 200cc of high purity water to the reactor outlet and starting the stop watch as soon as bubbles began to emerge from the fritted glass cylinder. The temperature was checked at points TC1 through TC4 and recorded as were the manometer readings M1 and M2. The rotometer reading was also recorded. A change in the reading of manometer M2 was used to indicate leaks in the system during the course of a run and between runs. At the end of the run the spring clamp on the ball and socket joint between R1 and A1 was removed and the two pieces separated.

The solution was drained from the stopcock at the bottom of A1 into two clean flasks. The adsorber was refilled with 100ml of water for a two minute soak to remove the last traces of hydrogen peroxide. This has been shown to effectively remove all the hydrogen peroxide in the exit stream (119).

The solutions were acidified and titrated with standardized potassium permanganate solution according to the conventional McBride method (112). The hydrogen peroxide content in this solution can be calculated with an expected error of .2%. The hydrogen peroxide content is directly related to the exit concentration of the reactor. Changing the setting on a variable transformer reduced the reactor temperature and in this way a run can be made over the entire temperature range from room temperature to 200°C, or higher. Once the glass surface has been characterized from these results, the catalyst was placed

inside the reactor tube and the complete series repeated. The measurements described allowed the determination of the rate of decomposition.

b. Fluid jacketed reactor. The initial reactor was designed to obtain simultaneous kinetic and electrical characterization of a catalyst and is shown in Figure 3.3b. However, procedures were not refined enough to avoid contamination during construction and operation. As a result, it was found that the surfaces were too active to carry out the study below 100^o C.

The reactor tube was constructed from two, 15/16 inch I. D., $\text{F } 29/42$ Mercury seal joints. Perpendicular to the axis of this tube two 5mm glass tubes were joined on opposite sides of the reactor extending through its wall. A jacket was placed around the reactor tube. Within this jacket a coil was placed to serve as the reactant preheater. The gas entered the reactor tube near the bottom and left near the top. A $\text{F } 10/30$ outer joint for a condenser, a $\text{F } 24/40$ joint for a thermocouple well and a stopcock drain were all connected to the jacket as shown. The side arms were plugged during this study. They were to serve as electrode holders for the measurement of changes in the catalyst's electrical properties. These measurements were to be made in the same way as the high temperatures measurements described in section C of this Chapter. Sealing the moveable electrode to prevent leakage and masking any exposed active material was a problem. A Kel-F

dispersion, 3M KX633, was found useful in masking active materials.

The reactor system was made leak-free.

A thermocouple well extended through the upper end of the reactor tube along the central axis. Around the well there is a concentric larger tube which held up to 10 catalyst slices. This outer tube had been cut in evenly spaced intervals in a spiral configuration. The cuts were the same dimensions as the catalyst crystals, and allowed the orientated crystal faces to be placed perpendicular to the reactant flow. The bottom fitting served as either a plug or catalyst support.

Approximately 130 were performed using 50% H_2O_2 and 100 runs using 98% H_2O_2 , respectively, in the saturator, Sl. These runs gave encouraging but not conclusive results that decomposition was occurring on up to 22 pieces of crystal placed in the reactor. In an attempt to better understand the variables involved, it was decided to construct a simple tubular reactor which has been described.

During the initial testing of the first reactor tube, the catalysts were positioned by shaking. This procedure significantly increased the activity of the glass surface and in subsequent chargings a piece of nylon rod was used to position the catalyst in desired location (Appendix E).

6. Geometric Surface Area

For determining the kinetic parameters the surface area of the

catalyst is required. Since the crystals are in the shape of square faced or rectangular bricks with relatively smooth cleaved surfaces, the geometric surface area was used. This area was determined with a modification of a procedure given by Thomas (143). Each catalyst was individually weighed with an Ainsworth "Right-A-Weigh", type S, automatic balance. The thickness was then measured by means of a caliper micrometer. The cross sectional area of the sample was calculated using the density of 6.80 gms/cm^3 for NiO. The geometric surface area of the crystals was then calculated. See Appendix F. Calculated surface areas were within $\pm 7\%$ of the surface area obtained by using the dimensions of the crystal alone.

C. Electrical Measurements on NiO Single Crystals

The electrical properties measured in this work were the electrical conductivity and the Seebeck coefficient. The techniques used in the electrical measurements were designed so that they could also be used in the jacketed reactor. Each technique will be described and discussed below. The results are discussed in detail in Chapter IV.

1. Resistivity-Seebeck Coefficient Cell

Several methods were used in this work to measure the resistivity and Seebeck coefficient. Most of the reported measurements were taken in a cell similar to that used by Parravano and his students (109, 110, 135). Figure 3.4 is a diagram of this cell. The crystal is

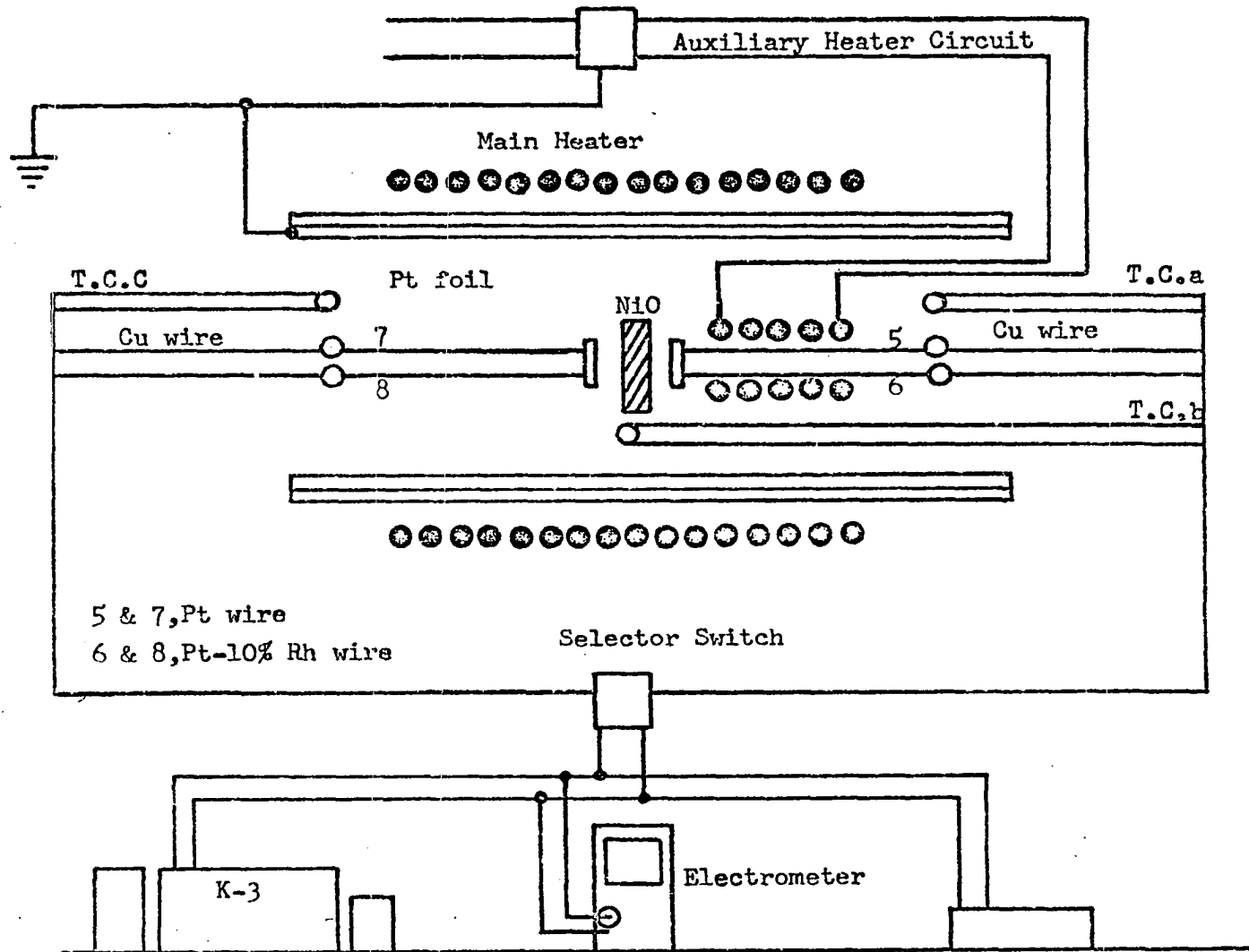


Figure 3.4. Resistivity-Seebeck Coefficient Apparatus.

mounted between two platinum foil electrodes, each 0.002 inches thick. The spring loaded electrodes are parallel to the cleavage plane of the crystal. One platinum wire and one platinum-10% rhodium wire were spotwelded to each foil. This was done with the assistance of Mr. Keith Warble of Avco Radiation Laboratory using their Hughes-Aircraft microspotwelder. These wires were L and N No. 28 AWG thermocouple wire. Ceramic insulation was used to separate these wires in the cell. General Electric Formex copper magnet wire was silver soldered to the platinum and platinum-10% rhodium wires. The two junctions were on opposite sides of the cell and, being in thermal contact with the main ceramic support, were not always at the same temperature. This made it necessary to compensate the Seebeck measurements. Iron-constantan thermocouples were used to measure the respective junction temperatures. This made it possible to compensate and calculate the Seebeck coefficient. The electrical system was completely shielded by grounded aluminum foil.

The average temperature of the crystal was controlled by setting a variable transformer connected to a Hevi Duty Electric Company 422 watt heater. Temperature fluctuations were eliminated by the electrical shielding which also eliminated external air currents.

To measure the resistance of the crystal a Keithley 610A electrometer was connected through a switch to the two opposite platinum wires of the cell. In some measurements DuPont No. 6216 electrical

conducting paint was fired on the crystal faces prior to placing in the apparatus. Proven ohmic electrical contacts with NiO are listed in Appendix H.

Thermal equilibrium was attained very slowly in this cell. Approximately three hours were required to reach steady state after a change in setting was made. Only steady state resistance measurements were taken. Calculation of the resistivity is covered in Appendix I.

The Seebeck coefficient was obtained by applying a temperature difference across the crystal by placing an auxiliary heater in contact with one side of the crystal. The other side was usually at a temperature of 2° to 25°C lower. A coil of nichrome wire was used as the auxiliary heater in this work. The temperature of the cold junction was determined by operating at steady state. Although the auxiliary heat could have been grounded during the measurement of the potential difference across the crystal, it was not necessary.

The potential difference across the crystal was measured using a L and N K-3 potentiometer with a L and N 9834 electronic null detector. Temperature differences across the crystal were measured using each electrode-thermocouple. Since the junctions of the thermocouple wires were not at the same temperature it was not convenient to use the differential method to obtain the temperature difference across the crystal. In addition to measuring the individual emfs generated by

the electrodes, it was necessary to measure the emf of the type J thermocouples at the noble metal-copper junctions. This EMF was measured with a L and N 8657-C portable potentiometer.

2. Two Point Probe Measurements

Contact resistance is a common source of error in semiconductor resistivity measurements. Modifications of the two point probe technique are often used to eliminate the effect of the contact resistance. It has been used successfully by several investigators with NiO (36, 97, 145, 160).

Figure 3.5 is a schematic drawing of the apparatus constructed to carry out this measurement. A small current from the dry cell battery was passed through the crystal via the outer two wrapped Englehard "Fibro" .013 inch O. D. platinum electrodes. These are electrodes 2 and 5 in Figure 3.5. This same current flowed through a General Radio M32K, 111.1 decade resistor connected in series. Knowing this resistance and measuring the voltage drop across this resistor permitted the calculation of the current through the crystal. The potential drop across electrodes 3 and 4 is measured with the potentiometer while allowing no current to flow through the detector circuit. The true resistivity of the crystal was calculated using the equation,

$$\rho = \frac{E_{34} A}{I_{12} l} \quad (29)$$

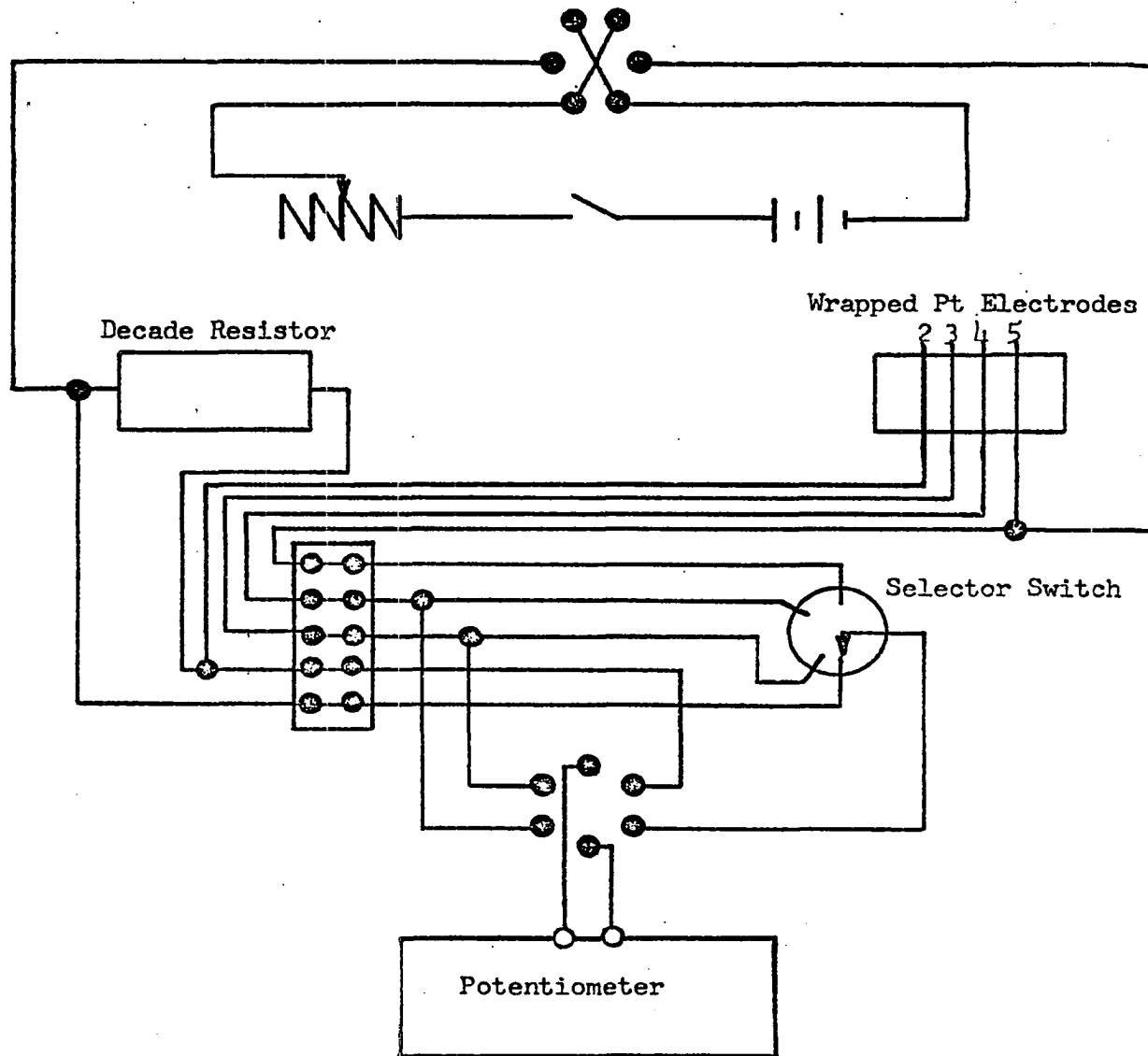


Figure 3.5. Two Point Probe Apparatus.

where E_{34} = voltage drop measured between electrodes 3 and 4,
 A = cross sectional area of sample,
 I_{12} = current through standard resistor,
 l = distance between electrodes 3 and 4.

In the conventional measurement of resistivity the outer electrodes are of the same uniform geometry as the sample. If the crystal is isotropic and homogeneous the resistivity can be calculated as the product of the potential gradient in the direction of current flow and the cross sectional area divided by the current flowing. The precision of the measurement is limited by the measurement of the cross sectional area and the distance between probes. Valdes and others (148) developed a four probe technique from which the method outlined above originated. Equations are available for various probe configurations yielding a sheet resistivity for an infinitely thin slice. The bulk or body resistivity is obtained by multiplying the sheet resistivity by the thickness, but is meaningful only if the crystal has uniform resistivity.

Wrapped electrodes were used here so that a comparison could be made with published work on the electrical resistivity of the single crystals discussed in Chapter II, Section B.

The assumption used with these wrapped electrodes is that the bulk resistivity can be calculated with equation 29 (36, 97).

The cell is placed in the same 422 watt furnace section used in the resistivity-Seebeck coefficient cell. At temperatures below 150°C

two point probe measurements were not possible, apparently because of the high resistivity of the crystal. As the temperature increased the voltage drop across the potential probes could be measured readily. Mechanical difficulties were encountered in wrapping the crystal. At first gloves were used in handling, but this process was very time consuming. For the sake of efficiency, ungloved hands were used followed with a benzene rinse to degrease. The platinum wire would not withstand much handling. Lifetime of the wire could be increased through stress-relief annealing by heating to about 816°C for one minute followed by air cooling. Two point measurements were used to help relate results of this effort to the larger body of data available. See Appendix I.

3. Low Temperature Measurements

a. Seebeck coefficient. Thermoelectric methods to obtain the sign of the carriers and a rough indication of the homogeneity of the material has been used by several investigators (32, 52). Some preliminary measurements were made with this basic technique using the apparatus in Figure 3.6. A soldering iron with a 23-1/2 watt heating element was mounted in a fixed position inside a shielded box. The temperature differential across the crystal was controlled by means of a variable transformer connected to the iron. A spring-loaded copper electrode was mounted to allow crystals to be easily placed in the apparatus. The copper soldering iron tip acted as one electrode and was

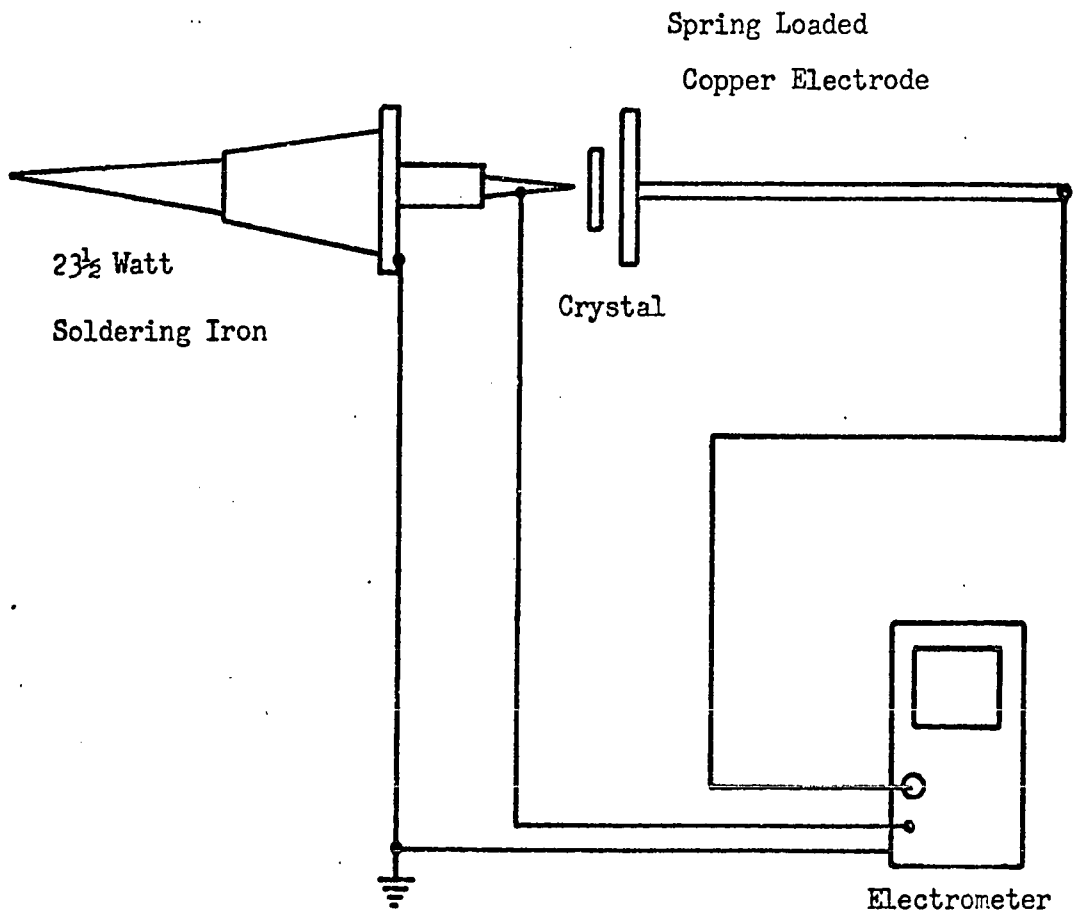


Figure 3.6 Low Temperature Seebeck Cell.

grounded with respect to the other electrode. Voltage differential was measured with a 610A Keithley electrometer. The sign of the cold electrode indicated the sign of the current carrier. With NiO the cold electrode is expected to be positive. For a given powerstat setting the temperature differential at steady state had previously been determined with type J thermocouples silver-soldered onto each electrode. Zhuravlev et. al., (163) used a modification of this technique to measure a distribution of what was called the thermoelectromotive force over the surface of a polycrystalline sample of CuO. A quantitative interpretation was placed on the value of the voltage difference divided by the temperature difference. This procedure would be preferred if it does produce the same results as the cell with the platinum electrodes because of the ease and rapidity.

b. Resistivity. Techniques to separate and measure the surface and bulk resistivities based on the work done at John Hopkins University (2, 3) have been applied to some high resistivity materials (98, 111). Although one must realize that a problem of contact resistance complicates the results, some measurements of this type were made on nickel oxide single crystals using the apparatus shown in Figure 3.7. This required fired-on silver electrodes using DuPont No. 6216 conductive preparation. The firing is described in Appendix H.

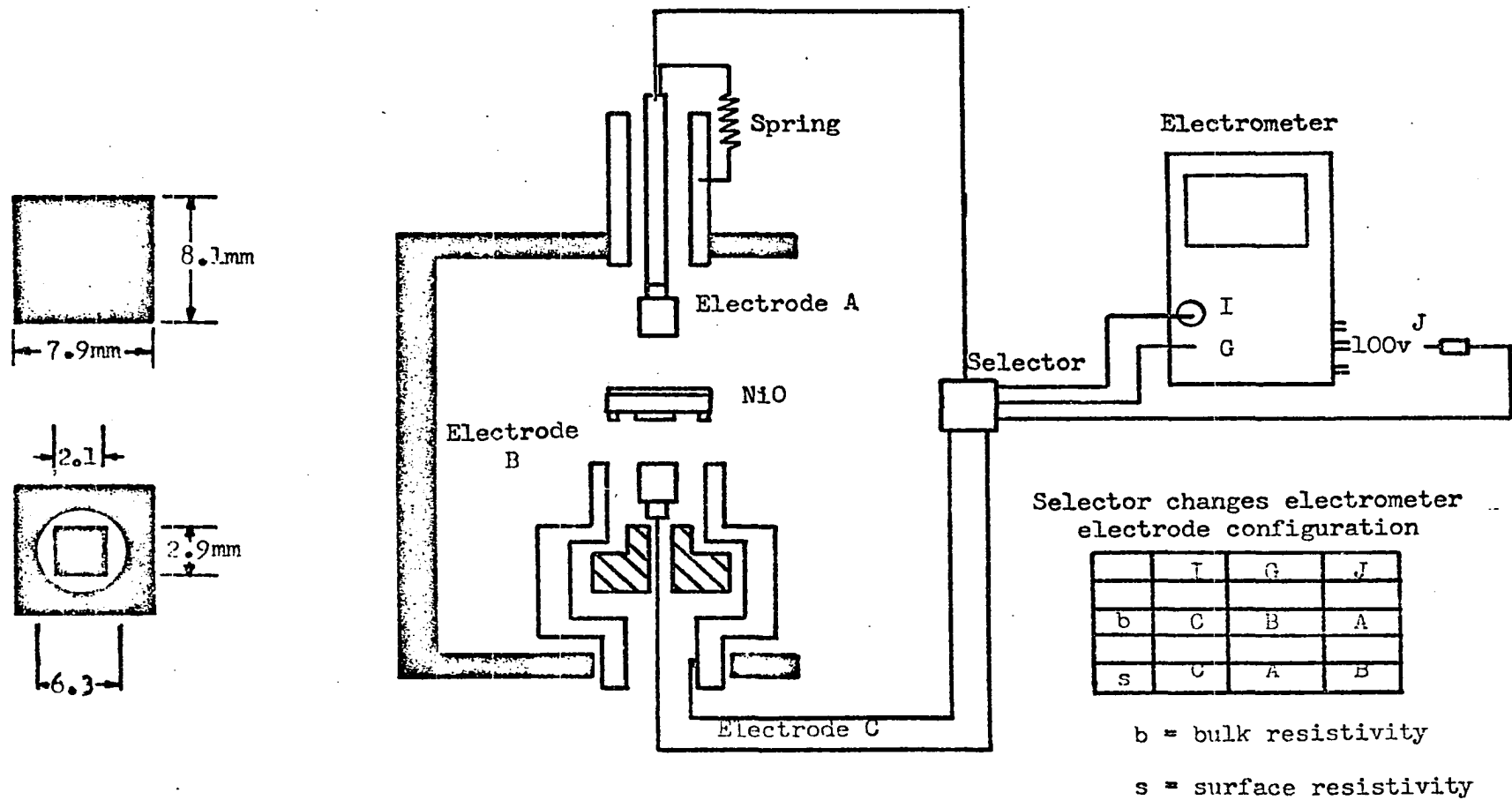


Figure 3.7. Low Temperature Resistance Measuring Apparatus.

4. Attempted Measurement of Electrical Properties

During Reaction

An attempt was made to obtain some information about simultaneous electrical conductivity-kinetic measurements in the jacketed reactor, Figure 3.3b. Two tungsten points were put through the bottom plug. These points were connected to the external measuring system via insulated copper leads. The contact with the NiO single crystal was made by gravity. Open circuit behavior indicated these electropolished electrodes were either being oxidized or not making adequate contact. The low temperature of 95^o C and the corresponding high catalyst resistance could have caused the difficulty also.

The problems encountered in making suitable electrical measurements using the electrode holding side arms of the reactor are complicated by the fact that hydrogen peroxide is decomposed catalytically on most materials. Electrodes identical to those in the Resistivity-Seebeck cell are designed to enter and hold the catalyst crystal. The fixed electrode could be sealed through glass with the use of a tungsten junction. The exposed platinum must then be covered with Kel-F as described in the Appendix J. The movable electrode will be more of a problem because one has to seal the system from the surroundings.

In preliminary tests, Teflon tape was wrapped around sample electrodes to insure a snug fit in the holders, but it was not adequate. To minimize gas leakage the Teflon-glass gap could possibly be filled

with Fluorolube. The similarity between this design and that of the Seebeck-Resistivity cell insures a valuable overlap of information.

CHAPTER IV

EXPERIMENTAL RESULTS AND DISCUSSION

A. Kinetic Results

In the chapter on procedure it was mentioned that the initial reactor with 35% and 50% solutions of hydrogen peroxide in the saturator gave unsatisfactory NiO catalytic results. It could not be conclusively verified that reaction was occurring on anything but the reactor walls. Flow rates used were between 50 and 200 cc/min. The reactor temperature was always below 100°C. Initially, it was thought that the low temperature combined with the low surface area of the catalyst was the problem. The addition of "Hitec" high temperature salt to the reactor jacket was considered to permit operation at a higher temperature. Before the heat transfer salt was added to the glass reactor's jacket it was decided to check out the possibility of reducing the water partial pressure. This had been shown to definitely depress the rate of reaction (55, 118). This reduction was accomplished by increasing the concentration of hydrogen peroxide in the saturator to 98%. However, the same results were obtained with a large amount of decomposition observed on the glass surface. This indicated that a better

glass pretreatment technique was required.

A simple borosilicate tube reactor was then used but showed the same high glass activity in decomposing hydrogen peroxide. Accidental breakage of a section of a borosilicate trial tube reactor occurred. Subsequent repair gave a surface of a significant less activity. This was positive evidence of the importance of glass pretreatment. The final procedure is discussed elsewhere.

System variables used in obtaining the kinetic data are listed below.

Experimental Conditions

Saturator concentration	98% hydrogen peroxide
Saturator temperature	13.5° C and 24° C
Room temperature	24 ± .5° C
Flow rate	40-200 cc/min
Average system pressure	33.90 inches H ₂ O above atmospheric
Atmospheric pressure	72.5 to 73.6 cm Hg
Carrier gas	N ₂
Reactor temperature	25° - 220° C

By following the procedure in Chapter III one can calculate for a given set of experimental conditions and catalysts the milliliters of standardized KMnO₄ required to standardize the absorber solution. This volume is proportional to the milligrams of H₂O₂ in the solution. Dividing by the time required to collect the sample, one has a number

which is related to the exit concentration. It is convenient to define an exit concentration parameter by

$$C \equiv \frac{\text{milliliters of standardized KMnO}_4 \times 10^3}{\text{time to collect sample, sec}} \quad (30)$$

The fraction of hydrogen peroxide decomposed is defined by

$$D \equiv \frac{\text{moles decomposed on NiO catalyst}}{\text{moles hydrogen peroxide in feed}} \quad (31)$$

or

$$D = \frac{C_W - C_H}{C_R} \quad (32)$$

where C_R = exit concentration parameter with no decomposition,

C_W = exit concentration parameter for glass at given conditions,

C_H = exit concentration parameter with glass and NiO.

If negligible reaction takes place on the Pyrex at 25°C,

$$C_R = C_W \text{ at } 25^\circ\text{C} \quad (33)$$

Equation (33) is verified in Appendix O.

From previous studies outlined in Chapter II, the assumption that the decomposition of hydrogen peroxide vapor is first order with respect to hydrogen peroxide is a reasonable assumption. The rate R , is defined as the moles of hydrogen decomposed per unit area per unit time,

$$R \equiv \frac{\text{moles hydrogen peroxide decomposed}}{(\text{cm}^2) (\text{time})} \quad (34)$$

For a first order reaction,

$$R = k (\text{H}_2\text{O}_2) \quad (35)$$

If the concentration of the hydrogen peroxide is given in g-mole/cm³, the specific rate constant has units of cm/time. Substituting (35) into the species balance assuming negligible decomposition at the reactor inlet one finds the specific rate constant is,

$$k = \frac{F}{A_S} \ln \left[\frac{1}{1-D} \right] \quad (36)$$

where F = flow rate of the reactor feed, cc/min

A_S = geometric surface area of the catalyst, cm²

1. Effect of Temperature

Since it was necessary to evaluate the specific rate constant over the complete range of operating temperatures it was convenient to express the experimentally determined exit concentration parameters by an expression of the form:

$$C = a + bt + dt^2 + et^3 + ft^4 + \text{etc.} \quad (37)$$

By using the orthonormal least squares technique of Hall and Canfield (50) it is possible to obtain the best fit of the data to this equation. In addition to eliminating random errors, one can then interpolate in a more reliable manner between actual data points.

The experimental values of the concentration parameter and the calculated values of the coefficients in equation (37) are given in Appendices L and M, respectively. The University's Osage Computer was used to evaluate these coefficients, as well as an estimate of the

sample variance. In general the least square curve produced from the determined coefficients fit the data quite well. An example of the results is given in Figure 4.1. In the figure, the exit concentration parameters for the empty reactor C_W and for the runs with various amounts of NiO single crystals are shown as a function of temperature in degrees Centigrade. The points are experimentally determined and the curves correspond to the computer fit.

In characterizing the activity of the catalyst the conventional approach of fitting the specific rate constant, k , to the Arrhenius equation (38) was followed.

$$k = k_0 \exp \left(\frac{-E(\text{apparent})}{RT} \right) \quad (38)$$

The Osage Computer was used to calculate the decomposition, D , and the specific rate constant, k , as a function of temperature using equation (37). The Arrhenius parameters are found with a least squares treatment of the logarithm of k and the corresponding reciprocal absolute temperature data. Figure 4.2 is an example of a graphical presentation of the above.

In the numerical calculations it was found convenient to drop the F/A_s coefficient in equation (36) and these so called "pseudo" rate constants are reported in Appendix N along with the corresponding F/A_s terms.

This does not change the values of the apparent activation

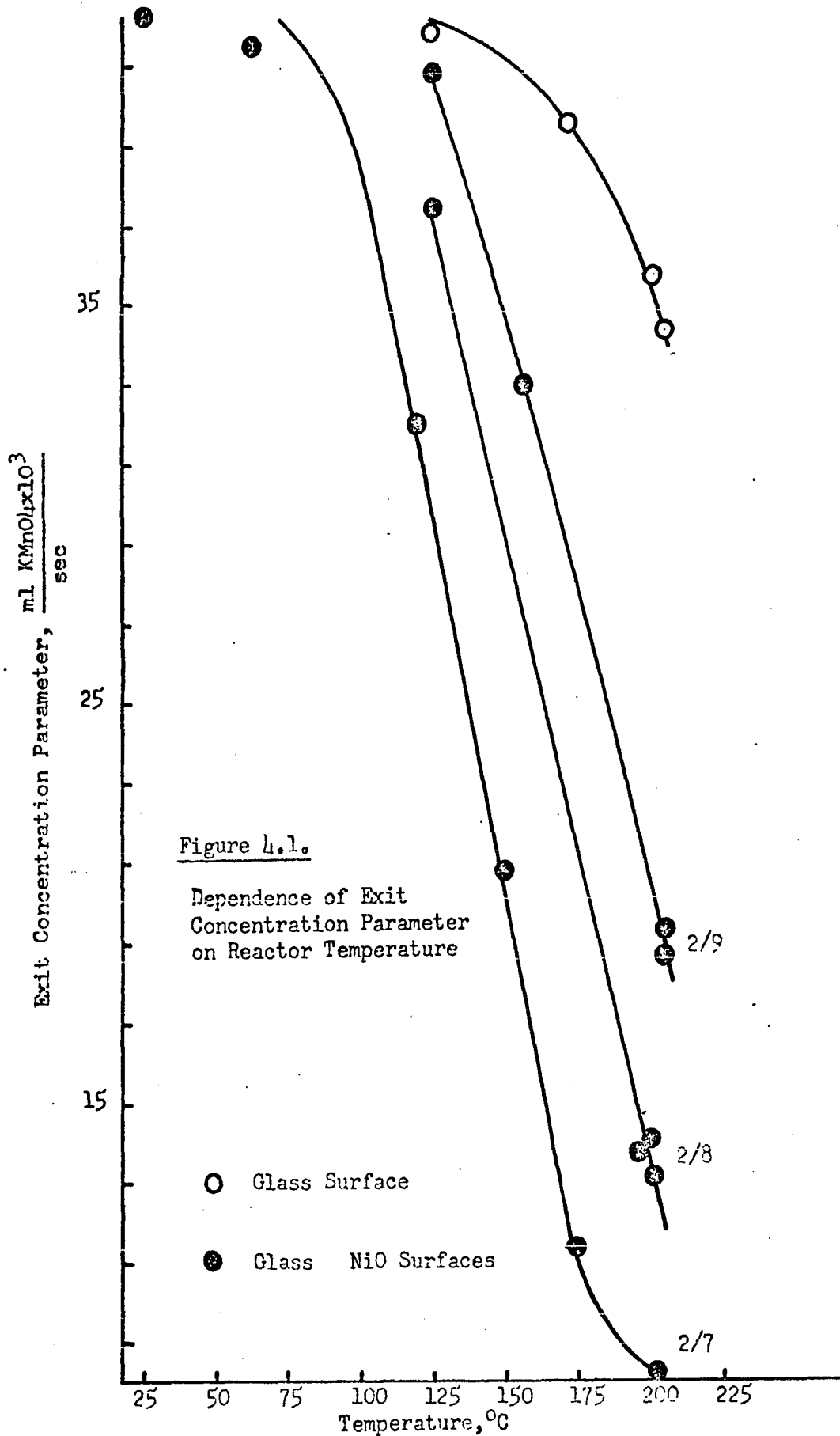


Figure 4.1.

Dependence of Exit Concentration Parameter on Reactor Temperature

- Glass Surface
- Glass NiO Surfaces

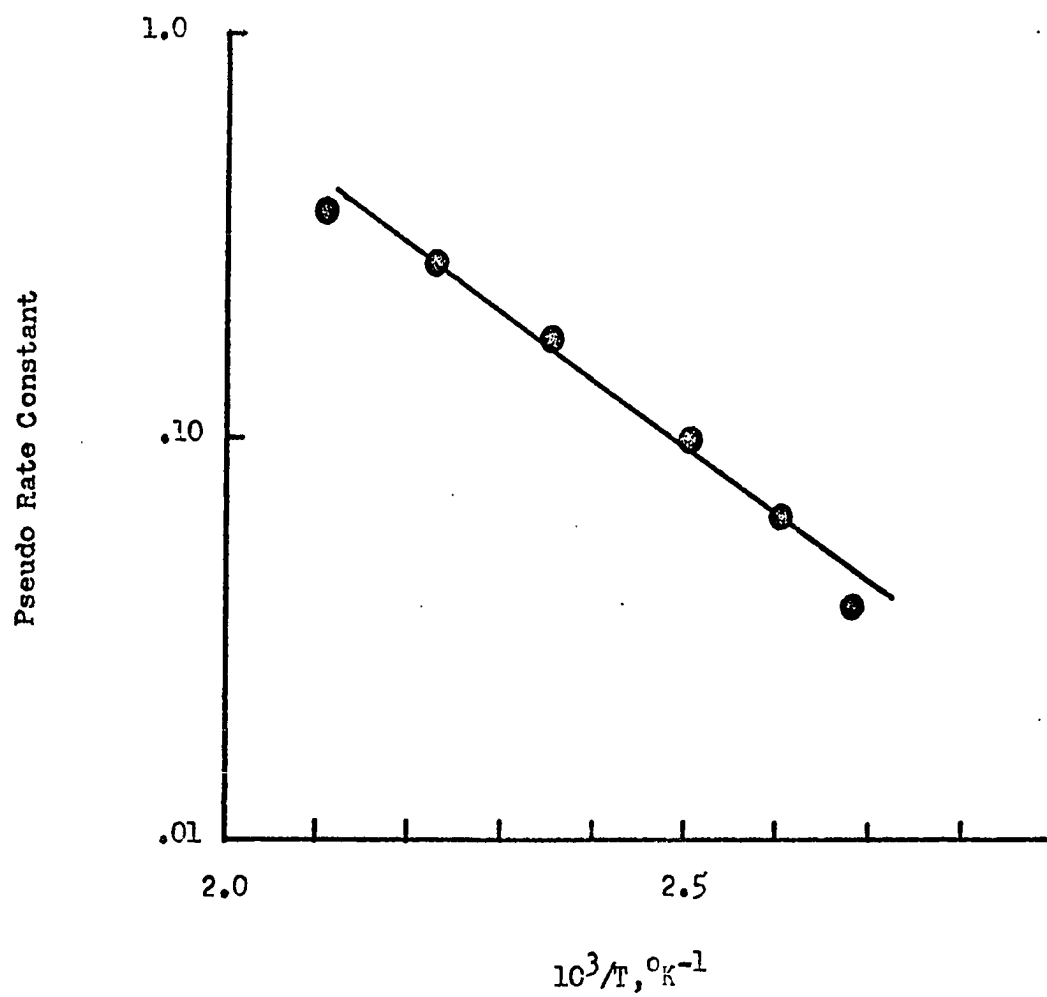


Figure 4.2. Representative Arrhenius Plot
of Kinetic Data, Run 2/12B.

energies, although the calculated values of the frequency factor must be corrected. These corrections, along with the kinetic parameters for the incompletely defined crystals (Runs 2/1 through 2/6), are presented in Appendix N. The kinetic parameters for the crystals with well defined surfaces, that is, only cleavage planes, are presented in Table 4.1.

TABLE 4.1

EXPERIMENTAL KINETIC PARAMETERS OBTAINED WITH NiO
SINGLE CRYSTAL HAVING ONLY CLEAVED SURFACES

Run	E_{apparent} kcal/g-mole	Standard Deviation	log k_0	Temperature Range °C
2/7	8.98	.61	5.8280 6.2190*	85 - 125
2/8	9.53	.48	5.6833 5.9595*	125 - 195
2/9	9.61	.04	5.9624	150 - 200
2/10	9.77	1.30	6.2669	125 - 200
2/11	6.85	.58	4.9652	75 - 200
2/12	7.65	.09	5.1269	125 - 200
2/13	6.02	.14	4.2924	100 - 200

* Extrapolated surface area (See Section A4 of this Chapter).

These values are based on a least squares treatment of the calculated rate. The temperature ranges included in this table were set to

include as many calculated data points as possible yet discard points based on extrapolation of actual experimental data. Hart and Ross (118) using oxidized flashed nickel film reported a temperature coefficient of $11.0 \pm .5$ kcal/mole in the temperature range from 60° to 160°C with a hydrogen peroxide partial pressure of 0.88 mm Hg. In the same range these authors found that with NiO on a metal slip the temperature coefficient was 13.0 ± 0.5 kcal/mole.

Two complications should be mentioned at this point with respect to the interpretation of the activation energies. For a first order process the apparent activation energy is the true activation energy reduced by the heat of adsorption of the reactant (85). The second problem exists if the reaction is diffusion limited. The diffusional falsification of activation energy has been discussed by Rosner (117). Since the heat of adsorption was not determined it is not possible to work with true activation energies. The diffusional falsification has been estimated in Appendix P.

2. Compensation Effect

By plotting the logarithm of the so called frequency factor, k_0 , versus the apparent activation energy given in Table 4.1, a straight line relation is observed. This relationship is shown in Figure 4.3 and is expressed by:

$$\log k_0 = a E_{\text{apparent}} + B \quad (39)$$

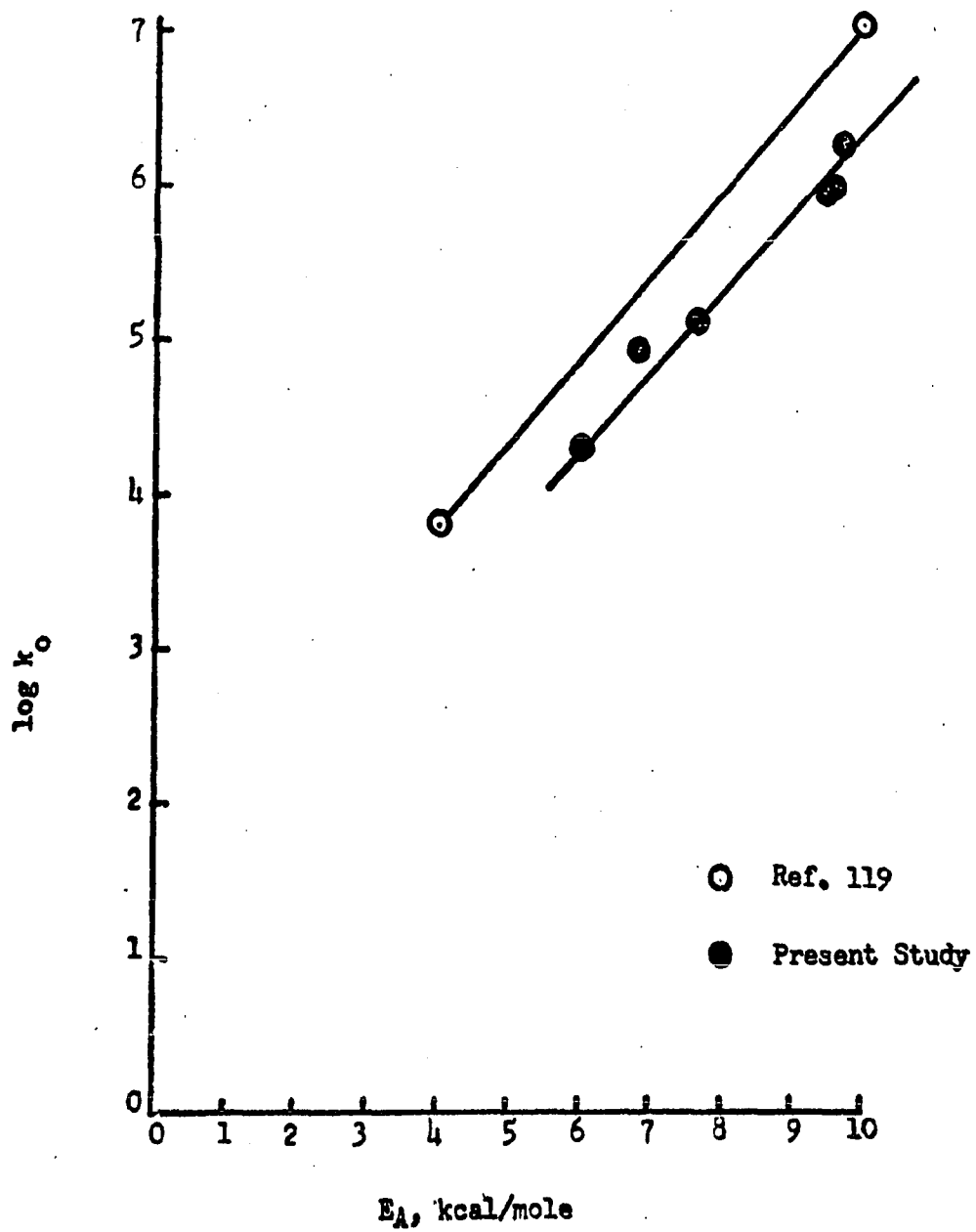


Figure 4.3. Compensation Effect on NiO.

where a and B are experimentally observed constants. The value of a in this system is .526. Ross (119) observed the same compensation effect on lithium-doped NiO. It is interesting to note that this effect has been shown to be operating in many heterogeneous reactions. Reviewing the literature (15, 26) reveals that while this effect imparts great significance on the activation energy (5) no definite explanation is known (17). One interpretation given by Cremer (26) for compensation that resulted when the pretreatment temperature of the catalyst was changed was that a catalyst surface may have more than one kind of active center, each kind having a different energy of activation. Pretreatment changes the relative concentrations of the different active centers, so it is to be expected that the observed activation energy will change.

3. Order of Reaction

The literature indicates that the overall reaction rate with respect to hydrogen peroxide decomposition on catalytic surfaces is first order (162, 55). On nickel oxide under the experimental conditions used here, the reaction has been shown to be first order (118, 119). To verify these observations the same catalyst was used in two runs, 2/4 and 2/5, changing only the inlet concentration. This was done by using two different saturator temperatures. Unfortunately, a new procedure was tried during the run with the saturator at 22°C which made all the data questionable except the experimental points at 165°C. The change was

an attempt to obtain data in the minimum time by allowing only one hour to reach steady state after each reactor temperature change. In some cases the $N_2 - H_2O_2$ stream was not allowed to flow through the reactor until fifteen minutes before the absorber was connected and the run began. This procedure resulted in a high level of fluctuation in the experimental values, so much so, that it was impossible to calculate the amount of decomposition reliably.

At 165° , on the other hand, a direct comparison between the decomposition at the two hydrogen peroxide compositions was made and the values appear in Table 4.2.

TABLE 4.2

DECOMPOSITION AT TWO DIFFERENT HYDROGEN
PEROXIDE CONCENTRATIONS AT $165^\circ C$

Run	Absorber Temperature, $^\circ C$	Mole Fraction $Y_{H_2O_2}^*$	Decomposition % D
2/4	22	2.044×10^{-3}	18.20
2/5	13.5	1.568×10^{-3}	19.56

*See Appendix O.

From equation (36) it is seen that for a first order reaction the percent decomposition is independent of the inlet concentration. The above data indicates for a 23% change in hydrogen peroxide concentration the amount of decomposition is relatively constant. This gives a rough check on the assumption of first order kinetics.

4. Effect of Surface Area

The initial check on the effect of surface area was done in a qualitative way in the first tube reactor (Appendix Q). Five pieces of catalyst were tested and found to decompose 55.91% of the vapor at 173°C. The measured decomposition with 3 and 2 crystals, respectively, was 16.58 and 11.92%. A linear relationship exists between the amount of decomposition and the number of crystals as the number of crystals varied from zero to three. The decomposition obtained with five crystals is more than the linear relation would predict. The geometric surface areas were not estimated as the crystals still had the rough production edges.

Runs 2/7 through 2/9 were carried out under as nearly the same conditions as possible except that the number of catalyst crystals in the reactor was varied. As the catalyst was uniformly pretreated it was of interest to compare the effect of the number of crystals or geometric surface area on the catalytic activity. This activity is characterized by the amount of decomposition at 165°C in Table 4.3.

Graphically these points fell along a straight line as shown in Figure 4.4. This means that the percentage decomposition is a linear function of the geometric surface area. However, it is clear that the total geometric surface area in Run 2/7 does not really represent the effective surface area, as the gas stream is not in contact with all the crystals. The specific rate constant calculated for Runs 2/7 - 2/9 at

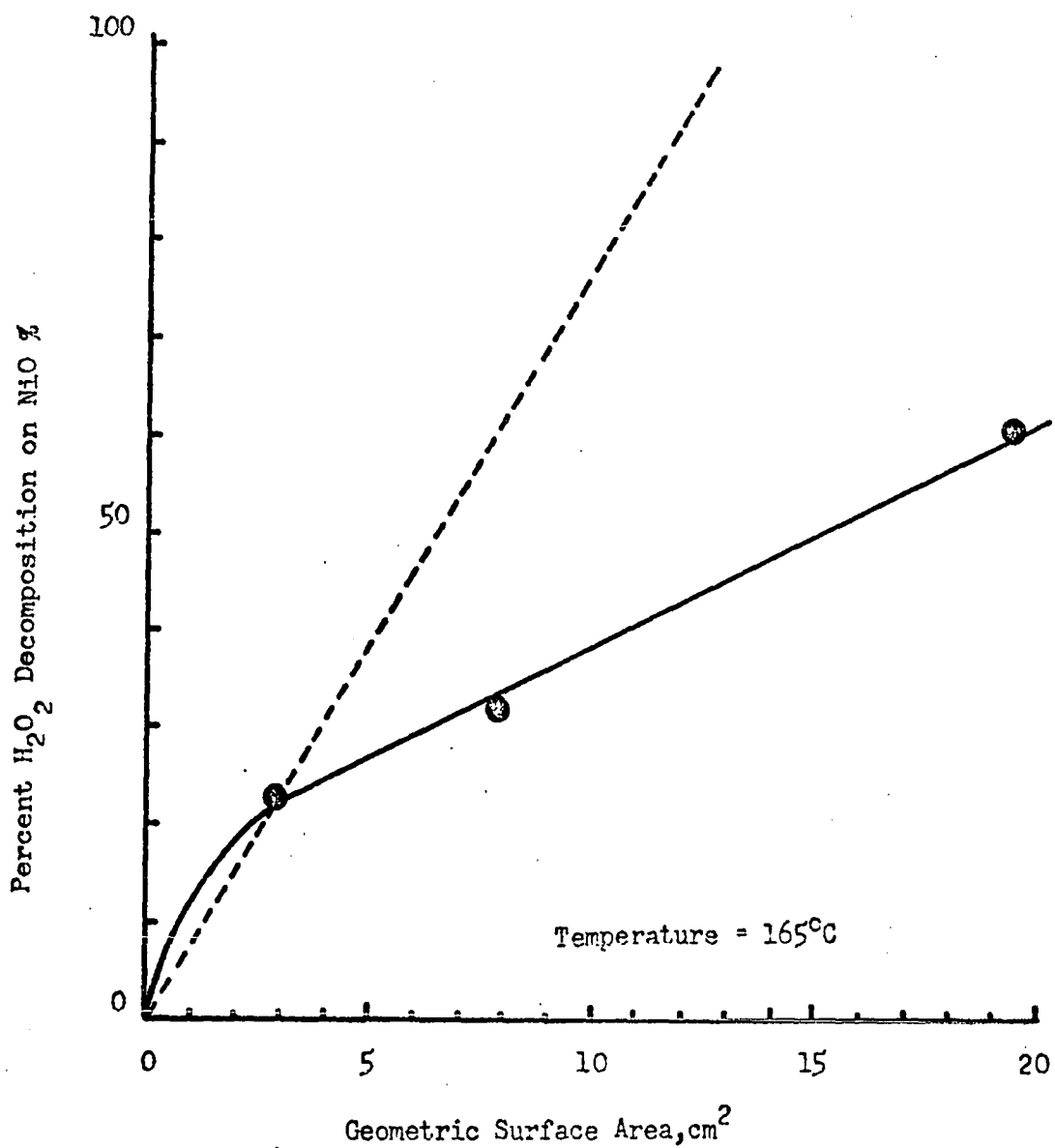


Figure 4.4. Effect of Geometric Surface Area on
H₂O₂ Decomposition, Runs 2/7-2/9.

TABLE 4.3

EFFECT OF CRYSTAL SURFACE AREA ON
DECOMPOSITION OF H_2O_2 AT $165^\circ C$

Run	Total Geometric Surface Area, cm^2	Decomposition %	Number of Crystals*
2/7	19.40	60.44	83
2/8	7.89	32.05	16
2/9	2.88	22.82	6

*For distribution, see Appendix E.

$165^\circ C$ were 9.082, 9.254, and 17.086 cm/sec, respectively. In Run 2/9 where only 6 crystals were distributed over the reactor length it will be assumed the gas contacts the complete surface. Based on this and also assuming the conventional linear effect of surface area on the rate (35), one can draw a line through the origin on a graph of percent decomposition D versus geometric surface area. This is shown in Figure 4.4. An effective area for Run 2/7 and 2/8 can then be found by going along a line of constant D until the dotted line is intersected. The geometric surface area corresponding to this point can be read. The values of the specific rate constant calculated from these estimated surface areas are given below.

<u>Run</u>	<u>Estimated Surface, cm^2</u>	<u>Estimated k, cm/sec</u>
2/7	7.88	23.36
2/8	4.18	17.47
2/9	2.88	17.09

Agreement between the specific rate constants is expected. It can be seen that using these corrected geometric surface areas produces rate constants that are essentially the same.

5. Effects of Flow Rate

The data from Run 2/12 (Appendix R) show the effect of changing the flow rate on the kinetic parameters. In this series seven pieces of catalyst were placed into the tube reactor. The comparison of the observed results appears in Table 4.4.

TABLE 4.4

EFFECT OF FLOW RATE ON OBSERVED KINETICS IN RUN 2/12

Run	N ₂ Flow cc/min	Decomposition %	Reaction Rate Factors*, $\frac{\text{g-moles H}_2\text{O}_2}{\text{cm}^2 \text{- sec}}$
2/12B	196	.1882	36.9
2/12C	293	.0573	16.8
2/12D	488	.0193	9.41

*Y_{H₂O₂} was taken as unity in these calculations.

In this table a new parameter is introduced, overall rate factor \bar{R} . It is defined by the equation,

$$\bar{R} = Y_{\text{H}_2\text{O}_2} F_{\text{N}_2} D \quad (40)$$

where the symbols have the same meaning as before.

It is worthwhile to compare these results in Figure 4.5 with the

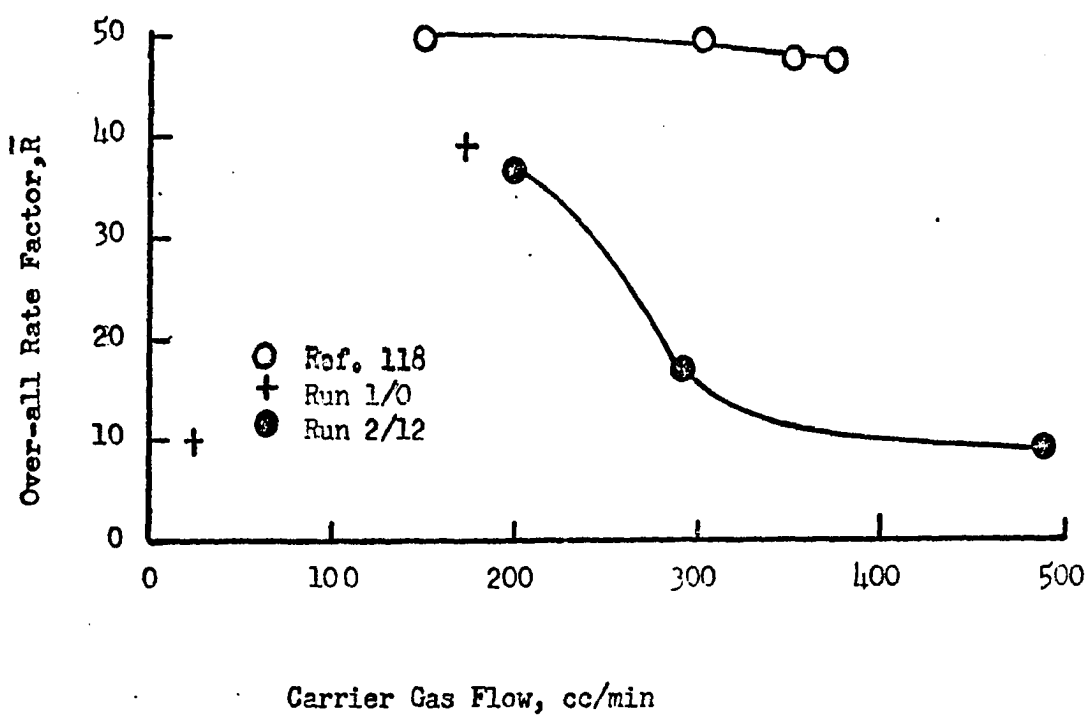


Figure 4.5. Effect of Flow on Over-all Rate Factor.

published work of Hart, McFadyen, and Ross (55). It is shown in their published study that only a slight deviation in this rate factor occurs. In this study it was found that as the flow rate increased the observed rate factor decreased. This is the same behavior observed in the above paper on oxidized nickel metal strips at flow rates greater than 300 ml/minute.

In chemical kinetic studies one must continually be on guard for diffusion limitations and a corresponding falsification of derived kinetic parameters. If diffusion were controlling here one would expect that the rate of reaction would increase with flow rate until a leveling off occurred. The opposite trend here can be explained by considering the equation (40). The mole fraction of hydrogen peroxide vapor appears as a coefficient in the equation. It is calculated by assuming equilibrium in the hydrogen peroxide saturator. As the flow rates of carrier gas through the H_2O_2 in the saturator increases it is clear that the system departs farther from the equilibrium conditions assumed in the calculations. The decrease in the mole fraction can account for the observed behavior.

It is desirable to operate in the region where the rate is independent of flow rate and several arguments follow which justify the claim that the flow rates used were adequate to eliminate significant diffusional effects.

In one of the early runs in tube reactor No. 1 the decomposition

was measured on 5 catalyst crystals at two different flow rates (Appendix Q). The results of these runs are shown in Figure 4.5. It is evident from the figure that at a temperature of 173°C and a flow rate of 25 cc/sec, a diffusional effect exists.

Somewhere between 25 cc/min and 190, one might eliminate both the diffusional effects and also remain near saturation. The latter point is the easiest to verify as a comparison can be made of the saturation hydrogen peroxide content at the given conditions and the actual measured content. This calculation has been performed in Appendix O and the results show that operating at 190 cc/min provides an inlet concentration that is saturated.

In considering a check on the effect of diffusion, the criteria of Hart, McFadgen and Ross (55) offers some help. These authors concluded that since the activation energy they measured was sensitive to the differences in the various oxide surfaces they studied and were high, diffusion control could be ruled out.

The system they used to obtain the published data consisted of an annular reactor formed between two concentric glass tubes. The catalyst was deposited on the inner surface of the larger diameter tube. Observed activation energies ranged from 4.6 kcal/g-mole on $\text{Ag}/\text{Ag}_2\text{O}$ to 19.7 kcal/g-mole on $\text{Fe}/\text{FeO}/\text{Fe}_2\text{O}_3$. The corresponding temperature range was between 38° and 183°C and the flow was laminar with a Reynolds number on the order of 7 for the flow rates between 150 and 350

cc/min. The partial pressure of hydrogen peroxide was 0.88 mm.

The fact that the same effects were observed here (Table 4.1) for similar operating conditions (55, 119) suggests the criteria would be useful.

From these considerations it appears that diffusional effects in the reported results will be small or negligible. A further calculation using an interesting correlation is included in Appendix P.

One final comparison can be made with respect to the observed behavior when diffusion is possibly controlling. Run 2/7 is related to Runs 2/8 and 2/9 as the catalyst had the same annealing treatment. This one run, however, had 87 small crystals distributed in 5 piles (see Appendix E). The exit concentrations for this series of runs is represented in Figure 4.1. One can see at the highest temperature that some of the temperature sensitivity has been lost in Run 2/7. This lack of dependence on temperature is characteristic of a diffusion controlled reaction. The behavior of the logarithm of the pseudo rate constant versus reciprocal absolute temperature is different from either Runs 2/8 or 2/9. Because of the agreement of the activation energy in Runs 2/8 and 2/9 and the lower value observed in Run 2/7, it is evident diffusion is occurring in this particular run.

6. Reproducibility

In treating the data it is helpful to know the reproducibility of each point. In the least squares fit of the data an estimate of the sample

variance was included in the calculations. These values are reported in Appendix M along with the constants that give the best fit using the criteria given by Hall and Canfield (50).

Experimentally it was found that for a given catalyst it was possible to reproduce the value of C in Equation 26 for a given temperature almost exactly, regardless of when the two runs were made. This can be seen by looking at the raw data in Appendix L or the graphical representation of this information such as Figure 4.1.

More interesting is the comparison of crystals that have had the same thermal treatment. Runs 2/7 through 2/9 have already been mentioned. These two runs have the same activation energy. The activation energies of Runs 2/1 and 2/11 are 4.32 and 6.85 kcal/g-mole, respectively. The only difference between these runs is that Run 2/1 had the smoothed production edges (undefined) while Run 2/11 used the same crystal after the edges had been cleaved. By plotting the exit concentration parameter, C , versus temperature, T , the conversion curve, it is found that the two catalytic lines have essentially the same slope. In this series the new edges were not re-annealed so the observed activation energy should not be expected to be the same.

Run 2/5 consisted of using the same catalyst as in Run 2/2 after several weeks of storage, an ethanol rinse, and an activation in hydrogen peroxide vapor (Run 2/4). The activation energy observed in Run 2/2 was 14.39 kcal/g-mole, while in Run 2/5, 9.80 kcal/g-mole.

It has been shown by Ross (119) that hydrogen peroxide reduces the black NiO surface. This same effect was observed in Runs 2/1 through 2/6 where the rough, undefined edge was on the perimeter of the well defined face. This rough edge would change to a greenish black color after exposure to hydrogen peroxide vapor. Where only cleaved edges existed this effect was not observed visually. Also, the results of Runs 2/8 and 2/9 show no such change in activation with time of exposure to the hydrogen peroxide vapor. Thus, one must look for another cause for the activation energy change.

Ho (64) has found that when a freshly annealed NiO surface is rinsed with ethanol a stain forms on the surface of the crystal that is quite difficult to remove. This suggests that the reaction may be complicated by the presence of some other material adsorbed on the surface.

In Run 2/6 the undefined edges of the same catalyst used above was coated with Kel-F. After firing, care was taken to remove the Kel-F visible on the surface of the crystal with an Exacto blade. It was observed that the undefined edge definitely had a complete covering of Kel-F. Kinetic measurements were made, and the parameters calculated. The data indicated that within experimental error no significant conversion had taken place. Since only the crystal's edges were covered, a majority of the surface was still exposed. This led to the conclusion that: (1) Kel-F is a very effective masking agent, (2) this Kel-F

acts as a poison with respect to the vapor decomposition of hydrogen peroxide, and (3) the key to its effectiveness may well be the strong adherence of the Kel-F film or the solvent used such as observed with ethanol.

In summary, within a run the kinetic data are reproducible. If the catalyst is removed and replaced, one expects the same temperature coefficient will be observed unless the surface is contaminated. This occurs easily and films are formed on the surface by water, acetone, nitric acid, and ethanol (64).

B. Electronic Characterization of Catalyst

1. Electrical Conductivity

Extensive electrical measurements were made using the cell described in section C.1 of Chapter III. The logarithm of the resistance measured versus the reciprocal of the absolute temperature in degrees Kelvin were plotted and fitted with a straight line by the method of least squares. The typical behavior is shown in Figure 4.6. These measurements were made on random samples from each of the sets of catalyst after the kinetic runs were made. Table 4.5 lists the resistivity temperature coefficient and the standard deviation (in parenthesis), in electron volts, according to catalytic run group.

Comparing these values with the heat treatment temperature specified in Table 3.2 resulted in Figure 4.7. This figure brings out

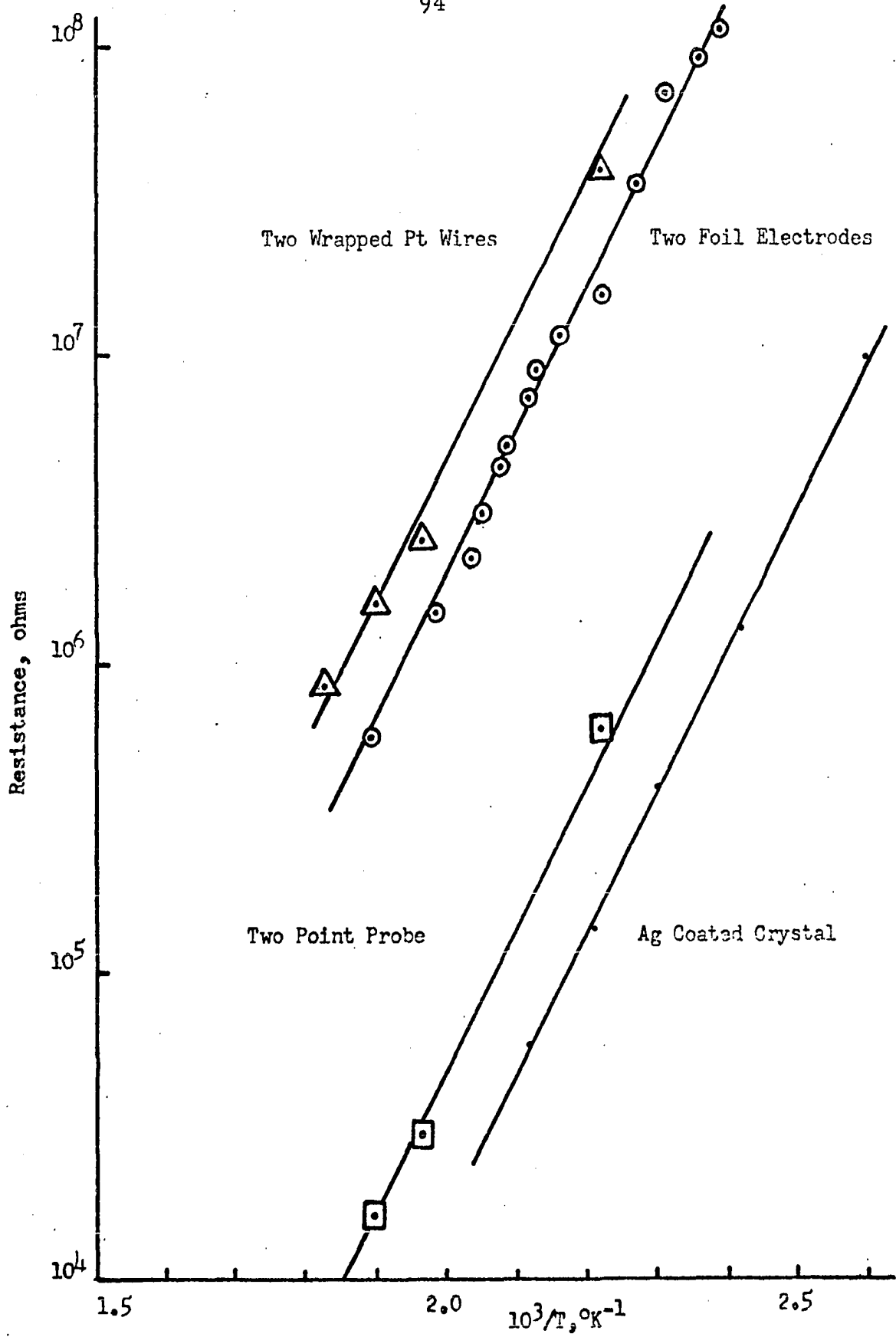


Figure 4.6. Temperature Dependence of Resistance for NiO.

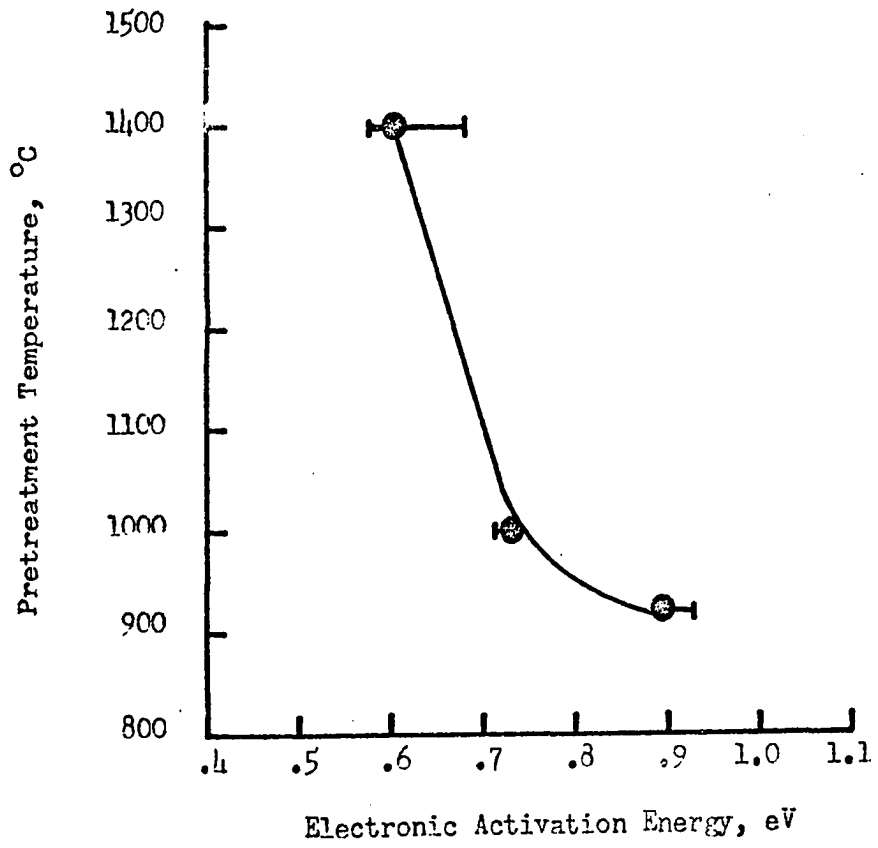


Figure 4.7. Annealing Temperature vs. Electronic Activation Energy of NiO.

the fact that the temperature coefficient is strongly dependent on the heat treatment temperature. Cooling rates and oxygen partial pressures of Runs 2/7-9 and 2/12, as well as 2/10 and 2/13, are not controlling factors under the chosen conditions. The observed temperature coefficients fall within the range of those previously reported in Chapter II, Section 3. Electrical characterization was attempted only on the catalysts which had well defined surfaces.

TABLE 4.5

RESISTIVITY TEMPERATURE COEFFICIENTS OF NiO
CRYSTALS, ELECTRON VOLTS

Temperature Range: 25° to 205° C				
Crystal 2/7-9	Crystal 2/10	Crystal 2/11	Crystal 2/12	Crystal 2/13
.894(.010)*	.598(.070)	.716(.009)	.929(.021)	.598(.022)
.814(.024)	.591(.105)*	.718(.014)	.925(.006)*	.604(.026)
	.660(.021)	.713(.008)	.930(.019)	
	.630(.023)			
	.630(.021)			
	.681(.028)			

*Obtained with Ag paste applied.

To obtain resistivity values from this cell it was necessary to apply silver paste to two opposite faces in order to know the cross sectional

area. This introduces an unknown contact resistance. If it is assumed that the effect is the same in all cases, the resistivities calculated from the measured resistances will be useful on a comparative basis.

2. Comparison with Two-Point Probe

The comparison of the resistivities with those in the literature should be done on the basis of the two-point probe results. The experimental points using the procedure outlined in Chapter III, Section C2, have been plotted on Figure 2.1. The experimental results fall within the previously reported low temperature results. When comparing the two-point probe measurement with resistance measurements between the two platinum electrodes one notes that the temperature coefficient of the resistivities are the same (see Figure 4.6).

3. Estimation of the Concentration of Nickel Vacancies

Ideally it would be possible to obtain the nickel vacancy concentration by analytical techniques. Iodometric determinations have been used frequently on sintered specimens to obtain both surface and bulk concentration (14, 21, 28, 105). The dimethylglyoxime method can also be used (112). One problem in using these techniques in single crystal work is in putting the sample into solution in a quantitative manner. It was found that the nickel oxide single crystal would not readily dissolve in boiling phosphoric acid, hydrochloric acid, nitric acid or aqua regia. Errors in determining the excess oxygen by the determination

of nickel have been mentioned by Haber (47). The quantitative analysis work done in the literature has, as far as the author knows, all been done with solid mass spectrographs, on single crystals.

From the implications of Mitoff's work and the similarity evident in comparing the work of various authors, over all the temperature regions, it seemed reasonable to estimate the vacancy concentration based only on electrical measurements. The same ideas have apparently been applied by Herbst and Friedbery (63) using sintered specimens and obtaining the relative stoichiometry from a relation between the intermediate and equilibrium region.

The derivation of the equations used to obtain an estimate of the defect concentration is given in Appendix A. The inherent assumption in both Appendices A and I seems reasonable on the basis of existing data. Further studies may indicate some of the values assumed are in error, requiring the numerical results to be modified. Relative values give the most reasonable interpretation of the estimates based on the sample for which the two-point probe measurements have also been made. Table 4.6 gives the relative vacancy concentrations with respect to the sample from Run 2/12.

TABLE 4.6

ESTIMATION OF THE RELATIVE Ni VACANCIES

Run	$Ni_{\square}/(Ni_{\square})_e$
2/7-9	280
2/10	76
2/11	39.9
2/12	1.0
2/13	no measurement made

These values were calculated using the equations in Appendix A, taking the average of the resistivity temperature coefficients in Table 4.5. The vacancy concentration in Run 2/12 was calculated to be 8.29×10^{-6} atoms per molecule NiO.

4. Room Temperature Measurements of Resistance

The only successful room temperature electrical measurements made were with the apparatus shown in Figure 3.7 using silver paste electrodes. Resistance was measured with a Keithley 610A electrometer. The resistance reading on the crystals using copper pressure contacts showed a large variation in scale reading depending on the electrometer setting. Some typical results are given below.

Resistance of NiO Single Crystals, ohms
Cu Pressure Contacts

Electrometer Scale	Run 506	Run 507	Run 507
10^7		47	
10^8		6	
10^9	8.5	.72	
10^{10}	1.05	.071	73
10^{11}	.215		11.1
10^{12}	.121		

Resistance was measured between copper pressure contacts of the room temperature Seebeck cell, Figure 3.6, as a function of the position of the contacts on the crystal. On one sample the resistance

varied from 0.15 to 0.98 on the 10^9 scale as the crystal was moved.

The results obtained with the bulk-surface conductivity apparatus were encouraging. The sample used is the same as in the experiments described in Appendix H. The dimensions of the Ag paste electrodes are shown in Figure 3.7. The bulk resistivity was found to be 5.28×10^8 ohm-cm and the surface resistivity to be 724×10^8 ohm-cm. Calculations appear in Appendix S. Two limitations in using this technique are: (1) the crystals can have cross sectional dimension no less than 7.8 mm x 7.8 mm, and (2) these tests are destructive in that the Ag electrode is expected to leave the surface contaminated even after acid removal.

5. Seebeck Measurements

a. Low temperature. The results obtained with the room temperature Seebeck cell (Figure 3.6) were reproducible. Further, on moving the crystals a change in the Seebeck voltage was measured. This is to be expected from previous results (163). By silver-soldering thermocouples to the electrodes it was found that applying 40 volts to the 23-1/2 watt soldering iron a steady state temperature differential of 16°C was achieved. Several crystal prepared in the same manner as the crystals in the catalytic Run 2/2 gave similar results when tested under these conditions. The observed Seebeck voltage difference with respect to the hot tip ranged from + 0.018 to + .026 volts. The sign indicates that the current carriers have an effective positive charge. The

corresponding Seebeck coefficient is calculated to be + 1117 to 1614 $\mu\text{v}/^{\circ}\text{C}$ at an average temperature of 29.4°C . An unsteady state set of conditions was found almost as effective and more rapid. Applying 100 volts to the soldering iron for 30 seconds and waiting 30 seconds produced a temperature difference of 18°C across the crystal with an average temperature of 33°C . The corresponding Seebeck voltage is taken to be the final voltage reading minus the initial voltage reading. For example, a set of crystals was pretreated by heating in air for four hours at 400°C . A comparison of the resistance and Seebeck voltage measurements is given below. These same catalysts were used in Run 1/0 (Appendix Q) and the same measurements were performed after reaction on one crystal.

<u>Crystal</u>	<u>Resistance ohms $\times 10^{-9}$</u>	<u>V(volts)</u>
a	.22	+ .0395
b	.12	+ .043
c	.12	+ .040
d	.15	+ .039
e	.33	+ .035
a*	.25	+ .044

*after reaction.

The Seebeck coefficient calculated is of the order of $2230 \mu\text{v}/^{\circ}\text{C}$. Nachman has observed Seebeck coefficients ranging from 160 to $700 \mu\text{v}/^{\circ}\text{C}$ at this temperature in air. These measurements indicate that a quantitative

estimate of the Seebeck coefficient cannot be directly obtained with this technique. A measure of the homogeneity of the surface and a verification of the sign of the charge carrier can be made.

b. High temperature. Following the procedure outlined in Chapter III, section C.1, it was possible to measure the Seebeck coefficient as a function of temperature. The calculations appear in Appendix T and the results in Table 4.7.

TABLE 4.7

SEEBECK COEFFICIENTS, $\mu\text{v}/^{\circ}\text{C}$

(Crystal prepared similar to catalyst in Run 2/10
with Ag paste electrode)

Run	111	111	111	112*
Average Temperature, $^{\circ}\text{C}$	137	172	201	210
ΔT , $^{\circ}\text{C}$	12.7	12.1	11.6	10.
θ , $\mu\text{v}/^{\circ}\text{C}$	99.4	90.2 - 99.2	71.2	154.8

* no Ag paste electrodes.

These values are much lower than obtained in the previous section and are in better agreement with the literature (104). It can be seen that if the temperature difference had been determined by the differential method the accuracy of these high temperature results would be expected to be higher. As mentioned elsewhere, however, errors introduced at the platinum-copper junctions can be large. Estimating a 2 or 3 $^{\circ}$ temperature

gradient within a few degrees is not accurate enough. The values in Table 4.7 have been obtained by attempting to correct these steady state measurements by compensation techniques, and were the best obtainable with this system. These measurements were obtained by applying a.c. current to the nichrome wire auxiliary heater. The average temperature was controlled by the voltage applied to the main heater. This work demonstrates that the design is useful as it now is to obtain qualitative information. One concludes that, if junction differentials are avoided by using a sufficient length of wires, that true Seebeck coefficients can be obtained on single crystals in any atmosphere.

C. Correlation between Electrical and Kinetic Properties

The object here is to connect the results obtained in the two previous sections where possible.

In catalysts which exhibit a compensation effect there are two conventional ways of characterizing activity of the catalyst (15). The first method (used in this work) is to compare rate of reaction or conversion at a representative temperature. The other approach is to compare the temperature required to affect a given conversion.

It has been shown that a relationship exists between the electronic activation energy and the annealing temperature. It is of interest to inquire whether a relationship to the activity exists. Figure 4.8 indicates the type of behavior observed for a temperature of 175°C . The

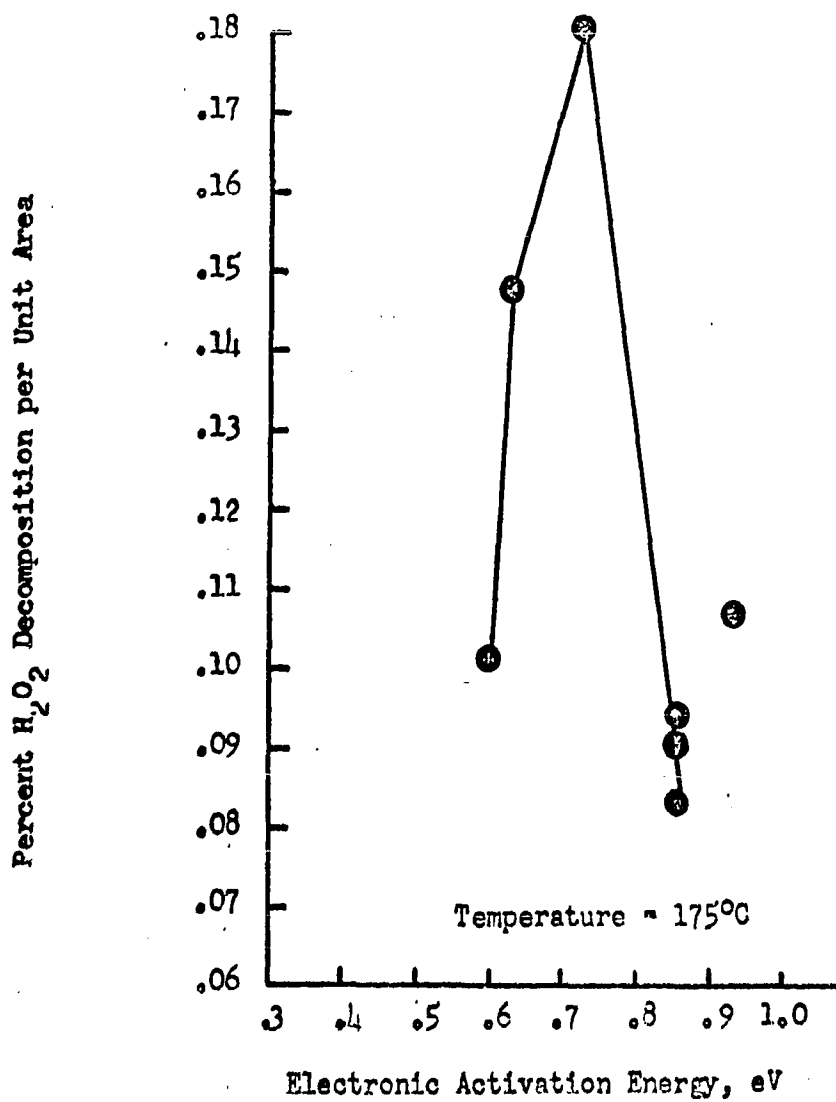


Figure 4.8. Catalytic Activity versus Electronic Activation Energy of NiO.

maximum in activity corresponds to an electronic temperature coefficient of .717 eV and an annealing temperature of 1000°C. On the other hand, no clearly defined trend is observed between the kinetic activation energy and the electronic temperature coefficient.

The electronic activation energy at low temperature is reportedly related to some property of the nickel vacancies present in the crystal (61). The nickel vacancy concentration is related to the conductivity or resistivity of the solid. It will be of interest then to apply the equations developed in Appendix A to relate the catalytic activity to the estimated nickel vacancy concentration. The relative values calculated have been given in Table 4.6.

An attempt must be made to determine if these results are meaningful or not. The only comparison that can be made is with the data of Nachman (104). In Figure 4.9, Nachman's chemically determined nickel vacancy concentration is plotted against the temperature at which he calcined nickel carbonate to form nickel oxide. Since in this study only air annealing was carried out, only one point can be used in the comparison. However, one run was made where the partial pressure of oxygen was only slightly higher than in air. It is shown on Figure 4.9. A straight line connecting Nachman's data is evident and a straight line is also drawn between the data reported here. This suggests that as the temperature of the pretreatment increases, the concentration of nickel vacancies increases. No data on cooling rate is presented in Nachman's

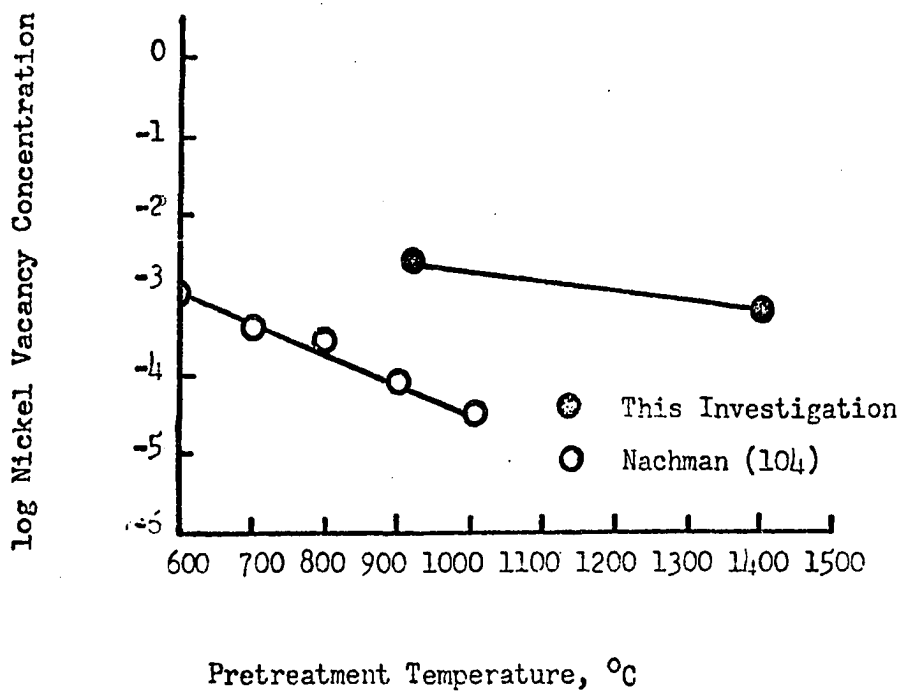


Figure 4.9. Effect of Pretreatment Temperature on Nickel Vacancy Concentration in NiO.

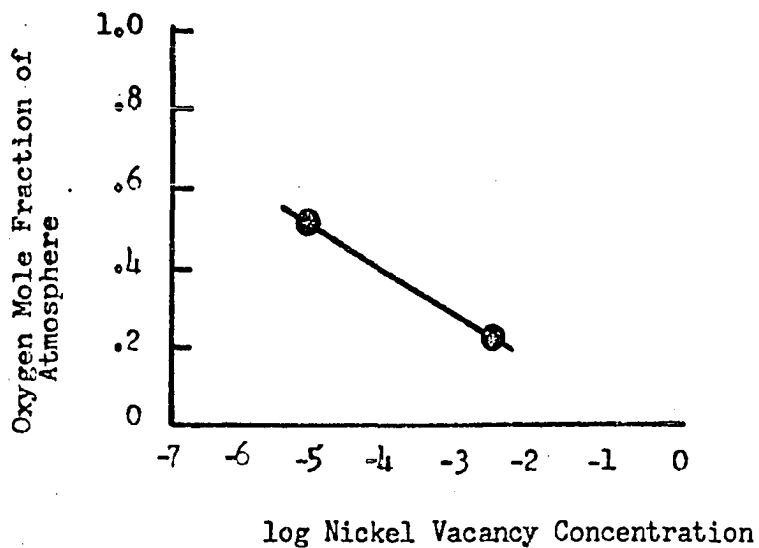


Figure 4.10. Effect of Oxygen Mole Fraction of Atmosphere on Nickel Vacancy Concentration in NiO.

paper. One further pretreatment effect shows that at a given temperature an increase in the oxygen content of the atmosphere decreases the vacancy concentration (see Figure 4.10). Figure 4.11 represents the activity parameter, percent decomposed per unit area, related to the nickel vacancy concentration. Initially there is a temptation to draw a straight line through the points showing an increase in activity with increase in nickel vacancy (as expected from previous work (55, 119)). The data, however, seem to be fitted best by a curve showing a maximum similar to the trend shown with the electronic activation energy. Crystals treated at 1000° and 1400° C show a catalytic activity directly related to the concentration of nickel vacancies.

No clear trend is recognized between the kinetic activation energy against the vacancy concentration.

Because of the tentative nature of some of the equations and interpretation of some of the results in the preceding sections the conclusions that follow must be accepted with those reservations.

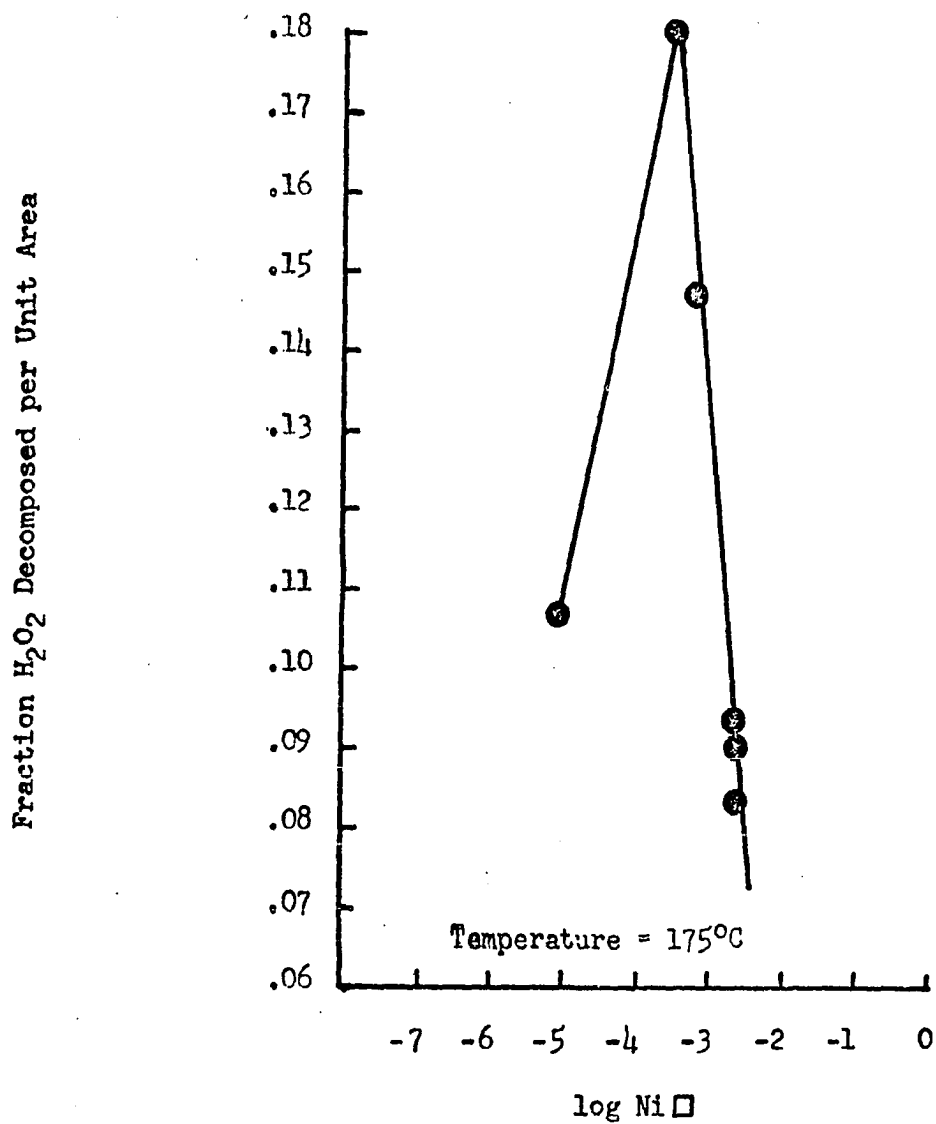


Figure 4.11. Effect of Nickel Vacancy Concentration on Catalytic Activity.

CHAPTER V

CONCLUSIONS

1. The decomposition of hydrogen peroxide vapor has been studied on nickel oxide single crystals with only cleavage planes exposed. The rate of reaction was measured on catalysts with less than two square centimeters total geometric surface area.

2. Using a first order specific rate constant, Arrhenius parameters were found. A correlation effect was shown between the frequency factor and the apparent activation energy for the series of non-stoichiometric catalysts used.

3. The catalytic activity is characterized by the amount of decomposition per unit geometric surface area. This activity is sensitive to the pretreatment of the nickel oxide.

4. Arrhenius type parameters of the resistance of nickel oxide were determined. A relationship between these parameters and the corresponding parameters of the resistivity was observed. The temperature coefficient was related to the pretreatment temperature.

5. A maximum in catalytic activity occurs as the pretreatment of the crystals is changed. It appears that this can be related to the

non-stoichiometry of the crystal. As the number of estimated vacancies increases the activity first increases then decreases.

6. The experimental techniques demonstrated here will prove useful in future studies in which the electrical measurements can be made simultaneously with reaction.

LITERATURE CITED

1. Aigrain, P. and Dugas, C., Z. Electrochem., 56, 363 (1952).
2. Amey, W. and Hamberger, F., "A Method for Evaluating the Surface and Volume Resistance Characteristics of Solid Dielectric Materials," Proc. A. S. T. M., 49, 1079 (1949).
3. A. S. T. M., A. S. T. M. Standards, American Society for Testing and Materials, Philadelphia (1964).
4. Baker, B. E. and Ouellet, C., Can. J. Res., B23, 167 (1945).
5. Balandin, A. A., "New Data on the Multiplet Theory of Catalysis," Catalysis and Chem. Kinetics, ed. Balandin, et. al., Academic Press, New York (1964).
6. Balandin, A. A., Z. Physik. Chem., B2, 288 (1929).
7. de la Banda, J. F. G., "Semiconductivity and Catalytic Activity: The Dehydration of Isopropyl Alcohol on Zr-Cr₂O₃ Catalysts," J. Cat., 1, 136 (1962).
8. Baranskii, P. I. and Lashkarev, V., "Measurement of Bulk Thermal Emf in Germanium," Journal of Tech. Physics (USSR), 27, 1161 (1957).
9. Batta, I., Solymosi, F. and Szabo, Z., "Effect of Spinel Formation on Catalytic Activity and Electrical Properties of NiO-Chromium Oxide System," Kinetics and Catalysis, 5, 737 (1964).
10. Baumback, H. H. and Wagner, C., Z. Physik. Chem., B24, 59 (1934).
11. Baxendale, J. H., "Decomp. of H₂O₂ by Catalysts in Homogeneous Aqueous Solutions," Adv. in Cat., 4, 31 (1952).

12. Berkowitz, A. E. and Greiner, J., "Interactions between Ni and NiO," J. App. Phys., 35, 925 (1964).
13. Bielanski, A., "Some Applications of Electrical Conductivity Measurements to the Investigation of Catalytic Processes on Semi-conducting Oxide Catalysts," Catalysis and Chem. Kinetics, 93, Academic Press, New York (1964).
14. Bielanski, A., "Physico-Chemical Properties of Alkali and Iron Doped NiO," Trans. F. Soc., 58, 166 (1962).
15. Bond, G. C., Catalysis by Metals, Academic Press, New York (1962).
16. Boreskov, G. K., "Theoretical Basis of the Selection, Preparation, and Use of Industrial Catalysis," Proc. Third Intern. Congress on Catalysis, 163, Interscience Pub., New York (1965).
17. Boudart, M., "Correlations in Heterogeneous Catalysis," C. E. P., 57, No. 8, 33 (1961).
18. Bronsted, J., Chem. Rev., 5, 231 (1928); Tran. F. Soc., 34, 1 (1938).
19. Calbick, C., "Electron Microscopy of Glass and Quartz Substrate Surfaces for Thin Films," Trans. 8th An. Vac. Symposium, Pergamon Press, New York (1962).
20. Cech, R. E. and Alessandrini, E., "Preparation of FeO, NiO, and CoO Crystals by Halide Decomposition," Trans. ASM, 51, 150 (1959).
21. Charman, H. B., Dell, R. M. and Teale, S. S., "Chemisorption on Metal Oxides, Pt. I-NiO," Trans. F. Soc., 59, 453 (1963).
22. Choi, J. S. and Moore, W. J., "Diffusion of Ni in Single Crystals of NiO," J. Phys. Chem., 66, 1308 (1962).
23. Cheaney, D. E. and Walsh, A. D., "HF Treatment of Silica and Pyrex Vessels Used for Combustion Studies," Fuel, 35, 258 (1955).
24. Cimino, A., Molinari, E. and Romero, G., "Magnetocatalytic Effects and Electrical Anomalies at the Néel Point of NiO," Z. fur Physikalische Chemie Neue Folge, Bd. 16, 101 (1958).

25. Coue, J., et. al., "Mechanism of Cat. Oxidation of CO on NiO," Proc. Third Congress on Catalysis, 748, Interscience Pub., New York (1965).
26. Cremer, E., "Compensation Effect in Heterogeneous Catalysis," Adv. in Cat., VII, 75 (1955).
27. deBoer, J. H. and Verwey, E., Proc. Phys. Soc. (L), 49, 66 (1937).
28. Deren, J., "Physicochemical and Catalytic Properties of the System Chromium Oxides-Oxygen-Water," J. Cat., 2, 161 (1963).
29. Deren, J., Haber, J. and Stechowski, J., "Influence of Surface Structure of CrO₃-Al₂O₃ Catalysts on the Mechanism of Redox Catalytic Reaction," Proc. Third Intern. Congress on Catalysis, 993, Interscience Pub., New York (1965).
30. Dickens, P. G., "Recombination of Oxygen Atoms on Oxide Surfaces, I. Activation Energies of Recombination," Trans. Far. Soc., 60, 1272 (1964).
31. Dowden, D. A., "Heterogeneous Catalysis, Pt. I. Theoretical Basis," J. Chem. Soc., 153, 242 (1950).
32. Dunlap, Jr., W. C., "Conductivity Measurements on Solids," Methods of Experimental Physics, 6B, ed. Lark-Horovitz, et. al., 32, Academic Press, New York (1959).
33. Ebisuzaki, Y., "Preparation of Monocrystalline Cuprous Oxide," J. App. Phys., 32, 2027 (1961).
34. Ehrlich, G., "Chemisorption on Solids," Proc. Third Congress on Catalysis, 113, Interscience Pub., New York (1965).
35. Emmett, P. H., "Measurement of Surface Area of Solid Catalysts," Catalysis, ed. Emmett, 31 (1954).
36. Eror, Jr., N. G., "Electrical Conductivity and Thermogravimetric Studies on CoO, NiO, and MnO," Ph.D. Thesis, Northwestern University, Evanston (1965).
37. Foex, M., Compt. Rend., 227, 193 (1948).
38. Garrett, C. G. B., "Quantitative Considerations Concerning Catalysis at Semiconductor Surfaces," J. Chem. Phys., 33, 966 (1960).

39. Giguere, P. A. and Liv, I. D., "Kinetics of Thermal Decomposition of Hydrogen Peroxide Vapor," Can. J. Chem., 35, 283 (1957).
40. Giguere, P. A., "Thermal Decomposition of H₂O₂ Vapor," Can. J. Res., 25B, 135 (1947).
41. Golodets, G., "Utilization of Thermodynamic Characteristics of Substances and Reactions in the Selection of Catalysts," Intern. Chem. E., 4, 632 (1964).
42. Gray, T. S., "Semiconductivity and Catalysis in the NiO System," J. Phys. Chem., 60, 209 (1956).
43. Gray, T. J., "Defect Structure and Catalysis," The Defect Solid State, ed. Gray, Interscience Pub., 239 (1957).
44. Gray, T. J., Garner, W. and Stone, F., Proc. Roy. Soc., A197, 294 (1949).
45. Grimley, R. T., Burns, R. and Inghram, M., "Thermodynamics of the Vaporization of NiO," J. Chem. Phys., 35, 551 (1961).
46. Haber, J. and Stone, F. S., "Crystal Field Effects in the Adsorption and Desorption of Oxygen at a NiO Surface," Trans. F. Soc., 59, 192 (1963).
47. Haber, J., "Discussion," Proc. Third Congress of Catalysis, 789, Interscience Pub., New York (1965).
48. Haensel, V., "Industrial Catalysis," I. E. C., 57, No. 6, 19 (1965).
49. Hall, J. W., "Effect of Dislocations in Catalysis," Ph. D. Dissertation, University of Texas, Austin (1963).
50. Hall, K. R. and Canfield, F. B., "Optimal Recovery of Virial Coefficients from Experimental Compressibility Data," to be published, Physica, 1966.
51. Hanson, R. A., I. E. C., 49, 1523 (1957).
52. Harman, T. C., "Measurement of Thermoelectric Materials and Devices," Semiconductor Products, Sept. (1963).
53. Harris, E. J., Trans. Far. Soc., 44, 764 (1948).

54. Hart, A. B. and Ross, R. A., "Catalytic Decomposition of Hydrogen Peroxide by Equimolar Mixed Oxides," Nature, 193, 1175 (1962).
55. Hart, A. B., McFadyen, J. and Ross, R. A., "Solid State Oxide Catalyzed Decomposition of H₂O₂ Vapor," Trans. Far. Soc., 59, 1458 (1963).
56. Hauffe, K., "Gas Reactions on Semiconducting Surfaces and Space Charge Boundary Layers," Semiconductor Surface Physics, ed. R. H. Kingston, University of Pennsylvania Press (1957).
57. Hauffe, K., Glang, R. and Engell, H., Z. Physik. Chem. (Leipzig), 201, 223 (1952).
58. Hauffe, K., Z. Phys., 113, 367 (1939); 118, 539 (1942).
59. Hauffe, K., "Role of Electrons, Holes, and Lattice Defects in Heterogeneous Catalysis," An Real Soc. Esp. Fis. Quim., LXI(B), 277 (1965).
60. Hauffe, K., "Reactions of Electrons and Lattice Defects with CO at NiO and ZnO Surfaces," Transition Metal Compounds, ed. E. R. Schatz, 37, Gordon and Breach, New York (1964).
61. Heikes, R. R., "Electron Transport Properties of Transition Metal Compounds," J. Pure and App. Chem., 7, 407 (1963).
62. Heikes, R. R. and Johnston, W., "Mechanism of Conduction in Li-Substituted Transition Metal Oxides," J. Chem. Phys., 26, 582 (1957).
63. Herbst, R. J. and Friedberg, A. L., "Mechanical Characteristics of Polycrystalline NiO," Ceramic Eng. Annual Prog. Report 2, Univ. Illinois, Sept. (1962).
64. Ho, Lee, Unpublished Results, University of Oklahoma, Norman (1966).
65. Hoarse, D. E., et. al., "Thermal Decomposition of H₂O₂ Vapor," Trans. Far. Soc., 55, 548 (1959).
66. Hogarth, C. A., "Some Conduction Properties of Oxides of Cd and Ni," Proc. Phys. Soc. (L), 64B, 691 (1951).

67. Honig, J. M. "Electrical Properties of Metal Oxides which have Hopping Charge Carriers," J. Chem. Ed., 43, 76 (1966).
68. Hubbard, J., "Correlation Effects in Partially Filled Narrow Bands," Transition Metal Compounds, ed. E. Schatz, Gordon and Breach, New York (1964).
69. Huston, A. R., "Semiconducting Properties of Some Oxides and Sulfides," Semiconductors, ed. N. B. Hannay, Reinhold Pub. Co., 541 (1959).
70. Jongepier, R. and Schuit, G., "Photodesorption from a NiO Surface," J. Cat., 3, 464 (1964).
71. Keating, K., "Effect of Deformation on Cat. Activity of Pt on Decomposition of H_2O_2 ," J. Cat., 4, 608 (1965).
72. Keier, N. P., Kinetics and Catalysis, 1, 74 (1959).
73. Keier, N. P., "Regularities of Catalysis on Chelate Polymers," Proc. Third Congress on Catalysis, 1021, Interscience Pub., New York (1965).
74. Klier, K., "Spectra of Pure NiO and NiO with Adsorbed Gases," Kinetics and Catalysis, 3, 51 (1962).
75. Klier, K. and Jiratora, K., "Interaction of Gases in the Surface of NiO," Proc. Third Congress on Catalysis, 763, Interscience Pub., New York (1965).
76. Kobozev, N. I., Krilova, L. and Shashkov, A., "Effect of Electron Properties of Support upon Exo-Electron Emission and Catalysis," Proc. Third Congress on Catalysis, 614, Interscience Pub., New York (1965).
77. Koide, S., "Electrical Properties of $Li_xNi_{(1-x)}O$ Single Crystals," J. Phy. Soc., Japan, 20, 123 (1965).
78. Kondoh, H. and Takeda, T., "Observation of Antiferromagnetic Domains in NiO," J. Phys. Soc., Japan, 19, 11 (1964).
79. Kotel'nikov, V. A., "On the Photodesorption of Oxygen from a NiO Surface," Kinetics and Catalysis, 5, 498 (1964).

80. Kozawa, A. and Yeager, E., "The Electrochemistry of Oxygen on NiO," AD-615495 Tech. Report 1, Nov. 1964; A. Adams, et. al., Fuel Cells, ed. W. Mitchell, 158, Academic Press, New York (1963).
81. Kroger, F. A. and Vink, H. J., "Relationship between the Concentration of Imperfections in Crystalline Solids," Solid State Physics, 3, 307 (1956).
82. Ksendzov, Ya. M., et. al., "Investigation of the Carrier Mobility in NiO with Li Impurity," Soviet Physics-Solid State, 5, 1116 (1963).
83. Kuchynka, K., "Mechanism of Cat. Decomp. of Nitrous Oxide on NiO; 1. Adsorption of Reactant and Formation of Oxygen Ions; 2. Rate Limiting Step," Coll. Czech. Chem. Comm., 30, 613 (1965).
84. Kuchynka, K. and Klier, K., "Adsorption of Oxygen on NiO Low Pressures," Coll. Czech. Chem. Comm., 28, 148 (1963).
85. Laidler, K. J., Chemical Kinetics, McGraw-Hill, New York (1965).
86. Laidler, K. J. Glasstone S. and Eyring, H., J. Chem. Phys., 8, 667 (1940).
87. Langmuir, I., J. Am. Chem. Soc., 40, 1361 (1918).
88. Law, J. T., "Semiconductor Surfaces," Semiconductors, ed. N. B. Hannay, Reinhold Pub. Co., 699 (1959).
89. Lee, V. J., "The Charge Transfer Theory of Gas-Surface Interactions and Heterogeneous Catalysis on Semiconductors," Ph.D. Dissertation, University of Michigan (1963).
90. Lee, V. J., "The Charge Transfer Theory of Heterogeneous Catalysis on Semiconductors," Proc. Third Intern. Congress on Catalysis, 556, Interscience Pub., New York (1965).
91. Lennard-Jones, J., Tran. Far. Soc., 28, 333 (1932).
92. Mackenzie, R. C., Ritchie, M., Proc. Roy. Soc. (L), A185, 207 (1946).
93. Matsuura, I., Kubokawa, Y. and Toyama, O., "Decomposition of H₂O₂ on ZnO and NiO," J. Chem. Soc., Japan, 81, 1209 (1960).

94. McKee, D. W., "Oxidation of Propane by Doped NiO," Nature, 202, 177 (1964).
95. McLane, C., J. Chem. Phys., 17, 379 (1949).
96. Minnesota Mining and Manufacturing Co., "Kel-F Brand Plastic Dispersions-Technical Data Sheets."
97. Mitoff, S. P., "Electrical Conductivity and Thermodynamic Equilibrium in NiO," J. Chem. Phys., 35, 882 (1961).
98. Mitoff, S. P., "Bulk Versus Surface Conductivity of MgO," J. Chem. Phys., 41, 2561 (1964).
99. Morin, F. J., "Oxides of the 3d Transition Metals," Semiconductors, ed. N. B. Hannay, Reinhold Pub. Co., 600 (1959).
100. Morin, F. J., "Electrical Properties of NiO," Phys. Rev., 93, 1199 (1954).
101. Morooka, Y. and Azaki, A., "Regularities in Catalytic Prop. of Metal Oxides in Propylene Oxidation," J. Cat., 5, 116 (1966).
102. Mott, N. F., Proc. Phys. Soc., A62, 416 (1949); Phil. Mag., 6, 287 (1961).
103. Mott, N. F. and Gurney, P., Electronic Processes in Ionic Crystals, Oxford (1940); Dover (1964).
104. Nachman, M., Cojocaru, L., and Ribco, L., "Electrical Properties of Non-Stoichiometric NiO," Phys. stat. sol., 8, 773 (1965).
105. Nachman, M., et. al., J. Phys. Chem. Solids, 20, 307 (1961).
106. Nyrop, J. E., "Surface Electrons," Phys. Rev., 39, 967 (1932).
107. O'Keefe, M. and Moore, W. J., "Electrical Conductivity of Monocrystalline Cuprous Oxide," J. Chem. Phys., 35, 1324 (1961).
108. Pariisky, G. B. and Kasansky, V., "The ESR Study of Free Radicals Adsorbed on Catalysts," Proc. Third Congress on Catalysis, 367, Interscience Pub., New York (1965).
109. Parravano, G., "Thermoelectric Behavior of NiO," J. Chem. Phys., 23, 5 (1955).

110. Parravano, G. and Domenicali, C., "Thermoelectric Behavior of Solid Particulate Systems NiO," J. Chem. Phys., 26, 359 (1957).
111. Peters, D. W., Feinstein, L. and Peltzer, C., "High Temperature Electrical Conductivity of Alumina," J. Chem. Phys., 42, 2345 (1965).
112. Pierce, W. C. and Haenisch, E., Quantitative Analysis, 3rd ed., John Wiley (1954); Pierce, Haenisch, and Sawyer; 4th ed., Chapman and Hall (1958).
113. Price, J. B., Private Communication, Northwestern University, Evanston, Illinois (1965).
114. Pollard, W. G., "Use of Surface States to Explain Activated Adsorption," Phys. Rev., 56, 325 (1939).
115. Roeser, W. F., "Thermocouple Thermometry," NBS Handbook 77, II, 68, National Bureau of Standards (1961).
116. Roginskii, S. Z., Z. Physik. Chem., A138, 21 (1928).
117. Rosner, D. E., "The Apparent Chemical Kinetics of Surface Reactions in External Flow Systems: Diffusional Falsification of Activation Energy and Reaction Order," A. I. Ch. E., 9, 321 (1963).
118. Ross, R. A. and Hart, A. B., "The Catalytic Decomposition of Hydrogen Peroxide Vapor by NiO and Promoted NiO," J. Cat., 2, 251 (1963).
119. Ross, R. A., "The Catalytic Decomposition of Hydrogen Peroxide Vapor on Metallic Oxides," Ph.D. Thesis, The University, Glasgow (1957).
120. Roth, W. L., J. Appl. Phys., 31, 2000 (1960).
121. Rouse, T. O. and Weininger, J. L., "Electrochemical Studies of Single Crystals of Lithiated NiO," J. E. S., 113, 184 (1966).
122. Sabatier, P., Compt. rend., 135, 87 (1902).
123. Saito, S., "X-Ray Diffraction Micrographs on Twin Structure of Antiferromagnetic NiO," J. Phy. Soc., Japan, 17, 1287 (1962).

124. Saltsburg, H., Snowden, D. and Garrison, M., "Transient Ionic Species Resulting from Gas-Solid Interactions: Oxygen Adsorption on NiO," J. Phys. Chem., 68, 3765 (1964); "Transient Oxygen Species on NiO Single Crystal Surfaces," Surface Sci., 2, 288 (1964).
125. Satterfield, C. N. and Yeung, R. S. C., "Diffusion and Heterogeneous Reaction in a Tubular Reactor. The Decomposition of Hydrogen Peroxide Vapor," I. E. C. Fundamentals, 2, 257 (1963).
126. Satterfield, C. N. and Stein, T. W., "Decomposition of Hydrogen Peroxide Vapor on Relatively Inert Surfaces," I. E. C., 49, 1173 (1957).
127. Schatz, E. R., ed., "Informal Proc. of the Buhl International Conference on Materials-- Transition Metal Compounds--Transport and Magnetic Properties," Gordon and Breach, New York (1964).
128. Schuit, G. C. A., "A Summary of Opinions on Heterogeneous Catalysis," An. Real Soc. Exp. Fis. Quim., LXI(B), 475 (1965).
129. Schumb, W. C., Hydrogen Peroxide, Reinhold Pub. Co., New York (1955).
130. Schwab, G. B., "Conductivity and Surface Chemistry of Crystals," Angewandte Chemie, Intern. Ed., 2, 59 (1963).
131. Schwab, G. B., "Experiments Connecting Semiconductor Properties and Catalysis," Semiconductor Surface Physics, ed. R. H. Kingston, 283, Univ. Penna. (1957).
132. Schwab, G. B. and Gossner, K., "Heterogeneous Catalysis," Annual Rev. Phy. Chem., 14, 177 (1963).
133. Slack, G. A., "Crystallography and Domain Walls in Antiferromagnetic NiO Crystals," J. App. Phys., 31, 1571 (1960).
134. Snowden, D. P. and Saltsburg, H., "Hopping Conduction in NiO," Phy. Rev. Letters, 14, 497 (1965).
135. Squires, R. G. and Parravano, G., "Hydrogen Deuterium Exchange Reaction on Cobalt Ferrite," J. Cat., 2, 324 (1963).
136. Stone, F. S., "Chemisorption and Catalysis on Metal Oxides," Adv. in Cat., 13, 1, (1962).

137. Stone, F. S., "Chemisorption on Semiconductors," Chemisorption, ed., Garner, Academic Press (1958).
138. Swalin, R. A., Thermodynamics of Solids, John Wiley, New York (1962).
139. Takeda, T. and Kondoh, H., "Chemical Etch Pits of NiO Crystal Annealed at High Temperature," J. Phy. Soc., Japan, 17, 1315 (1962).
140. Takuro, N., et. al., "Antiferromagnetic Magnetostriction in CoO and NiO Single Crystals," J. Phys. Soc., Japan, 17, Supp. B-1, 214 (1962).
141. Taylor, H. S., Proc. Roy. Soc., A108, 105 (1925).
142. Tichane, R., "Cleaning Processes for Borosilicate Glass," J. Am. Cer. Soc., 42, 441 (1963).
143. Thomas, F. L., "Precision Resistors and Their Measurement," NBS Handbook 77, Vol. 1, National Bureau of Standards (1961).
144. Thomas, W. J., Tran. Frad. Soc., 55, 624 (1959).
145. Thornton, H. R., "Effect of Grain Boundaries on the Electrical Conductivity of NiO," Ph. D. Thesis, University of Illinois, Urbana (1963).
146. Uhara, I., et. al., "Dislocations as Active Centers of Catalysis and Chemical Action in Ag.," J. Phys. Chem., 69, 880 (1965).
147. Uhara, I., "Structure of Active Centers in Ni Cat.," J. Phys. Chem., 67, 996 (1963).
148. Valdes, L. B., "Resistivity Measurements on Ge for Transistors," Proc. I.R.E., 42, 420 (1954).
149. Vanderslice, T. A., et. al., "Detection of Helium in Silicon by Cleavage in a High Vacuum," G. E. Res. Lab. Report No. 63-RL-3519E (Nov. 1963).
150. Van Houten, S., "Semiconduction in $\text{Li}_x\text{Ni}_{(1-x)}\text{O}$," J. Phys. Chem. Solids, 17, 7 (1960).

151. Van Houten, S., "Mechanical and Dielectric Relaxation in Transition Metal Oxides," Transition Metal Compounds, ed. E. Schatz, Gordon and Breach, New York (1964).
152. Verneuil, A., Compt. Rend., 135, 791 (1902).
153. Volkenstein, F. F., The Electron Theory of Catalysis on Semiconductors, Adv. Cat., 12, 189 (1960); Macmillan Co. (1963).
154. Volkenstein, F. F., J. Chem. Fiz. (USSR), 24, 9 (1950).
155. Wagner, C. and Hauffe, K., Z. Electrochem., 44, 172 (1938).
156. Walsh, A. D., "The Mode of Action of Anti-Knocks," Low Temperature Oxidation, ed. W. Jost, 283, Gordon and Breach, New York (1961); 7th Symposium on Combustion, 183, Butterworths Sci. Pub. (1959).
157. Weisz, P. B., "Effects of Electronic Charge Transfer between Adsorbate and Solid on Chemisorption and Catalysis," J. Chem. Phys., 21, 1531 (1953).
158. Winter, E. R. S., "Decomposition of Nitrous Oxide upon Doped NiO," Dis. Far. Soc., 28, 183 (1959).
159. Wright, R. W. and Andrews, J., "Temperature Variation of Electrical Properties of NiO," Proc. Phys. Soc. (L), 62A, 446 (1949).
160. Yamaka, E. and Sawamoto, K., "Electrical Conductivity of NiO near the Curie Temp.," Phys. Rev., 112, 1861 (1958).
161. Yamashita, J., "Electronic Structure of TiO and NiO," J. Phys. Soc. Japan, 18, 1010 (1963); "Band Picture or Localized Model," Transition Metal Compounds, Gordon and Breach (1964).
162. Yeung, S. C., "Decomposition of H₂O₂ Vapor in Tubular Reactor," Ph.D. Thesis, M.I.T. (1959).
163. Zhuravlev, V. A. and Kolosova, L., "The Relationship between the Distribution of Thermoelectromotive Force on the Surface of Cupric Oxide and its Catalytic Activity," Kinetics and Catalysis, 5, 260 (1964).

164. Zhuravlev, V. A., Kozak, M. and Kuzhelyuk, A., "Relationship between Catalytic Activity and Work Function of Semiconducting Catalysts during Aging," Kinetics and Catalysis, 4, 269 (1963).
165. Zhuze, V. P. and Shelykh, A., "Hall Effect in NiO," Soviet Physics-Solid State, 5, 1278 (1963).
166. Zirin, M. H. and Trivich, D., "Thermoelectric Effect in Single Crystal Cuprous Oxide at High Temp.," J. Chem. Phys., 39, 870 (1963).

NOMENCLATURE

- A = cross sectional area, (centimeters)².
- A_s = geometric surface area, (centimeters)².
- C = exit concentration parameter, ml standardized KMnO₄
(seconds)⁻¹10³.
- D = moles H₂O₂ decomposed on NiO per mole H₂O₂ in feed.
- D = Fick diffusivity, (centimeters)² per second.
- E = activation energy low temperature conductivity.
- E_{apparent} = apparent activation energy, kcal/g-mole.
- E_f = Fermi level.
- E_i = impurity energy level.
- E₃₋₄ = EMF between two conductivity probes, volts.
- e = electronic charge, coulombs per carrier.
- F = flow rate of nitrogen carrier gas, cubic centimeters per
minute.
- G = electronic activation energy, electron volts.
- k = Boltzmann's constant.
- k = specific rate constant, centimeters per second.

- k_0 = frequency factor, centimeters per second.
 l = length between two point probes.
 N = carrier concentration, carriers per cubic centimeter.
 N = normality.
 $Ni\Box$ = nickel vacancies, atoms per molecule NiO.
 (Ni^{3+}) = electron hole concentration, carriers per cubic centimeter.
 \bar{P} = partial pressure.
 P_p^o = vapor pressure of anhydrous hydrogen peroxide.
 R = gas constant.
 R = rate of reaction, moles H_2O_2 decomposed per unit time per unit geometric surface area.
 \bar{R} = overall rate factor, defined by equation 40.
 S^2 = variance.
 t = thickness of NiO crystal.
 t = temperature, degrees centigrade.
 T = absolute temperature, degrees Kelvin.
 T_i = temperature of i -th conductivity region, degrees Kelvin.
 T_i^* = transition temperature of i -th conductivity region, degrees Kelvin.
 $Y_{H_2O_2}$ = mole fraction hydrogen peroxide in vapor.
 α = proportional to.
 γ_p = activity coefficient of hydrogen peroxide.

ΔE	=	Seebeck voltage, microvolts.
ΔT	=	temperature across crystal, degrees centigrade.
θ	=	Seebeck coefficient, microvolts per degree centigrade.
μ	=	carrier mobility, (centimeter) ² per volt second.
π	=	Peltier coefficient.
π	=	total pressure.
ρ	=	density of crystal, grams (centimeters) ⁻³ .
ρ	=	electrical resistivity, ohm-cm.
σ	=	electrical conductivity, (ohm-cm) ⁻¹ .
Φ	=	electronic work function.

Subscripts

c	=	after chemisorption.
D	=	donor.
e	=	nickel vacancy concentration of run 2/12.
E	=	equilibrium conductivity region.
H	=	kinetic parameter obtained on glass and NiO surface.
I	=	intermediate conductivity region.
L	=	low temperature conductivity region.
o	=	before chemisorption.
R	=	kinetic parameter obtained on glass surface at 24 ^o C.
W	=	kinetic parameter obtained on glass surface.

APPENDIX A

DERIVATION OF RELATION BETWEEN CONDUCTIVITY PARAMETERS AND NICKEL VACANCY CONCENTRATION

Basic in this derivation are the results of Mitoff (97). The equation relating the nickel vacancy concentration to the absolute temperature in the equilibrium region in air is:

$$\text{Ni}\square = 0.848 \exp(-8963/T^{\circ}\text{K}) \quad (41)$$

In general the electrical conductivity, σ , can be written:

$$\sigma_i = C_i \exp\left(\frac{-\Delta G_i}{kT}\right) \quad (42)$$

where C = constant temperature coefficient

G = temperature coefficient of the i -th conductivity region

k = Boltzmann constant

T = Temperature, $^{\circ}\text{K}$

i = E- equilibrium region

I- intermediate region

L- low temperature region

At the equilibrium transition temperature T_E , $\sigma_E = \sigma_I$. Using equation

(42) an expression can be written for C_I in terms of C_E , ΔG_E , ΔG_I , and T_E . At the low temperature transition temperature, T_T , $\sigma_I = \sigma_L$. Thus an expression can be written relating C_I to C_L , ΔG_L , ΔG_I , and T_T .

Elimination of C_I gives:

$$\frac{C_E}{C_L} = \frac{\exp\left(\frac{-\Delta G_L}{kT_T}\right) \exp\left(\frac{-\Delta G_I}{kT_E}\right)}{\exp\left(\frac{-\Delta G_I}{kT_T}\right) \exp\left(\frac{-\Delta G_E}{kT_E}\right)} \quad (43)$$

Expressions for C_E and C_L can be obtained using equation(42) for the condition that the conductivity has a value of 1. The temperature corresponding to this point is denoted by T^* , thus:

$$C_E = \exp\left(\frac{\Delta G_E}{kT_E^*}\right) \quad (44)$$

$$C_L = \exp\left(\frac{\Delta G_L}{kT_L^*}\right)$$

Substituting equation(44) into(43) allows one to solve for the equilibrium transition temperature.

$$T_E = \frac{(\Delta G_E - \Delta G_I)}{\frac{\Delta G_E}{T_E^*} - \frac{\Delta G_L}{T_L^*} - \frac{1}{T_T} (\Delta G_I - \Delta G_L)} \quad (45)$$

If this equation can be solved on the basis of experimental results, substitution into equation(41) allows calculation of the vacancy concentration.

Based on the discussion in Chapter II, Section 3, it is reasonable to take $G_E = 1.01$ eV and $G_I = 0.239$ eV. One must then experimentally determine only G_L , T_T , and T_L^* .

The working equation is then:

$$\text{Ni}\square = 0.849 \exp \left[-11625 \left[(.787 \times 10^{-3} \frac{\Delta G_L}{T_L^*}) - \frac{1}{T_T} \left[.239 - \Delta G_L \right] \right] \right] \quad (46)$$

This equation was tested on the data of Nachman (104) on the electrical properties of polycrystalline non-stoichiometric NiO. The parameters needed in equation (46) were determined from conductivity plots presented earlier. The calculated defect concentrations are compared with the reported non-stoichiometry determined chemically as shown in Table A1.

TABLE A1

NICKEL VACANCY CONCENTRATION, ATOMS
PER NiO MOLECULE

Reported (104) $\times 10^4$	Predicted $\times 10^4$	ΔG_L , eV (104)
9.7	17.8	.22
3.7	9.3	.28
2.5	7.7	.35
.7	6.6	.41
.2	7.6	.45

The agreement between the two is remarkably good considering the difference in the materials on which some of the numerical values were obtained.

APPENDIX B

IMPURITY CONCENTRATION OF NiO SINGLE CRYSTALS GROWN BY VERNEUIL METHOD (152)

No quantitative analysis was performed. However, by reviewing the literature a range of impurity concentration can be assumed as follows:

<u>Element</u>	<u>Impurity Concentration, PPM</u>
Ag	0.15 - 5
Al	0.24 - 500
Ca	1 - 50
Co	1 - 500
Cr	5 - 140
Cu	1 - 100
Fe	10 - 4400
K	1 - 27
Mg	5 - 100
Pb	10
S	470
Si	25 - 700
Sn	42

These data are based on the work reported in references 36, 97, 113, and 145 .

APPENDIX C

DEIONIZED DISTILLED WATER

High purity water is of importance in both the analytic work and in cleaning the glassware coming in contact with the hydrogen peroxide. It was, therefore, necessary both to process the water supply available and monitor its quality. The need for water with a specific resistance greater than 2×10^6 ohm-cm to be used in cleaning glassware for stability studies was taken as a guide to the quality of water desired.^a

To monitor the conductivity of the water a flow cell was constructed using a piece of 1/4" O.D. polystyrene tubing. Two pieces of 99.0+ % Ni wire, .08 in diameter, furnished by the E. H. Sargent and Co., were mounted perpendicular to the axis of the plastic tube .63 mm apart. The resistance of the water was determined by allowing it to flow through this cell and reading a Keithley 610A electrometer connected across these nickel electrodes. This resistance was compared with the resistance reading of various water samples using an Industrial

^aSolvay Product Division, "Analysis of Hydrogen Peroxide," Allied Chemical Corporation, Technical Bulletin.

Instruments' CEL-C2 dip cell and a Mueller Cell. This latter cell was designed by Dr. Marvin Mueller and consisted of two specularly finished, gold plated brass plates with a Teflon spacer. The cell constants of both these latter cells were known. Flow cell resistance readings for various samples are as follows:

<u>Water Sample</u>	<u>Resistance, ohms</u>
Distilled followed by Ion-Exchange	8×10^6
Minimum acceptable (corresponds to 2×10^6 ohm-cm)	6.8×10^6
Distilled	2.9×10^6
Tap	0.9×10^6

In all the experimental work water had a resistance of greater than 6.8×10^6 ohms. Production of this water consisted of processing tap water with a Barnstead still and then passing this distilled water through an deionizing column. Amberlite MB-1, furnished by Rohm and Hass Company, was used to deionize the water in a gravity feed column. The deionized distilled water was stored in polyethylene carboys.

APPENDIX D

CALIBRATION OF THERMOCOUPLES

Iron-constantan thermocouples were used to measure the temperature in the high temperature conductivity cell, the 2-point probe cell, the reactor and saturator. Calibration consisted of checking the compensated emf at room temperature and comparing with a standard thermocouple. This standard thermocouple was checked at one point by means of an L and N Type G-2 Mueller Bridge and NBS calibrated platinum resistance thermometer. The temperature was maintained constant with a water bath. The thermocouple emf was measured with L and N K-3 Galvanometer and Electronic Null detector. The zero degree reference junction was designed according to ASTM E 207-62T. The following data were recorded at the calibration point.

Temperature from platinum resistance thermometer using NBS conversion tables	$26.96^{\circ}\text{C} \pm .1^{\circ}\text{C}$
Thermocouple EMF (wrt 0°C)	1.3693 mV
Thermocouple temperature from NBS conversion tables ^b	26.77°C

^bNBS Circular No. 561.

On the basis of these results it is assumed the temperature is known to $\pm .25^{\circ}\text{C}$. If a given thermocouple checks with the reading the standard thermocouple gives when connected to the L and N 8657C portable millivolt indicator, the accuracy is taken to be $\pm .5^{\circ}\text{C}$.

APPENDIX E

LOCATION OF CRYSTALS IN THE TUBE REACTOR

<u>Run</u>	<u>Location (Refer to Figure 3.3a)</u>
2/1	one crystal placed every three inches with respect to reactor inlet, total 3.
2/2	one crystal below each T.C.P., total 3.
2/3	one crystal at center T.C.P.
2/5	one crystal below each T.C.P., total 3.
2/6	one crystal below each T.C.P., total 3.
2/7	83 crystals in 5 equal piles under T.C.P. and between.
2/8	9 crystals under 1st T.C.P., 3 between 1st and 2nd, 4 under 2nd and 6 under 3rd T.C.P.
2/9	5 between 2nd and 3rd T.C.P. and 1 between 1st and 2nd.
2/10	8 evenly spaced with the 3rd, 5th, and 7th crystal under T.C.P.
2/11	6 evenly spaced with 2nd, 4th, and 6th crystal under T.C.P.
2/12	5 evenly spaced 1st and 4th crystal under T.C.P.
2/13	4 evenly spaced with 1st and 4th crystal under T.C.P.

abbreviation: T.C.P. = thermocouple position

APPENDIX F

GEOMETRIC SURFACE AREAS

Geometric surface areas, A_s , in Runs 2/7 through 2/13 were calculated using:

$$A_s = 20 \left(\frac{W}{t\rho} \right) + \left[P \sqrt{\frac{W}{t\rho}} \right] t$$

where W = weight of crystal, grams

t = crystal thickness, mm

ρ = density of crystal, grams/cm²

P = shape parameter based on crystal type

Using the reported density of 6.80,^{c, d} the following surface areas are obtained. In three runs a comparison is given with surface area calculated with dimensions of the crystal only.

<u>Run</u>	<u>S. A., cm²</u>	<u>S. A. (from dimensions)</u>
2/7	19.40	
2/8	7.89	

^cHague, J. R., "Refractory Ceramics of Interest in Aerospace Applications," Battelle Memorial Inst., AD 423400 (1963).

^dHarrison, W., "Fabrication and Fracture of Polycrystalline NiO," Honeywell Research Center, AD 614263 (1965).

<u>Run</u>	<u>S. A., cm²</u>	<u>S. A. (from dimensions)</u>
2/9	2.88	2.71
2/10	2.96	
2/11	1.53	1.50
2/12	2.33	
2/13	1.72	1.48

Estimate of error is taken as the maximum deviation between the samples, namely, $\pm 7\%$.

The shape parameter, P , is equal to 4 if the edges of the large face are equal and the crystal is classified as type 1. If the edges of this face are in the ratio of 2:1 or 3:1, P takes on a value of 4.25 or 4.62, respectively. For convenience the latter are classified as type 2 and 3.

The geometric surface areas in Runs 2-1 through 2-6 were not expected to be representative of the true surface area. The edges of these crystals were sanded as grown edges. This meant that the surface of the edge was not well defined and rough compared to cleaved surfaces. The crystals were placed on a piece of photographic paper then exposed to room light. After developing, the images were cut out and weighed. Knowing the average weight of the paper for a unit area, it was possible to calculate the surface area. The estimated surface areas so calculated are listed below.

These estimates are expected to be in error by $\pm 10\%$. This is

based on a comparison between the actual weight of the crystals and the weight estimated from the dimensions.

<u>Run</u>	<u>Estimated Surface Area</u>
2/1	2.098 cm ²
2/2, 2/4-2/6	2.010
2/3	0.820

The data from which the geometric surface areas in Runs 2/7 through 2/13 were calculated appear below.

<u>Run</u>	<u>W, grams</u>	<u>t, mm</u>	<u>Type</u>	<u>W, grams</u>	<u>t, mm</u>	<u>Type</u>
2/7	all of those in 2/9 and 2/8 plus:					
	.0351	.9	type 1 only	.0373	1.1	
	.0163	.2		.0252	1.6	
	.0444	.8		.0107	.9	
	.0097	.8		.0315	.9	
	.0406	1.1		.0146	.4	
	.0407	.9		.0282	.9	
	.0056	1.1		.0313	1.0	
	.0496	.9		.0367	1.3	
	.0415	.9		.0235	.8	
	.0391	1.0		.0077	.7	
	.0523	1.6		.0272	.9	
	.0472	.9		.0368	1.0	
	.0442	1.0		.0150	.4	
	.0475	1.1		.0075	.6	
	.1002	1.2		.0189	1.1	
	.0451	1.0		.0323	1.0	
	.0473	.9		.0173	.4	
	.0454	.9		.0196	1.5	
	.0406	1.0		.0296	1.1	
	.0432	.9		.0338	1.3	
	.0312	1.7		.0199	.6	
	.0163	.6		.0221	1.3	
	.0087	1.0		.0171	1.3	
	.0273	1.1		.0055	.4	
	.0416	1.4		.0146	.7	
				.0116	.4	

<u>Run</u>	<u>W, grams</u>	<u>t, mm</u>	<u>Type</u>	<u>W, grams</u>	<u>t, mm</u>	<u>Type</u>
2/7 cont'd:						
	.0170	.7	type 1 only	.0101	.8	
	.0150	.7		.0101	1.0	
	.0207	.6		.0106	.7	
	.0094	.7		.0143	.8	
	.0183	.6		.0108	.3	
	.0309	1.1		.0038	.2	
	.0183	.9		.0029	.3	
	.0136	.9		.0048	.4	
	.0065	.6		.0105	.9	
	.0119	.7		.0145	.7	
	.0185	.9		.0005	--	
	.0158	.7		.0035	--	
2/8	all of those in 2/9 plus:			.0660	.9	
	.0733	.9	type 1 only	.0677	1.3	
	.1107	1.0		.0605	1.2	
	.0705	1.0		.0296	1.0	
	.0874	.9		.0241	.3	
	.1108	1.1		.0406	.8	
	.0622	1.0		.0257	.9	
	.0671	1.3		.0395	1.0	
2/9	.0780	.8	1	.1387	1.2	2
	.0999	1.0	1	.0602	1.0	1
	.1631	1.0	2	.0705	.8	1
				.0215	.7	1
2/10	.0576	1.0	2	.0182	.6	3
	.0815	.9	1	.0286	.8	3
	.0305	.8	2	.0424	1.0	2
	.0296	.5	2	.0282	.6	3
	.0698	.9	2	.0162	.9	1
	.0538	.9	2	.0136	.7	1
				.0179	.3	1
2/11	.1402	1.2	1	.0268	1.0	2
	.0368	1.0	2	.0210	.7	4
	.0423	1.0	1	.0187	.9	2
				.0186	1.0	1

<u>Run</u>	<u>W, grams</u>	<u>t, mm</u>	<u>Type</u>	<u>W, grams</u>	<u>t, mm</u>	<u>Type</u>
2/12	.1067	1.1	2	.0515	.9	3
	.1075	.9	1	.0504	1.0	2
	.0980	1.1	2	.0306	1.1	1
				.0383	1.0	2
2/13	.0992	1.0	1			
	.0768	1.0	2			
	.1091	1.0	1			
	.0877	1.0	2			

APPENDIX G

CALCULATED KINETIC PARAMETERS RUNS 2/1-2/6

Run	E_{apparent} , kcal/g-mole	$\log k_0^*$	Temperature Range $^{\circ}\text{C}$
2/1	4.32	1.781	50 - 200
2/2	14.39	6.358	125 - 200
2/3	33.20	14.44	125 - 200
2/4			
2/5	9.80	4.206	125 - 200
2/6	7.44	7.44	165 - 200

* pseudo rate constant.

The catalytic parameters were all obtained on NiO surface that had, in addition to the cleaved 100 planes, a rough undefined area present on the edges.

APPENDIX H

ELECTRICAL CONTACTS

Good electrical contact is extremely important in making electrical studies with a semiconductor like NiO. One must find a material that acts as an ohmic contact and also has a minimum contact resistance. The true resistance of the semiconductor can then be obtained. Contacts that proved to be ohmic in previous investigations with NiO are listed in the Table below.

ELECTRICAL CONTACTS FOR NiO

<u>Contact Material</u>	<u>Reference</u>
Silver, paint, print, paste, evaporated	e
Platinum, paste, clips	63,124
Gold, evaporated	e
Brass, pressure contacts	e
Aluminum, evaporated	e
Nickel, gold-30% nickel alloy	e

^eGibbons, J. F. and Beadle, W., "Switching Properties of NiO Films," Solid State Electronics, 7, 785 (1964).

In order to obtain specific contact geometries Du Pont No. 6216 conductive silver preparation, furnished by E. I. Du Pont de Nemours and Co., was used in the present study. The paste was painted on. Firing took place in the following sequence: (1) furnace set to reach a temperature of 425°C in 20 minutes, (2) the crystal was removed and the furnace allowed to cool, (3) the other side of the crystal was painted and replaced, (4) the furnace was set to reach 677°C in 19 minutes followed by a 10 minute bake at this temperature, (5) and, finally, a quench in air to room temperature. One should be aware that with Ag contacts above $100\text{-}200^{\circ}\text{C}$ diffusion into the specimens almost invariably occurs.

The fired-on silver electrodes cannot be scraped off but can be removed by soaking the crystal in nitric acid at 25°C for one hour. Typical results using silver electrodes in both the room temperature Seebeck apparatus (Figure 3.6) and the low temperature conductivity apparatus (Figure 3.7) are given below.

Electrical Properties Using Silver Paste Electrodes

Run	Conductivity Cell, Resistance, ohm $\times 10^{-8}$	Seebeck voltage, final observed voltage	Treatment after Measurement
1	.28	+ .0062	HNO_3 soak, fire 15 min and 30 min
2	.396	+ .0062	HNO_3 soak
3	18.1	+ .0062	paint with Ag, fire 1 hour

<u>Run</u>	<u>Conductivity Cell Resistance, ohmx10⁻⁸</u>	<u>Seebeck voltage, final observed voltage.</u>	<u>Treatment after Measurement</u>
4	.775	+ .0058	fire 1 hour
5	.91	+ .0065	fire 1/2 hour
6	1.32	+ .0073	HNO ₃ soak
7	1.88	+ .0082	test concluded
8	7.2		

This indicates that as the firing time increases so does the observed overall resistance of the crystal.

APPENDIX I

CALCULATION OF RESISTIVITY

In order to estimate the defect concentration using equation (46) in Appendix A, one needs to have resistivity versus temperature data. Ideally this would be obtained by the two-point probe method eliminating contact resistance and allowing one to calculate the true resistivity of the material. Unfortunately, this technique could not be used below 150°C. If the contact resistance was known the low temperature measurements with the platinum foil electrodes could be used. Experiments were performed to compare the resistivity value using the 2-point probe, Ag-painted crystals, 2-Pt foil electrode and 2 wrapped Pt electrodes. The experimental points all fell on lines with the same temperature coefficient, but with varying values of resistivity. At a temperature of 178°C the ratio of the 2-Pt foil electrodes to the 2-point probe resistivity had a value of 1.64×10^2 or a conductivity ratio of 6.08×10^{-3} .

A further complication arises in that the operating limit of the conductivity apparatus is near 250°C. This is because of the upper temperature limit on the Temp-R-Tape used to give strength and stability

to the apparatus and to insulate it electrically. These Teflon and fiberglass tapes were furnished by the Connecticut Hard Rubber Co. This meant that the low temperature transition could not be experimentally determined with this equipment. The literature indicates a range of transition temperature values of NiO. A value of 394^o C is assumed to be representative of the single crystals used here as it is most often found to come within the range of reported results.

It is of interest to see if resistivity data from the Pt foil electrodes using Ag coated NiO crystals and an assumed transition temperature yield at least relatively correct values of the defect concentration. By applying this technique the ratio of the nickel vacancies calculated is:

$$\frac{(\text{Ni}\square) \text{ foil}}{(\text{Ni}\square) \text{ 2 point}} = 7.56 \times 10^{-3}$$

This value is close to the conductivity ratio actually measured on the crystal. It is not expected that the absolute value of the vacancy concentration has any significant meaning. Using this calculation as a relative measure may be satisfactory and certainly worth considering when experimental data is not available.

APPENDIX J

KEL-F COATINGS

A continuous film coating of Kel-F could be applied using "Kel-F" plastic dispersion types KX-633 and 643, furnished by Minnesota Mining and Manufacturing Co. The final coating procedure which was adopted made it possible to coat crystals, glass, and metal parts with a coating which proved to be relatively inert in the hydrogen peroxide vapor under the conditions of the experiments.

Crystals with undefined edges were masked by coating with KX633. After air drying for 30 to 60 minutes, any "Kel-F" that had accidentally spread onto the large crystal face could be easily scraped off with a razor blade, taking care not to damage the crystal. A 584-watt Hevi-Duty tubular furnace unit was used for the heat treatment. In the first 30 minutes the furnace reached 216°C . The furnace was set to 227°C for 10 minutes, 238°C for 10 min, $260\text{-}271^{\circ}\text{C}$ for 20 minutes and a final bake at 260°C for 2 hours. Pieces of larger dimensions were coated with "Kel-F" by painting and air drying as above. They were then placed in a drying oven and heated to about 400°C for four hours, then air quenched. The procedures deviate somewhat from the manufacturers recommended procedures (96).

APPENDIX K

DECOMPOSITION OF HYDROGEN PEROXIDE

VAPOR ON BOROSILICATE GLASS

Several investigators have found that borosilicate glass is the best material of construction with respect to inertness to hydrogen peroxide vapor (55, 125, 126). During the preliminary catalytic studies no increase in reaction due to the presence of a catalyst could be detected on as many as 22 pieces of NiO crystals. It was thought that the problem was the low concentration of the solution in the saturator (35%, 50%) and the fact that the reactor had a maximum operating temperature of 100°C. It was later discovered that the glass itself was completely obscuring the effect of the catalyst. Turning to the literature, it was clear that preparing the glass reactor might well be the key to a successful study. A summary of the various treatments that have been used is given in Table K1. A common step in most of the work is some type of acid wash.

In the present study each of the glass reactors was degreased with ethanol before use, rinsed with water, then soaked in various

concentrations of nitric acid, then rinsed before it was used. The actual treatment given the three reactors constructed and the subsequent activity of the glass in terms of the exit concentration parameter C are listed in Table K2. The significant improvement in going from the large reactor to tube No. 1 is related to better control of the treatment.

Several conclusions can be made from the results on tube No. 1. The most obvious is that initially cleaning the glass before glassblowing greatly improves the inertness. It appears that the value of C increases with time exposed to the hydrogen peroxide vapor, however, not indefinitely. Continued acid washing and rinsing does nothing in the way of improving the glass. It was reported in the literature that fusing the glass at 490°C causes an decrease in the activity (126) as much as a factor of 20. Helium gas was passed through tube No. 1 as it was heated to 490°C and held for as much as 200 minutes. The only effect was initially a large increase in activity followed by a gradual decrease. These treatments of the glass do not seem to effect the overall activity of the glass. This heat treatment may result in loss of surface Si-OH groups, or surface dehydration which might alter the surface reactivity (23).

It is interesting to put the exit concentration parameters on the same basis with respect to KMnO_3 normality. If this is done the values of C in x2/10 and Z/12 become 40.6 and 42.2, respectively. An increase in flow rate of the gas would cause an increase in C of 1.58. This is

in agreement with the observed values.

The second thing one observes in Table K-3 is the change in activation energy. Satterfield and Stein (126) have shown that there is no correlation between activation energy and surface activity of the glass. Their acid treated glass annealed at 490°C showed the lowest surface activity and the highest activation energy, 10 kcal/g-mole, compared with between 3.5 to 7 kcal/g-mole for acid washed borosilicate glass. Initially the activation energy on reactor tube No. 2 is low but begins to increase. This deactivation is expected, however, after Run 6 the activation energy is much larger. This suggests that since a Kel-F coating covered the crystal edges in Run 2/6, which reduces the activity of the catalyst, the same effect may be responsible for this. Indeed, the temperature may have been high enough to "contaminate" the reactor, so to speak.

These experiments, together with the information from earlier studies, resulted in a treatment for the reactor tube No. 2 in which most of the kinetic work was taken. The treatment began with rinsing the original pieces of glass with ethanol, draining and adding a small amount of HNO_3 , steeping, and rinsing with deionized distilled water before glass-blowing. After blowing, the reactor was annealed to 600°C with the ends covered loosely with degreased aluminum foil. At this point the reactor was rinsed with ethanol, drained, filled with 3 ml of conc. HNO_3 and after steeping, rinsed only twice with deionized distilled water. Additional

water rinses would increase the activity. The improved initial results obtained with this procedure are also indicated in Table K2.

Reactor tube No. 1 was reactivated somewhat by coating the inside of the reactor with the Kel-F dispersion following procedures similar to those in Appendix J. At 200°C one coat reduced the decomposition from 66.1 to 41.8%. A second coat further reduced activity, giving a decomposition of 28.8%. The flow rate used above was 192 cc/min and the saturator temperature was 13.5°C.

Sodium content of the glass, adsorbed heavy metal ions, imbedded dirt, and localized defects (19, 126, 142) are all variables on the glass surface and indicate that a combination of both chemical and thermal treatments are required to obtain reproducible surfaces. Cheaney and Walsh suggest that the acid treatment causes a film of silicic acid to be deposited on the surface (23). Such a surface is acidic, and not completely anhydrous. The fact that no significant change in the glass activity was observed might be because of exposure to the atmosphere (60% relative humidity) after heat treatment. Fire-polishing the glass has been found to definitely reduce the activity. Similar findings are reported (40). Such treatment followed by acid rinsing gives a glass surface approaching the fracture type (142). A freshly fractured piece of glass provides the cleanest surface of a single glass phase.

The considerations shed some light on the nature of the problem. By paying attention to the details and applying the treatment here,

one can obtain a surface which is inert enough to allow study of the reaction on a very small surface area of catalyst.

Finally, in reactor tube No. 1, after the initial glass activity study was made, considerable work was done in studying the activity of NiO single crystals. It was observed that the activity of the glass increased significantly after the catalyst had been removed relative to the initial activity. Since no reaction is expected between the NiO and the surface of the glass at this temperature, the increase was most likely due to scratching of the surface during charging and unloading the catalyst or introduction of some impurities with the crystals. In subsequent work the catalysts were positioned with the aid of a Nylon rod. No similar activation was observed in reactor tube No. 2.

TABLE KI

TREATMENTS OF BOROSILICATE GLASS IN HYDROGEN
PEROXIDE VAPOR DECOMPOSITION STUDIES

Chemical Treatment	Thermal Treatment	Comments	Reference
Soak in warm chromic acid 5 min., repeated H ₂ O rinse, final rinse with redistilled H ₂ O	Fusing: glass brought to softening point in flame of Meker burner	Activity of glass reduced by factor of 20. Rinsing with hot water increased activity	40
Rinse, sat'd soln. boric acid in ethanol, dry 1 hr. at 200°C, overnight at 500-520°C		Film of silicic acid decreases activity	95
40% HF wash, cold H ₂ O rinse	Heat treatment 500°C increases activity (causes complete dehydration)	Further H ₂ O rinsing or with non-ionic detergent or alkali increases activity	23
2N HNO ₃ , 4N H ₃ PO ₃ , or 1% HF, followed by water rinsing	"Fusing" at 490°C	Acid and heat treatment reduce activity by factor of 10	126

TABLE K1--Continued

Chemical Treatment	Thermal Treatment	Comments	Reference
Ethanol rinse, conc. HNO ₃ , dilute HNO ₃ soak, immersion rinse in H ₂ O dry at 100°C		No decomposition below 136°C, 3.5% in range 135-183°C	119
40% HF rinse	950°C in vacuum 10 min.	Preserves gaseous H ₂ O ₂	65
Acid treated glass gives most inert surface along with coating of silicic, boric or phosphoric acid. Repeatedly washed acid treated surface comparable to activity of metal oxides, and hydroxides			156
Ethanol and HNO ₃ reaction and seeping, soak in conc. HNO ₃ rinse doubly distilled H ₂ O rinse, dried in filtered air 110°C, repeat a maximum of 6 times		Decomposition of less than 1% at 140°C	f

^fRoss, R. A., Private Communication, College of Technology, Belfast (1966).

TABLE K1-Continued

General Remarks on Borosilicate	Reference	
HF rinse gives H ₂ O free surface. 1 min. treatment with boiling 1% HF rough surface. Etch 10 min in 1% NaOH followed by acid rinse	Fractured surface provides cleanest surface of a single phase glass. Imbedded dirt can not be removed without introducing additional defects	142
Polishing debris minimized by cleaning.	Exhibit fine structure on range 100-500A shows polish scratches while additional larger defects such as gouges and grossly rough areas may be present, 1 part in 10 ³	19

TABLE K2

ACTIVITY OF PYREX GLASS

Pretreatment	$C^* \frac{\text{ml KMnO}_4}{\text{sec}} \times 10^3$	Temperature of Reactor °C	Nitrogen Flow cc/min
<u>Initial Reactor</u>			
o, l, j, d, l, j, k	2.94	61	40
	36.8		176
m, o	1.85	92	54
n	1.44		54
	28.1		177
o	1.57		54
m	1.89 - 2.3		54
<u>Tube No. 1</u>			
b, q, e			
a, c, d, b, h	4.38	30	55
	6.15		
	5.21 - 5.44		
	5.25 - 5.35		
	4.52 - 4.38		
a, b, d, a, g	3.82, 4.28	173	181
a, c, d	3.78 3.84		
b, j	4.14		
i	3.73 3.84		

TABLE K2--Continued

Pretreatment	$C^* \frac{\text{ml KMnO}_4}{\text{sec}} \times 10^3$	Temperature of Reactor °C	Nitrogen Flow cc/min
<u>Tube No. 1</u>			
j	3.42		
a, c, d, b, g	3.33		
b	3.11		
f-490/30m	2.80		
i	3.55 3.90 4.11		
f-345	3.96		
b, f-490/3h20m	2.99 3.44		181
i	3.79		
b, j, g	3.46		
a, c, d, f-490/30m	3.54 3.61		
	0.61 - 1.00	247	
i	4.30 4.44		
<u>Tube No. 2</u>			
j, a, c, j-d, j, g-200f/2h			
q, e	5.80	24	57
	3.54	159	
a, c, d, j-twice	34.8	167	181
	30.8 31.8	226	

TABLE K2--Continued

Pretreatment	$C^* \frac{\text{ml KMnO}_4}{\text{sec}} \times 10^3$	Temperature of Reactor °C	Nitrogen Flow cc/min
	20.1	285	
	32.4	168	
	34.2	24	

*These exit concentration parameters are all based on a common KMnO_4 normality of 0.011N.

TABLE K2

LEGEND

<u>Symbol</u>	<u>Corresponding Treatment</u>
a	degrease in ethyl alcohol (absolute)
b	rinse with deionized H ₂ O
c	HNO ₃ reacting with trace of ethanol
d	HNO ₃ soak
e	anneal in air - to 600°C
f	anneal in the atmosphere
g	dry in oven
h	dry with N ₂ flow on stream
i	left overnight with N ₂ flow
j	H ₂ O soak, or rinse
k	N ₂ flow at same conditions
l	HNO ₃ vapors passed through (in N ₂)
m	catalyst added - used - removed
n	other material added - used - removed
o	reactor modified
p	used in previous studies
q	blown

TABLE K3

ACTIVITY OF PYREX GLASS REACTOR NO. 2

Run	Decomposition %	Temperature of Reactor °C	C_R $\frac{\text{ml KMnO}_4 \times 10^3}{\text{sec}}$	E_{apparent} kcal/g-mole
2/3	4.18	100	41.04	3.67
	6.89	150		
	9.59	200		
2/5	2.78	100	43.5	3.31
	4.44	150		
	6.09	200		
2/6	.87	100	43.0	7.98
	3.48	150		
	4.35	200		
2/9	0	100	43.	11.74
	4.46	150		
	17.60	200		
2/10	.34	100	45.2	14.77
	2.40	150		
	20.99	200		
2/12	2.38	150	47.	16.95
	8.58	175		
	18.38	200		

The KMnO_4 normality used in Runs 2/2 through 2/9 is 0.0096N and .00862N in 2/10 through 2/12.

APPENDIX L

EXPERIMENTAL EXIT CONCENTRATION PARAMETERS

Run	Catalyst				Blank			
	C	T	C	T	C	T	C	T
2/1	40.23	23	18.11	203	34.14	22		
	39.69	23	18.46	203	39.69	137		
	39.28	23	21.63	185	39.30	24		
	38.04	86	21.43	186	37.20	202		
	25.85	90	21.74	186	36.49	201		
	39.67	90	32.65	124	39.13	67		
	36.71	90	33.31	120	43.86	24		
	35.63	91	34.21	120	36.16	24		
	18.79	195			45.31	57		
	17.82	203						
2/2	40.04	25	30.14	162	39.43	23	41.24	23
	40.16	25	38.87	96	37.88	845	41.32	67
	40.00	89	39.57	96	40.68	85	40.33	68
	39.84	89	32.62	159	40.66	85		
	37.12	131	40.27	240	29.94	186		
	22.43	197	30.97	158	38.79	183		
	22.21	198	39.18	161	39.86	120		
	32.17	161			41.26	23		
2/3	40.95	86	36.10	163	36.13	215		
	39.18	134	33.20	196	37.87	95		
	28.58	214	37.35	183	40.78	96		
	37.47	163			40.39	24		
2/5	43.44	94	24.21	203	40.23	207		
	41.24	94	24.47	202	41.27	206		
	42.05	94	40.95	118	43.37	24		
	30.58	176	43.57	24				
	30.00	177	43.47	24				

Run	Catalyst				Blank			
	C	T	C	T	C	T	C	T
2/6	43.04	63	40.29	185	41.20	186	42.51	25
	41.38	123	43.00	25	41.51	186		
	40.27	172			42.39	124		
	41.08	170			43.30	63		
2/7	44.17	64	8.18	201	see 2/9			
	32.09	119	20.80	149				
	31.65	120	42.29	24				
	11.36	174	43.23	24				
	11.07	173	41.49	62				
2/8	41.94	24	13.84	196	see 2/9			
	14.11	199	37.30	124				
	13.02	200						
2/9	19.24	203			34.38	204	41.39	183
	18.76	203			35.77	200	39.53	171
	40.81	123			40.93	124		
	33.02	155						
2/10	40.25	125	43.18	73	44.40	170	45.09	64
	38.58	125	31.86	148	42.20	170	44.76	64
	16.90	189	21.33	178	33.77	205	43.80	137
	25.41	161	20.52	179	45.28	123	39.63	179
					44.10	123	45.19	24
2/11	21.39	204			56.10	117	31.82	197
	39.55	131			57.11	117	32.47	197
	33.18	162			51.23	117	48.77	160
	43.47	73			42.27	183	50.41	157
					56.93	67		
2/12	46.45	24	38.80	150	45.00	165	38.14	201
	25.83	189	46.00	75	43.67	165		
	42.83	119			47.07	112		
2/13	43.00	123	39.69	153	see 2/12			
	44.79	62	24.99	203				
	43.34	127						

C represents the experimental concentration parameter and T the reactor temperature in degrees centigrade.

APPENDIX M

BEST FIT COEFFICIENTS TO CONCENTRATION
PARAMETER-TEMPERATURE RELATION

$$C = \frac{\text{ml KMnO}_4}{\text{time}} = A + BT + DT^2 + ET^3 + FT^4$$

H = catalyst and glass

W = glass

<u>Run</u>	<u>A</u>	<u>B</u>	<u>D</u>	<u>E</u>	<u>F</u>
2/1 H	39.68453	.00718887	.0005621	0.0	0.0
W	38.7691	.067182	-.00039196	0.0	0.0
2/2 H	41.2955	-.07025	.00116	-.00000652	0.0
W	41.54717	-.02222	0.0	0.0	0.0
2/3 H	79.40603	-.887014	.0065268	-.00001630	0.0
W	41.54717	-.02222	0.0	0.0	0.0
2/5 H	41.907729	.0863298	-.0008564	0.0	0.0
W	43.717912	-.0143793	0.0	0.0	0.0
2/6 H	43.75004	-.0182117	0.0	0.0	0.0
W	41.002177	.07938404	-.00081661	.00000215	0.0
2/7 H	45.5071316	-.2425802	.0069557	-.00007245	.0000001933
W	see 2/9				
2/8 H	38.4735776	5.1820333	-.0015482	0.0	0.0
W	see 2/9				

Run	A	B	D	E	F
2/9 H	59.159902	-.07439323	-.0006081	0.0	0.0
W	14.881393	.39040897	-.0014383	0.0	0.0
2/10 H	-28.39797	1.8897692	-.0148046	.000032205	0.0
W	48.302288	-.1607728	.00207517	-.00000793	0.0
2/11 H	36.02227	.1999038	-.001332975	0.0	0.0
W	88.639156	-.9341191	.00874134	-.000027653	0.0
2/12 H	47.74196	-.077813	.0012658	-.00000775	0.0
W	27.833193	.32337193	-.0013537	0.0	0.0
2/13 H	48.012936	-.129030699	.00175405	-.000008262161	0.0
W	27.833193	.323372	-.0013537	0.0	0.0

Run	Variance (50) S ²	Exit Concentration Parameter Reactor Temperature 25°C	Carrier Gas Flow cc/min
2/1 H	8.284	39.552	180
W	8.9583		
2/2 H	5.804	40.161	180
W	7.837		
2/3 H	1.8373	41.036	179
W	7.837		
2/5 H	.4806	43.49	187
W	.5260		
2/6 H	.3028	43.30	190
W	.1268		
2/7 H	.9339	43.00	190
W	see 2/9		
2/8 H	.6146	43.00	189
W	see 2/9		

Run	Variance (50) S^2	Exit Concentration Parameter Reactor Temperature 25°C	Carrier Gas Flow cc/min
2/9 H	.1152	43.00	190
W	.1618		
2/10 H	.9297	45.197	193
W	1.63162		
2/11 H	.11274	46.00	194
W	4.549		
2/12 H	.5032	46.50	196
W	2.653		
2/13 H	.21559	46.50	196
W	see 2/12		

The KMnO_4 normality in Runs 2/1 through 2/9 is 0.0096N and 0.00862N in Run 2/10 through 2/13.

In cases where no experimental data on borosilicate exist at 25°C , C_R is estimated from the catalytic run data at this temperature.

APPENDIX N

CALCULATED PSEUDO RATE CONSTANTS AND DECOMPOSITION

<u>Run</u>	<u>Reactor Temperature, °C</u>	<u>Pseudo Rate Constant</u>	<u>Decomposition %</u>
2/1	100	.1882	.1715
	125	.2661	.2336
	150	.3583	.3011
	175	.4683	.3740
	200	.6018	.4522
2/2	100		
	125	.0217	.0215
	150	.0874	.0837
	175	.2245	.2011
	200	.4925	.3889
2/3	100		
	125		
	150		
	175	.0235	.0233
	200	.1142	.1079
2/5	100	.0070	.0070
	125	.0617	.0599
	150	.1477	.1373
	175	.2737	.2394
	200	.4560	.3662
2/6	100	.0233	.0230
	125	.0208	.0206
	150	.0180	.0179
	175	.0197	.0195
	200	.0307	.0302

Run	Reactor Temperature, °C	Pseudo Rate Constant	Decomposition %
2/7	100	.0392	.0385
	125	.3006	.2597
	150	.6750	.4908
	175	1.066	.6558
	200	1.010	.6356
2/8	100		
	125	.1021	.0978
	150	.2689	.2357
	175	.4743	.3777
	200	.7398	.5228
2/9	100		
	125	.0200	.0198
	150	.1711	.1573
	175	.3156	.2706
	200	.4461	.3599
2/10	100	.0069	.0069
	125	.1360	.1271
	150	.3538	.2980
	175	.5729	.4361
	200	.6132	.4584
2/11	100	.0888	.0850
	125	.1611	.1488
	150	.2384	.2122
	175	.3215	.2749
	200	.4111	.3371
2/12	100	.0387	.0380
	125	.1005	.0956
	150	.1756	.1610
	175	.2873	.2497
	200		
2/13	100	.0494	.0482
	125	.0887	.0848
	150	.1292	.1212
	175	.1910	.1739
	200	.3006	.2696

No values based on extrapolated data included in the tabulated values above.

APPENDIX O

APPROACH TO SATURATION

It is convenient to use the exit concentration parameter for the borosilicate reactor at 24°C as a reference in calculating the percent decomposition. The closer the value is to that expected for a completely saturated stream, the simpler the equations become in treating the kinetic data. A calculation is carried out in this section which shows that for all practical purposes the conditions used provide an inlet stream to the reactor that is saturated with hydrogen peroxide vapor.

For Run 2/12 the nitrogen flow rate through the system was 190 cc/min and the exit concentration parameter at 24°C on the borosilicate surface was 43×10^{-3} . The normality of the KMnO_4 used was 0.0096N. A ml of .1N potassium permanganate corresponds to 1.701 mg. of hydrogen peroxide and the molecular weight of hydrogen peroxide is 34.02 (129). The molar flow rate of hydrogen peroxide, \dot{M} , is determined by multiplying the product of the exit concentration parameter and the KMnO_4 normality as indicated below,

$$\dot{M} = \frac{(17.01)(60)}{(34.02)} \times 10^{-3} \text{ NC} = 1.238 \times 10^{-5} \text{ g-moles/min.}$$

Knowing the saturator temperature and the concentration of the hydrogen peroxide solution, it is possible to calculate \dot{M} based on the equations given by Schumb (129). This is accomplished by assuming that the nitrogen carrier gas leaving the saturator is in equilibrium with the solution, that is, its hydrogen peroxide concentration corresponds to a saturated vapor. At equilibrium the mole fraction of hydrogen peroxide in the vapor Y_p , is related to the mole fraction in the liquid, x_p , through the activity coefficient γ_p and the vapor pressure of anhydrous hydrogen peroxide, P_p^0 .

$$Y_p = \frac{x_p \gamma_p P_p^0}{\pi}$$

where π is the total pressure in the same units as the vapor pressure. For a 98% solution of hydrogen peroxide at 13.5 °C the mole fraction is 1.568×10^{-3} . The molar flow rate of hydrogen peroxide can now be calculated from this information since,

$$\dot{M} = Y_p F_{N_2} \frac{\pi}{RT} = 1.18 \times 10^{-5} \text{ g-moles/min.}$$

where F_{N_2} , the flow rate of nitrogen, is 190 cc/min measured at a pressure π and a temperature $T^{\circ}\text{K}$.

These two values agree within the experimental error associated with the flow measurement.

APPENDIX P

APPARENT ACTIVATION ENERGY OF SURFACE REACTION IN EXTERNAL FLOW SYSTEMS

Rosner (117) has derived general expressions for estimating diffusional falsification of activation energy and given approximate solutions for the case of a thin, non-turbulent diffusion layer which develops along an impermeable catalytic flat plate. The similarity of the model assumed and the system used in the present study suggests applying these published results to this kinetic study.

A knowledge of the true reaction order enables the determination of the falsification parameter E_a/E if one knows the Fick diffusivity, D . From the overall reaction rate and the apparent activation energy one can then estimate the true activation energy.

Assuming that the characteristic catalyst length is equal to the summation of the length of the seven pieces of catalyst, it is possible to apply Rosner's approximations to the data of Run 2/12. At 150°C the value of the diffusivity for the hydrogen peroxide a nitrogen system is calculated by Yeung (162) to be 0.287 cm/sec. . By graphical techniques

one finds,

$$\frac{E_a}{E} = \frac{\text{experimental apparent activation energy}}{\text{true apparent activation energy}} = 0.76$$

This was obtained by using a Schmidt number of 0.991 (162) and a Reynolds number of 14.8. This suggests that there is a slight diffusional falsification.

APPENDIX Q

EXPERIMENTAL RESULTS FROM TUBE REACTOR NUMBER 1

One series of useful runs was taken in reactor tube No. 1. The catalyst pretreatment consisted of heating the crystal to 410°C in air for five hours and cooling slowly. The bath temperature was 13.5°C and the concentration in the saturator was 98%. The results using a flow rate of 25 cc/min are given below.

<u>Blank</u>		<u>Catalyst, 5 crystals</u>	
Experiment Exit Concentration Parameter $\frac{\text{ml KMnO}_4}{\text{sec}} \times 10^3$	Reactor Temperature °C	Experiment Exit Concentration Parameter $\frac{\text{ml KMnO}_4}{\text{sec}} \times 10^3$	Reactor Temperature °C
1.91	241	8.94	24
1.94	242	8.03	52
10.20	24	0.58	129
8.34	165		

The decomposition is 100% with the catalyst and glass at 132°C.

The amount of decomposition on the glass alone at 200°C amounts to 33.2%.

Although the results at the higher flow rate were not as

reproducible some results were obtained at 173°C and with a flow rate of 175 cc/min. The number of crystals was changed and the decomposition measured.

5 crystals	55.91% decomposition
3 crystals	16.58% decomposition
2 crystals	11.92% decomposition

APPENDIX R

EXPERIMENTAL EXIT CONCENTRATION PARAMETERS

RUN 2/12-RATE OF FLOW VARIED

H = catalyst and glass surface

W = glass surface

<u>Run</u>	<u>Flow cc/min</u>	<u>Surface</u>	<u>Exit Concentration Parameter ml KMnO₄ x 10³ sec</u>	<u>Reactor Temperature °C</u>
2/12B	196		see Appendix L	
2/12C	293	H	49.65	187
			50.47	187
			66.49	150
			71.42	25
			70.62	71
			69.49	123
	293	W	67.34	169
			70.35	117
2/12D	488	H	98.63	191
			98.45	191
			144.76	153
	488	W	114.47	168
			119.08	114
			113.4	205

APPENDIX S

LOW TEMPERATURE RESISTIVITY

It was of interest to see if a low temperature determination of resistivity would be useful in characterizing the crystal. The guarding technique described in Chapter III, Section C.3 was used. The dimensions of the crystal and the fired on silver electrodes are given on Figure 3.6. Results are from a representative test.

The bulk resistivity was measured by placing electrode C in the 100v source on the Keithley 610A Electrometer. The current flow between electrode C and A were measured. Electrode B was connected to the Keithley ground. The case of the instrument was connected to a good water pipe ground. Applying the equations developed in ASTM D257-61 (3), the bulk resistivity can be calculated by,

$$\rho = \frac{A}{t} R_v = \frac{A(\text{mm}^2)}{1.4\text{mm}} R_v$$

where A = effective area of the guarded electrode,

t = average thickness of specimen,

R_v = volume resistance of specimen, ohms.

The volume resistance above is determined by,

$$R_v = \frac{100 \text{ volts}}{I_m} = \frac{100 \text{ v}}{2.0 \times 10^{-7} \text{ amp}} = 50 \times 10^7 \text{ ohms}$$

where I_m = the current measured with electrometer.

For rectangular electrodes the effective area is found to be 14.8 mm^2 using equations in the article cited. Thus the bulk resistivity is calculated to be $5.28 \times 10^8 \text{ ohm-cm}$.

Using the ASTM procedure a surface resistivity may be determined connecting C to the input terminal, A to the ground terminal and B to the guard ring. Current flow is then measured between B and C.

The surface resistivity is defined by,

$$\rho_s = \frac{P}{g} R_s$$

where R_s = surface resistance,

g = distance between electrodes,

P = effective perimeter of guarded electrode.

Following the convention for determining g and P (3), one calculates values of 1.9 mm and 17.6 mm respectively. The surface resistance for a measured current of 1.28×10^{-8} , with 100 volt applied is $78.1 \times 10^8 \text{ ohms}$.

The surface resistivity is then found to be $724 \times 10^8 \text{ ohms}$. The usefulness of this technique is limited by the fact a large sample is required and the effect of the silver contamination is untested.

APPENDIX T

CALCULATION OF THE SEEBECK COEFFICIENT

A steady state temperature differential is established across a NiO crystal in the high temperature resistivity-Seebeck coefficient cell (Figure 3.4) by applying a voltage across the auxiliary heater. In this appendix the data obtained following the procedure outlined in Chapter III, section C.1 is used to calculate the Seebeck coefficient. The NiO sample used has a pretreatment similar to the catalysts in Run 2/10. The data are given below.

Average temperature of crystal	210 ^o C
Thermocouple a EMF	3.39 mv
Thermocouple c EMF	2.11 mv
Thermocouple d EMF	1.2436 mv
Thermocouple e EMF	1.3112 mv
EMF across crystal, g	-0.0015477 v

To compensate thermocouples d and e and obtain the EMF's with respect to 0^o C, the procedure of Roeser (115) is used. This consists of determining the EMF corresponding to the junction and adding this

contribution to the observed reading. Thermocouples a and c indicate that junctions d and e are at a temperature of 65°C and 41°C , respectively. The corresponding EMF generated by d and e are 0.397 mv and 0.241 mv. The EMFs with respect to 0°C are found by adding this to the measured EMF, that is, d has a compensated value of 1.5522 mv while e has a compensated value of 1.6406. Thus,

$$\text{Temperature by d} = 214^{\circ}\text{C}$$

$$\text{Temperature by e} = 224^{\circ}\text{C}$$

The Seebeck coefficient is then determined to be,

$$\theta = + \left| \frac{1547.7 \text{ v}}{10^{\circ}\text{C}} \right| = 154.8 \mu\text{v}/^{\circ}\text{C}$$

The sign of the Seebeck voltage was such that the cold side was always positive with respect to the hot side. This verifies the P-type conduction. The usual sign convention for the Seebeck coefficient is $\theta = +|\theta|$ for P-type materials (52).